

ANDROGEN TOXICITY ON NEUROMUSCULAR PHYSIOLOGY IN A NOVEL MODEL
OF SBMA

By

Kentaro Oki

A DISSERTATION

Submitted to
Michigan State University
in partial fulfillment of the requirements
for the degree of

Neuroscience – DOCTOR OF PHILOSOPHY

2013

ABSTRACT

ANDROGEN TOXICITY ON NEUROMUSCULAR PHYSIOLOGY IN A NOVEL MODEL OF SBMA

By

Kentaro Oki

Spinal bulbar muscular atrophy (SBMA) is a progressive motor disease that appears only in men around mid-life and results in limb weakness, dysphagia (swallowing difficulties), and dysarthria (speech difficulties). The disease is believed to be neurogenic, originating from motoneuron dysfunction and its slow progressive death. Thus, most of the studies characterizing the disease in mice have focused on motoneuron as the site of disease although there is some clinical evidence suggesting skeletal muscle may be an important site of disease. SBMA is caused by a mutation that leads to an expansion of CAG repeats coding for glutamine in the androgen receptor (*AR*) gene, and the male-specific phenotype is believed to be androgen-dependent as females carrying the mutation have little to no symptoms. The male-specific disease phenotype has been replicated in mouse models expressing similar mutations and can be improved with castration, reinforcing that the disease is androgen-dependent. Furthermore, female mice in these models are asymptomatic and only exhibit disease symptoms with androgen treatment. Although a CAG expansion in the *AR* gene is thought to underlie the disease, a similar phenotype is observed in a transgenic (Tg) mouse line engineered to express a rat *AR* cDNA with a wild type (WT) number of glutamine residues (22) at very high levels exclusively in skeletal muscle fibers. Although alteration of gene and protein expression is exclusive to the skeletal muscles, mice from this myogenic (141) model exhibit a phenotype similar to the other CAG-expanded mouse models of SBMA. Tg 141 female mice that exhibit an androgen-dependent loss of motor function after 3-5 days of testosterone (T) treatment exhibit skeletal muscle

dysfunction, recorded by electrically stimulating isolated preparations of the extensor digitorum longus (EDL) and the soleus (SOL), prototypical fast- and slow-twitch muscles, respectively. Treatment in female 141 Tg mice over 3-5 days was enough to induce a precipitous decrease in force production in both muscles and alterations to kinetics during contractions in the EDL. To confirm that skeletal muscles could be a primary site of disease during SBMA, male mice of the same 141 model, as well as two other SBMA mouse models were examined. The other models were one expressing the full-length human AR with 97 CAG repeats (97Q model) and another expressing 113 CAG repeats in the first exon of the *AR* gene. Muscle dysfunction in the other models would further support myogenic contributions as being critical to the SBMA motor phenotype. Motor dysfunction was recorded in all mouse models, and male mice from the 141 and 97Q models exhibited dysfunction in the EDL and SOL. All muscles exhibited some deficit during force production, and contraction kinetics were altered in the EDL of Tg 141 males. These results indicate that severe muscle dysfunction can underlie the phenotype during SBMA, and androgens can act on the skeletal muscles to induce motor weakness. Furthermore, skeletal muscles may be an important target for therapeutics that could ameliorate disease symptoms.

ACKNOWLEDGMENTS

Thank you to Dr. Cynthia Jordan, my graduate advisor, who gave direction to my research and has given so much time and effort to guiding my writing. I hope that I can have a similar ability to guide so many different projects in the future. Thank you to Dr. Bob Wiseman who advised me on how to conduct studies on skeletal muscles. Without your collaboration and expertise, this work would not have been possible. Thank you to Dr. Marc Breedlove whose questions and insight at each step of the planning, benchwork, analysis, and writing helped us fill in missing details. Thank you to Dr. Cheryl Sisk and Dr. Peter Cobbett who comprised the rest of my committee and provided valuable guidance throughout my research. Thank you to Dr. Greg Demas who guided my first research project and whose enthusiasm for research influenced me to pursue a career in science.

Thank you to the other members of the Jordan and Breedlove laboratories, past and present, particularly Diane Redenius, Kate Mills, Kelsey Korabik, Jessica Poort, Mike Kemp, Jamie Johansen, Chieh Chen, and Kayla Renier as well as past and present members of the Wiseman laboratory, Jeff Ambrose, Natalie Pizzimenti, and Jon Kaspar for technical assistance and scientific discussions. Thank you to the individuals in ULAR who have cared for the mice used in this research. Thank you to Matt LaTourette and Chris Hunley for collaborating and guiding data analysis. Thank you to Irene Li who guided me in making figure illustrations in Adobe Photoshop. All of you have helped me in my research and allowed me to work smoothly in two laboratories on campus.

I am thankful for my friends at Michigan State University who were involved with the Navigators and the Ballroom Dance Team. You have all been amazing friends who have helped

me outside of academics. Thank you to Mulyanto Poort, Rehan Baqri, and Amit Shah for your collegiality in a professional environment as well as your personal friendship outside of our respective laboratories.

I am forever thankful to my parents and my brother, Tai, for their support, encouragement, and counsel throughout my life and all of my education. You have shaped me to be the person I am today and have stood by me through all things. You always encouraged me to strive towards my goals, especially through struggles, and I could not have done this without you. Thank you for everything. Finally, I am grateful to Robin Coan for her support and grace. You have made my life a much happier one, and I have truly enjoyed some of the best moments of my life with you. Your constant support was also critical in the latter stages of this work.

This work was supported by R01 NS045195 (CLJ) and DK095210 (RWW).

TABLE OF CONTENTS

LIST OF TABLES	viii
LIST OF FIGURES	ix
LIST OF ABBREVIATIONS	xv
INTRODUCTION	1
Motor Function	1
Neuromuscular Diseases	3
Spinal and Bulbar Muscular Atrophy	8
Experiments to determine disease origin	11
Anatomy and Physiology of Skeletal Muscle	13
Overview	16
CHAPTER 1: Androgen receptors in muscle fibers induce rapid loss of force but not mass: Implications for SBMA	18
Abstract	19
Introduction	19
Methods	21
Animals and hormone treatment	21
Motor function tests	22
In vitro studies to assess muscle mechanics	23
Histology	26
Androgen receptor protein expression	26
Protein gels	27
Testosterone levels	27
Data analysis and statistics	27
Results.....	28
Testosterone (T) treatment impairs motor function without loss of muscle mass	28
Skeletal muscles from T-treated female mice show striking androgen-dependent loss of force	29
Five Day Treatment	29
Tetanic Force	29
Muscle histology and protein content	30
Skeletal muscles from T-treated Tg females exhibit androgen-dependent changes in twitch force and kinetics	31
Twitch Force	31
Contraction Kinetics	32
Tetanic force production is reduced in the SOL but not EDL of Tg mice after three days of T treatment	32
Only the EDL from motor-impaired mice show deficits in fatigue resistance	33
Discussion	34

CHAPTER 2: Muscle dysfunction may underlie androgen-dependent motor dysfunction in mouse models of SBMA	40
Abstract	41
Introduction	41
Methods	44
Animals and treatment	44
97Q males	44
141 males	45
KI males	46
Motor function tests	46
In vitro studies to assess muscle mechanics	47
Histology	50
Testosterone levels	50
Data analysis and statistics	50
Results	51
Motor dysfunction correlates with muscle dysfunction in 97Q Tg mice	51
Motor dysfunction correlates with muscle dysfunction in myogenic Tg males	53
Histology	55
97Q Model	55
141 myogenic model	56
Knock-in model	56
Discussion	56
GENERAL DISCUSSION	65
General Findings	65
Overview of findings	65
Mechanisms of Muscle Dysfunction	69
Calcium Mechanisms	70
Trophic Factors	74
Metabolic Mechanisms	75
Future Directions	76
Conclusions	77
APPENDIX	78
REFERENCES	105

LIST OF TABLES

Table 1	Biometric data for female 141 mice. T, testosterone; mg, milligrams; nmol/L, nanomolar per liter; N/g, newtons/gram. Values are means \pm standard error of means. * $P < 0.05$	83
Table 2	Body weight, muscle mass and plasma testosterone (T) levels at end stage. Motor-impaired Tg male mice in each SBMA model show significantly decreased body weights compared to their respective WT controls. All but the soleus (SOL) muscle in 97Q males had significantly less mass. Circulating T levels were comparable between Tg and WT males within each line but notably higher for Tg and WT males in the 97Q model because these animals were castrated and given exogenous T starting at puberty. * $P \leq 0.05$ difference between transgenic mice and their respective WT controls, values = mean \pm standard error of mean	90
Table 3	Kinetics analysis of individual twitch traces for motor-impaired Tg males and their WT controls. Analyses revealed few significant effects of disease on twitch kinetic; only rise time (time to peak force) in the EDL muscle of 141 Tg males was significantly prolonged compared to WT controls. Note however a consistent trend toward slower twitch kinetics in diseased muscles of both models. * $P \leq 0.05$, values = mean \pm standard error of mean	91
Table 4	Muscle morphology for male mouse muscles. Total number of muscle fibers and percent of total number of fibers containing centralized (cent) nuclei for EDL and SOL of the two Tg SBMA models (141 myogenic and 97Q). Only the EDL from myogenic males had significantly fewer fibers than WT controls. Fiber number was unaffected in both the EDL and SOL of 97Q Tg males and also in the SOL of 141 Tg males. The EDL of 97Q males and the SOL of 141 males contain a higher percentage of fibers with centralized nuclei, indicative of an abnormal muscle state. Note that these two muscles also showed the severest loss in force (Figs 2, 4). n=5/group in all except 141 EDL (n=3) * $P \leq 0.05$, values = mean \pm standard error of mean. ¹ values from (Johansen et al., 2011); ² unpublished data (Johansen and Jordan).	92

LIST OF FIGURES

Figure 1 For interpretation of the references to color in this and all other figures, the reader is referred to the electronic version of this dissertation. The whole skeletal muscle is comprised of multiple fascicles with capillaries between fascicles providing a blood supply. Fascicles are then comprised of multiple myofibers. Myofibers are large, multinucleated individual cells of a skeletal muscle and are comprised of myofibrils.78

Figure 2 Large multinucleated myofibers contain the mitochondria on the muscle periphery to aid in muscle energetic. Myofibrils comprise the myofiber and are, in turn, comprised of myofilaments. Along myofibrils are sarcomeres, the most basic unit of a skeletal muscle that allows for a contraction. Upon electrical stimulation, multiple sarcomeres shorten within a muscle resulting in whole muscle shortening to produce a contraction.79

Figure 3 The myofilaments that comprise myofibrils and sarcomeres are shown when the overlying sarcoplasmic reticulum (SR) is removed from the myofibril. Myosin and actin form an interdigitating pattern throughout the myofibril to allow contractions. Myosin are anchored at the M line while actin is anchored by Z disks. Regions of the SR closer to the T tubules are termed the terminal cisternae. T-tubules that run on either side of the interdigitating region contain openings that form a triad with the terminal cisternae. These regions are where the electrical stimulus initiates muscle contractions.80

Figure 4 0) The first image at the top right lists the key proteins involved during a skeletal muscle contraction. A T-tubule is in contact with the sarcoplasmic reticulum (SR) containing calcium (Ca) ions that will initiate contraction. Ryanodine receptor 1 (RyR1) is closed, and sarcoendoplasmic reticulum Ca ATPase (SERCA) is inactive while Ca is within the SR. On the actin filament, tropomyosin covers the binding site preventing myosin heads from binding to actin. 1) With a voltage change, T-tubules conduct the electrical depolarization to initiate the opening of RyR1, releasing Ca from the SR. Upon Ca release from the SR, it binds to the Ca-sensitive subunit of the troponin complex. This also initiates SERCA function, but the large release of Ca into the cytosol is greater than the rate at which Ca is replaced into the SR. 2) Ca binding of troponin induces a conformational change in troponin removes the troponin-tropomyosin complex away from the actin filament, exposing the actin binding sites. 3) A myosin head to binds to the actin binding site, and 4) ATP is hydrolyzed, resulting in ADP and inorganic phosphate. Once phosphate is released, the myosin head turns. 5) With the release of ADP, the myosin head is turned even further, moving the actin filament, shortening the sarcomere, and resulting in a power stroke to initiate skeletal muscle contraction. This shortening in the sarcomeres produces the contractile force generated by muscles. In cases where ATP is depleted, the myosin head remains in this locked position on the actin filament. 6) As long as ATP is available, another ATP binds to the myosin head. 7) This releases the myosin head from the actin filament, returning the myosin head to its original position (same as step 2).

8) Once the skeletal muscle returns to resting potential, RyR1 closes, and SERCA, its function initiated when Ca entered the cytosol, is able to return Ca back to the SR against the Ca concentration gradient (dashed arrow). Consequently, TnC no longer binds Ca, and the troponin-tropomyosin complex returns to its resting state where tropomyosin covers the myosin binding sites on actin. 0) With Ca return to the SR, the entire region is ready for another contraction. ...81

Figure 5 Motor function declines rapidly in testosterone (T)-treated adult female transgenic (Tg) mice that express a wild-type androgen receptor (AR) transgene only in skeletal muscle fibers. Baseline performance at Day 0 before hormone treatment did not differ across treatment groups. T treatment induced a rapid decline in grip strength (A), hang time (B), and body weight (C) only in Tg females. By Day 5, motor performance on both tests was decreased significantly for T-treated Tg (T Tg) females compared to baseline or compared to the other groups, including asymptomatic females that were blank-treated wild-type (B WT), testosterone-treated wild-type (T WT), and blank-treated transgenic (B Tg). Each asymptomatic group maintained pre-treatment performance levels on both the grip strength and hang tests across the 5 days of treatment, indicating that only the combination of AR transgene expression in muscle fibers and male levels of androgens instigates motor dysfunction. Values are means \pm standard errors of means based on N = 5-6 mice/muscle and group. * $P \leq 0.05$, T Tg versus B Tg or T WT.84

Figure 6 Tetanic force produced by both EDL and SOL of motor-impaired female mice is reduced significantly compared to tetanic force produced by corresponding muscles of asymptomatic controls after 5 days of testosterone (T) treatment. Representative traces for T WT muscles and T-treated transgenic (T Tg) muscles are shown (A, B). Tetanic force produced by the EDL of T Tgs is about half of control females (C), whereas tetanic force produced by the SOL of T Tg females is about a quarter of T WT controls (D). Tetanic force produced by muscles of control-treated Tg females (B/Tg) is equivalent to that of WTs, indicating that AR transgene expression *per se* does not impair muscle strength. Comparable force deficits are observed at the beginning and end of experiments (indicated as first and last tetanus) for both EDL and SOL of T Tg mice, suggesting that force deficit is present *in vivo* and is not due to a more rapid deterioration of these muscles *in vitro*. Force (in Newtons-N) was normalized to muscle wet weight (grams-g). Values in histogram are means \pm standard errors of means, N = 5-6 mice/group. * $P < 0.001$, T Tg versus B Tg or T WT.85

Figure 7 Neither histopathology nor expression of the AR transgene explains the severe deficit in SOL force production of T-treated Tg mice. Cross sections of SOL muscle (scale bar = 500 μ m) from Tg females after 5 days of T treatment stained with H&E exhibit no signs of abnormal morphology (e.g. fiber atrophy/hypertrophy, centralized nuclei, A), nor alterations in fiber number (B) compared to the SOL from other treatment groups (N = 4-5 mice/group). Bars represent means \pm standard errors of means. AR immunoblot (C) shows AR expression levels in the EDL and SOL from asymptomatic (B Tg) versus symptomatic (T Tg) mice. We find no consistent differences in AR expression (~110 kD) between EDL and SOL muscles, indicating that a difference in AR protein content between the EDL and SOL is not likely to underlie the relatively greater force deficit in the SOL compared to the EDL in T-treated Tg mice. Actin

(~40 kD) loading control shows no consistent differences in protein loading between the EDL and SOL of Tg mice.86

Figure 8 Twitch kinetics are slowed only in the EDL of motor-impaired Tg mice after 5 days of T treatment. Representative twitches from the fast-twitch EDL and the slow-twitch SOL (A, B) reveal decreased peak twitch force for both muscles of T-treated Tg mice (see Table 1 for mean values) but altered twitch kinetics only for the EDL. Quantitative analysis of individual twitches (C – F) confirms a significant prolongation in the time it takes to reach peak twitch force (C) and to relax (E) in EDL, but neither parameter is significantly altered by T in the SOL muscle of Tg mice (D, F). Plotted values are means \pm standard errors of means, with N = 5-6 mice/group. * $P < 0.001$ T Tg versus B Tg or T WT.87

Figure 9 The SOL but not the EDL of motor-impaired mice shows the same deficit in peak tetanic force after 3 days of T treatment. Tetanic force in the slow-twitch SOL from T Tg mice was significantly decreased after 3 days of T treatment (A), comparable to the magnitude of the effect of 5 days of treatment (Fig 6). A subtle, but not significant difference was seen in EDL from the same motor-impaired mice (T Tg versus T WT mice, $p = 0.07$). However, peak twitch force in both muscles was significantly reduced in T Tg mice compared to T WT mice (B). Twitch kinetics were largely unaffected in T-treated Tg mice after 3 days of treatment (C, D) except that relaxation time was slowed significantly in EDL, consonant with the effect of T on this parameter after 5 days of treatment (Fig 8). N = 5-7/group. * $P < 0.05$88

Figure 10 The EDL but not the SOL from motor-impaired Tg mice showed compromised resistance to fatigue after 5, but not 3, days of T treatment. Fatigue resistance was measured as time in seconds from onset of tetanizing stimulation to when the muscles decreased in force by 50% of maximal tetanic force. The EDL from Tg mice after 5 days of T treatment fatigued significantly faster, dropping to half maximal force several seconds sooner than the EDL from either T-treated WT or blank-treated Tg mice (A). Interestingly, the EDL from blank-treated Tg mice showed a *greater* resistance to fatigue than the EDL from blank-treated WT (B Tg versus B WT), indicating a beneficial effect of the transgene itself on resistance to fatigue in the EDL. Five days of T treatment had no effect on fatigue resistance in SOL (B), and there was no effect of T on fatigue resistance after 3 days of treatment in either muscle from Tg mice (C and D). 5-day EDL: N = 5-6 mice/group; 5-day SOL, N = 5-6 mice/group; 3-day EDL, N = 6 mice/group; 3-day SOL, N = 4-7 mice/group. * $P \leq 0.05$89

Figure 11 Transgenic (Tg) males in both the 97Q and 141 ‘myogenic’ models of SBMA show the expected impairment in motor function. Mean number of rearings in an open field, taken as an indirect measure of hindlimb strength, was decreased significantly in Tg males of both the 97Q (A) and myogenic 141 (D) models of SBMA compared to their respective WT controls. Similar significant deficits were also found in mean frontpaw grip strength (B, E) and hang times (C, F). These measures indicate that Tg males in both models show the expected

SBMA phenotype. * $p \leq 0.05$ compared to WT controls. Error bars represent standard error of the mean, with $n = 6-7$ mice/group.93

Figure 12 Both the fast twitch extensor digitorum longus (EDL) and slow twitch soleus (SOL) muscles from motor-impaired 97Q Tg males show deficits in contractile force. Raw twitch and tetanic force (A,D, and G) were significantly reduced, with the one exception that raw tetanic force was unaffected in the SOL (J). However, twitch and tetanic forces once normalized to muscle mass were significantly decreased in both muscles, including tetanic force produced by the SOL (B, E, H, and K), indicating primary defects in contractile function of muscles of diseased 97Q Tg males that are independent of their mass. The force deficit is also readily apparent in examples of individual traces of EDL (C) and SOL (I) twitches. Although somewhat reduced, the twitch/tetanus (Tw/Tet) ratio in the diseased EDL was not significantly different than WT (F). In contrast, the Tw/Tet ratio in the SOL of diseased males was significantly reduced (L), suggesting defects in calcium handling mechanisms. Such defects in muscle function may contribute to if not underlie defects in motor function. * $p \leq 0.05$ compared to WT controls. Error bars represent the standard error of the mean, with $n = 4-7$ mice/group.95

Figure 13 Both the EDL and SOL from motor-impaired 97Q Tg males fatigue more rapidly. The fatigue profile for both the EDL and SOL indicates that both muscles in Tg males produce less force per gram muscle at the start of stimulation (A, C) followed by a drop in force for all muscles indicating muscle fatigue during tetanizing stimulation. While the Tg EDL loses less of its original force than the WT EDL over the stimulation period (A), the Tg EDL appears to fatigue faster, losing 50% of its original force (time to half of maximal force loss) significantly sooner than WT EDL (B). The Tg SOL also appears to have a faster time course of fatigue than WT SOL, losing 50% of its original force significantly sooner than WT SOL (D). * $p \leq 0.05$ compared to WT controls. Plotted values are means \pm standard error of the mean, with $n = 4-7$ mice/group.97

Figure 14 Both the fast twitch EDL and slow twitch SOL muscles from motor-impaired myogenic (141) Tg males show deficits in contractile force. Raw and normalized twitch and tetanic force were significantly reduced in both the EDL and SOL of motor-impaired males (A, B, D, G, H, J and K) with the exception of normalized tetanic force in Tg EDL (E). On the other hand, the deficit in raw tetanic force in the EDL probably is due to the deficit in fiber number in this muscle (Table 4). Samples of twitch traces reveal such deficits in twitch force (C, I). The Tw/Tet ratio is also significantly reduced in both the Tg EDL (F) and SOL (L), also suggesting that that calcium mobilization from intracellular stores may be perturbed. Muscles of myogenic 141 males show similar defects in contractile properties as 97Q males, although disease affects force most in the SOL of 141 males while affecting most the EDL in 97Q males. Nonetheless, these results suggest that motor dysfunction likely involves primary defects in muscle function. * $p \leq 0.05$ compared to WT controls. Error bars represent the standard error of the mean, with $n = 4-7$ mice/group.98

Figure 15 Only the SOL from motor-impaired 141 Tg males fatigues more rapidly. The fatigue profile indicates that the Tg EDL shows increased resistance to fatigue, losing less total force than WT EDL overall (A). However, both Tg and WT EDL appeared to fatigue at about the same rate, reaching a 50% drop at about the same time (B). The apparent increase in oxidative metabolism in the diseased EDL (Johansen et al., 2011; Monks et al., 2007) may help stave off some of the later losses in force exhibited by WT EDL. The SOL of diseased 141 Tg males on the other hand fatigues rapidly, losing 50% of its starting force in less than 9.8 ± 0.9 s compared to 42.1 ± 2.4 s in WT SOL. The marked increase in fatigue susceptibility of the SOL muscle in 141 Tg males also likely contributes to motor dysfunction in this model. $*p \leq 0.05$ compared to WT controls. Plotted values are means \pm standard error of the mean, with $n = 4-6$ mice/group.100

Figure 16 Muscles from diseased and healthy mice remain stable *in vitro* during the course of the experiment. Viability of each skeletal muscle was monitored with tetanus stimulations throughout an experiment. Force produced by tetani at the beginning of the experiment (open bar) was comparable to force produced at the end (filled bar). These data suggest that the force deficits found *in vitro* in diseased muscles likely reflect a genuine force deficit *in vivo*, rather than a defect that emerges *in vitro*. *In vitro* measurements were taken during a 2-3 hour window. Plotted values are mean \pm standard error of the mean.101

Figure 17 Representative photomicrographs of cross sections of muscle used for fiber counts. The EDL from the myogenic model was previously characterized (Johansen et al., 2011) and therefore not included. EDL muscle fibers in diseased 97Q Tg males are markedly heterogeneous in size, with some fibers notably smaller than the rest (arrow). EDL fibers from 97Q males also contain centralized nuclei (arrow). Since mass of the EDL from diseased 97Q males is reduced by half (Table 2) without loss of fibers (Table 4), it is likely that atrophy of individual fibers underlies the deficit in EDL mass. Note however that decreases in muscle mass contribute little to the deficits in twitch and tetanic force (Fig 2A, B, D and E) since a large proportion of the deficit persists once force measures are normalized to muscle mass. No major histological changes were observed in cross section of SOL from either 97Q males (middle panels) or myogenic (141) males (bottom panels) except for centralized nuclei which were more frequent in the SOL of 141 Tg males compared to WT SOL. Despite the lack of striking histopathology, SOL function is impaired in both models, but particularly in the 141 myogenic males, which show a three-fold loss of normalized force (Fig 14H, K). These data indicate that impairments in muscle function need not be accompanied by marked histopathology. Scale bar = 50 μ m.102

Figure 18 KI males with mild motor deficits show negligible deficits in muscle function. Measurements of forepaw grip strength and hang times are significantly decreased in KI males relative to WT controls (A, B), showing the expected impaired motor function in KI males. While force measures in the KI EDL suggest small deficits in twitch and tetanic force consistent with the mild motor phenotype in this model, these apparent deficits are not significant (C – H). Likewise, we found no significant deficits in twitch and tetanic forces produced by the SOL from

KI males (I - N). These data raise the possibility that motor deficits in KI males may reflect synaptic defects upstream to the skeletal muscles. * $p \leq 0.05$ compared to WT controls. Plotted values are mean \pm standard error of the mean, with n = 5-7 mice/group.103

LIST OF ABBREVIATIONS

ACh – acetylcholine

AChR – acetylcholine receptor

ALS – amyotrophic lateral sclerosis

AR – androgen receptor

B – blank

Ca – calcium

CK – creatine kinase

DHPR – dihydropyridine receptor

DM – myotonic dystrophy

DMD – Duchenne's muscular dystrophy

EDL – extensor digitorum longus

EMG – electromyography

GDNF – glial cell line-derived neurotrophic factor

H&E – hematoxylin and eosin

HSA – human skeletal α -actin

IGF-1 – insulin-like growth factor 1

KI – knock-in

N – newtons

PV – parvalbumin

RyR1 – ryanodine receptor

SBMA – spinal and bulbar muscular atrophy

SERCA – sarcoendoplasmic reticulum ATPase

SMA – spinal muscular atrophy

SMN – survival motor neuron

SOD1 – superoxide dismutase 1

SOL – soleus

SR – sarcoplasmic reticulum

T – testosterone

Tg – transgenic

TnC – troponin C

TnI – troponin I

TnT – troponin T

VEGF – vascular endothelial growth factor

WT – wild type

INTRODUCTION

The overall aim of the thesis is to determine whether skeletal muscle dysfunction has a role in the onset and/or progression of motor deficits in a neuromuscular disease known as spinal and bulbar muscular atrophy (SBMA). All experiments were conducted using mice as the model organism. This chapter briefly introduces motor function as a result of motor unit activity. It then presents how alterations to elements of the motor unit result in motor dysfunction, with a particular emphasis on SBMA, a male-specific motoneuron disease. It will discuss how skeletal muscle dysfunction might contribute to the symptoms of this disease based on case studies in humans and animal models of SBMA. Finally, a description of the mechanisms involved in skeletal muscle function is given to help readers understand the measurements that were used to assess muscle function in my studies.

Motor Function

Motor function is critical for survival in vertebrates and most invertebrates. Muscle contractions initiated by excitation-contraction coupling, i.e. when a presynaptic electrical stimulus is converted to a postsynaptic mechanical response (Sandow, 1952), generates the necessary *in vivo* force to perform locomotion and many other functions. Basic motor function in animals is generated by the motor unit, comprised of an α -motoneuron and the muscle fibers that it innervates. When a single motoneuron is excited above threshold, all the muscle fibers it innervates are stimulated to contract. This stimulus response follows an “all or none” pattern of activation where any stimulus below threshold will not induce a response, and any stimulus at or above threshold results in a complete response by the motor unit (Sherrington, 1929).

Different unit types are classified according to differences in size (i.e., the number of target muscle fibers a motoneuron innervates). Motor units and α -motoneurons vary in size where smaller motoneurons innervate fewer muscle fibers, and larger motoneurons innervate more muscle fibers. Smaller motoneurons and motor units are more easily recruited to contract and perform small tasks. As the need for greater muscle force arises, the larger motor units are recruited to accommodate the task. This phenomenon occurs as the smaller motoneurons have higher input resistance, resulting in a large change in potential with smaller input (rheobase) currents and a greater probability of being activated. Conversely, larger motoneurons have greater surface area and lower input resistance requiring larger rheobase currents to induce changes in potential, resulting in a lower probability of being activated. This model for motor unit recruitment has been called Henneman's size principle (Clamann and Henneman, 1976; Henneman, 1957; Henneman and Olson, 1965). Once motor units have been recruited, larger units with larger axons tend to have faster conduction velocities due to decreased resistance within the axon, and smaller motor units with smaller axons have slower conduction velocities due to increased resistance within an axon (Bawa et al., 1984). Order of motor unit recruitment based on size can also predict the metabolic properties of the skeletal muscles they innervate as being fast-twitch or slow-twitch (Zengel et al., 1985). Smaller motoneurons tend to innervate muscles that have higher fatigue resistance and can be tonically activated due to the greater levels of mitochondria and vascularization and the dependence on aerobic mechanisms in these muscles. Conversely, larger skeletal muscles innervated by larger motor units produce more force, but fatigue more easily and are only activated for shorter periods due to lower levels of mitochondria and vascularization but being dependent on anaerobic mechanisms (Burke et al., 1973; Henneman and Olson, 1965; Hennig and Lomo, 1985).

Proper motor function allows the execution for vital functions such as movement and respiration. However, dysfunction in α -motoneurons, junctions, or skeletal muscles can result in difficulties with vital functions, and such cases of motor dysfunctions, termed neuromuscular diseases, can be fatal.

Neuromuscular Diseases

Neuromuscular diseases are a group of conditions that affect the ability of an organism to move or coordinate movements. Although other diseases like Parkinson's and Huntington's diseases also exhibit a motor component, their underlying symptoms originate in brain regions, and the current review specifically focuses on diseases originating in the motor unit components. Neuromuscular diseases are characterized by motor performance deficits and are separated based on where the agents of disease are presumed to act. Neuromuscular diseases include myopathies (e.g. muscular dystrophies, mitochondrial myopathies), diseases directly affecting the junction (e.g. Lambert-Eaton myasthenic syndrome, myasthenia gravis), and diseases in which pathogenesis is presumed to originate in the motoneurons (e.g. amyotrophic lateral sclerosis – ALS, spinal muscular atrophy – SMA). Depending on the condition, symptoms may be apparent anywhere from infancy (seen in some cases of SMA) to the middle-later stages of life (seen in cases of ALS). The discussion will focus on two primary myopathies, Duchenne muscular dystrophy and myotonic dystrophy, and two motoneuron diseases, ALS and SMA.

Myopathies are conditions for which the agents of disease originate in skeletal muscles. They can be categorized based on how they present in patients and are divided as primary or acquired myopathies. Primary myopathies typically have an underlying genetic cause, whereas acquired myopathies result from an insult to the body, such as inflammation. The focus will be

on primary myopathies and their etiology. The most common myopathies are muscular dystrophies, conditions marked by progressive skeletal muscle degeneration and regeneration that result in weakness. Duchenne's muscular dystrophy (DMD) is the most frequently occurring dystrophy with an occurrence of 1 in every 3300 live births (Deconinck and Dan, 2007). DMD occurs due to a mutation in the *DMD* gene on the X chromosome (Lindenbaum et al., 1979). The gene codes for dystrophin, a structural protein found in the sarcolemma of skeletal muscles (Hoffman et al., 1987; Koenig et al., 1988; Zubrzycka-Gaarn et al., 1988). Males and females can carry the gene, but females rarely exhibit disease symptoms due to the X-linked recessive pattern of inheritance (Morton and Chung, 1959). Although the precise function of dystrophin is unknown, it is thought to stabilize the sarcolemma against the force imposed by muscle activity. In affected individuals, the absence of dystrophin removes the anchor between muscle cytoskeleton and the extracellular matrix, disrupting the costameric lattice (Ervasti and Campbell, 1993). This leads to muscle membrane fragility usually confirmed using orange Procion or Evans Blue (Matsuda et al., 1995), which enter only muscle fibers that lack intact plasma membranes. It is postulated that in DMD, multiple pathophysiological processes are activated due to the membrane fragility, and this may alter intracellular calcium (Ca) handling as increased Ca content has been recorded in skeletal muscle fibers from DMD individuals (Bertorini et al., 1982; Emery and Burt, 1980). Symptoms present in DMD patients between 3 and 5 years of age and are characterized by a delayed onset in walking, toe walking, or waddling. Serum creatine kinase is elevated 50-100 times normal levels in patients, indicative of damaged fibers (McMillan et al., 2011). Fatty replacement and fibrosis (pseudohypertrophy) manifest in calf muscles (Schreiber et al., 1987). Generally, loss of ambulation occurs between 7 and 12 years of age and death by the second decade (Eagle et al., 2002).

Another primary myopathy is myotonic dystrophy, the most common form of muscular dystrophy in adults with a minimum incidence of 1 in 8000. Myotonic dystrophy is classified into two types (DM1 and DM2), and both conditions have an autosomal-dominant inheritance pattern (Harper, 1989). DM1 (also referred to as Steinert's Disease in the literature) is the more common form of myotonic dystrophy that results from an expansion of the codon CTG in the untranslated 3' region of the myotonic dystrophy protein kinase (*DMPK*) gene (Harley et al., 1992). The CTG expansion in DM1 individuals ranges from 50 to >1000 repeats, and individuals screened for the disease are classified into three subcategories based on the number of repeats. DM1 patients are also classified on a spectrum based on symptoms and time of onset during the lifetime: congenital, childhood, adult, and late adult (Harper and Dyken, 1972). The variable age of onset is seen not just across affected families but also within a family and is correlated with the number of CTG repeats. Analysis of genetic markers also reveals that the repeat expansion can increase in size in successive generations, starting with a mild phenotype in early generations but resulting in a more severe and earlier onset of the disease in the later generations due to the lengthened expansion (Brook et al., 1992). Patients generally exhibit muscle weakness, and similar to DMD, have elevated levels of serum creatine kinase in the blood (Heatwole et al., 2006). Electromyographic recordings indicate delayed muscle relaxation and hyperexcitability in myofibers, and spontaneous activity resulting in myotonia (Romeo, 2012). The underlying mechanism for the abnormal muscle activity is thought to be aberrant splicing of a chloride (Cl) channel (*ClC1*) due to the CTG expansion. This leads to decreased Cl channel expression in the muscle membrane, decreased Cl conductance, and increased input resistance. Thus, muscles respond to a lower stimulus intensity, resulting in hyperexcitability and myotonia (Mankodi et al., 2002). Associated histopathology in human muscle biopsies

include centralized nuclei within muscle fibers, generally atrophic slow-twitch (type I) muscle fibers, and muscle fibers with ring-shaped myofibrils (Heidenhain, 1918 reviewed in (Romeo, 2012)).

Neuromuscular diseases also include conditions where motor function is characterized by motoneuron dysfunction and degeneration, such as ALS and SMA. Unlike primary myopathies, these conditions are classified as motoneuron diseases with muscle dysfunction and atrophy presumed to be secondary to the defects in motoneurons. ALS is a neurodegenerative disease marked by loss of motor coordination, muscle atrophy, and degeneration of upper and lower motoneurons. Symptoms include difficulties with movement, speech, and breathing that worsens progressively until the terminal stage. Onset generally peaks around the sixth decade of life, and life expectancy of a patient after diagnosis is generally 2-5 years though it varies from case to case (Gubbay et al., 1985; Haverkamp et al., 1995; Ringel et al., 1993). The first identified causative gene for ALS is a mutation in the superoxide dismutase 1 (SOD1) gene (Rosen et al., 1993). Cases with an underlying genetic defect are termed “familial” and account for roughly 2% of all ALS cases. Since the discovery of the mutant allele, much of the research on ALS has relied on mouse models expressing a mutated SOD1 allele, which codes for a metalloenzyme that protects cells from oxidative stress by catalyzing the dismutation of toxic superoxide to oxygen and hydrogen peroxide (McCord et al., 1971). Although the specific mutation in the SOD1 gene differs across models, the ALS mouse models generally exhibit a similar and predictable pattern of disease. Mice in these models generally exhibit paralysis in one or more limbs starting at around 3-6 months of age, lose body mass, eventually exhibit total immobility, and die shortly afterwards. Spinal cords from affected mice indicate motoneuron pathology or

loss resulting may underlie this phenotype (Bruijn et al., 1997; Gurney et al., 1994; Ripps et al., 1995; Wong et al., 1995).

SMA is a neuromuscular condition characterized by α -motoneuron degeneration in the spinal cord, resulting in proximal muscle weakness and paralysis. It is estimated to occur for 1 in every 6,000-10,000 live births (D'Amico et al., 2011). SMA is classified by 1) the underlying genetics and pattern of inheritance and 2) the age of onset and phenotype progression and severity. The causative gene was found to be the survival motor neuron (*SMN*) gene (Lefebvre et al., 1995) and is present in multiple copies in the genome (Burglen et al., 1996). Type 0 is designated for prenatally diagnosed individuals who rarely survive beyond 6 months of age. Type I is designated where age of onset is between 0-6 months of age. Type I patients are never able to sit unsupported and generally do not live beyond 2 years of age. Type II patients are able to sit unsupported but are never able to walk. These individuals generally experience proximal weakness in the legs more than the arms and generally live into their 30's but have shortened life expectancies. Type III patients are able to walk but experience weakness later in life and may require a wheelchair. In spite of the symptoms, individuals with type III SMA generally have a normal life expectancy (Dubowitz, 1995; Markowitz et al., 2012). The severity and spectrum of SMA result from the nature of *SMN1* deletion. SMA type I is generally caused by a homozygous deletion of the *SMN1* allele, whereas SMA types II and III result mostly from conversion of *SMN1* to *SMN2* (Campbell et al., 1997). Type II is due to a conversion event at one allele and a hemizygous deletion in the other allele while type III can be due to homozygous conversion of *SMN1* to *SMN2* (Hahnen et al., 1996; van der Steege et al., 1996). Sometimes referred to as X-linked SMA, spinal and bulbar muscular atrophy (SBMA) is a condition in which recent

evidence suggests that motor dysfunction may originate in the skeletal muscles. Thus, the dividing line between primary myopathies and motoneuron diseases is becoming blurred.

Spinal and Bulbar Muscular Atrophy

Spinal and bulbar muscular atrophy (SBMA) is a so-called polyglutamine as well as a motoneuron disease for which proper motor coordination is disrupted. SBMA is also known as Kennedy Disease for the researcher who characterized the disease (Kennedy et al., 1968). Unlike other forms of SMA, a mutation in the androgen receptor on the X-chromosome has been linked to SBMA. The mutated gene is passed on in an X-linked inheritance pattern where affected males have the mutation expressed in all somatic cells. In females, if the mutation is on one X chromosome, the mutation is expressed in roughly half of all somatic cells due to random X inactivation (Lyon, 1961, 1962). The mutation, itself, is due to an expansion of three nucleotides, similar to what is observed in myotonic dystrophy. A region of CAG codons, which code for glutamine in the N-terminus of AR, is expanded in SBMA (La Spada et al., 1991). All individuals have this expanded CAG region. However, whereas unaffected males have 10-37 repetitions, individuals affected by SBMA have 40-85 repeats. Thus, in addition to being classed as a type of SMA, the underlying genetic mutation has led to SBMA being classified as a polyglutamine disease, a group of neurodegenerative conditions which include Huntington's disease, dentatorubropallidoluysian atrophy, and spinocerebellar ataxia types 1, 2, 3, 6, 7, and 17 (Ross, 2002). Although all the conditions are progressively neurodegenerative and grouped together, the symptoms and localization of neurodegeneration differ across conditions. SBMA is unique among polyglutamine disorders because the function of the affected protein is well characterized (Fischbeck et al., 1999).

Although males and females can express the disease allele, SBMA is a male-specific disorder where affected individuals generally show symptoms sometime between their third to fifth decades of life (Rhodes et al., 2009). Recent evidence suggests that the reason only males are affected is because SBMA symptoms depend on male levels of androgen (specifically testosterone – T) rather than random X inactivation. T administration to an SBMA sufferer resulted in motor performance decline. Subsequent cessation of T administration allowed motor function to return to baseline (Kinirons and Rouleau, 2008). Additionally, females (one with two mutated X chromosomes) are unaffected or exhibit only minor symptoms, presumably because of a lack of testosterone (Schmidt et al., 2002).

AR is a ligand-activated transcription factor. Androgen receptors bind their ligand (testosterone or the metabolite dihydrotestosterone) to exert their effects, and the ligand-receptor binding results in receptor dimerization and translocation from the cytoplasm into the nucleus (Wong et al., 1993). Once ligand-receptor complexes are formed, co-activators are recruited to aid in binding DNA and increase protein translation (MacLean et al., 1997). Although testosterone normally promotes growth of skeletal muscles, the AR mutation linked to SBMA leads to dysfunctional AR signaling when bound to T and results in loss of motor function in men with SBMA. In addition to motor deficits, which are thought to arise through a gain of new and toxic functions of the mutant AR, individuals with SBMA also show a partial loss of normal AR signaling. Signs of partial androgen-insensitivity include gynecomastia (development of male breasts) and reduced virility of patients with decreased sperm count and testicular atrophy (Arbizu et al., 1983). Of note, XY individuals with a total loss of AR function because of a different mutation in the *AR* gene are feminized but report no difficulties with motor function,

arguing that a loss of normal AR function plays little to no role in the motor dysfunction caused by SBMA.

Deficits in motor coordination are seen in patients as they have limb muscle weakness, difficulties climbing stairs, and may require a cane or a walker for mobility. Tests have concluded there are delays in motor conduction velocities to limb muscles in SBMA patients compared to control patients (Suzuki et al., 2008). Results from postmortem analyses show that SBMA causes a loss of spinal motoneurons (Kennedy et al., 1968; Sobue et al., 1989). In addition, muscles are also clearly affected in SBMA but whether the effects of muscle are via a loss of innervations (neurogenic) or are due to the action of a mutant AR directly in muscle is not clear. Electromyographies (EMGs) have revealed fasciculations (Kennedy et al., 1968), and biopsies have revealed muscle atrophy, pathology typically attributed to a neurogenic origin but also split myofibers which is typically attributed to a myogenic origin, in patients suffering from SBMA (Arbizu et al., 1983). Additionally, consistently finding elevated creatine kinase levels in SBMA patients implicates primary myopathic mechanisms in SBMA (Chahin and Sorenson, 2009). Thus, the question of whether primary muscle involvement in SBMA should be assessed in considering the etiology of SBMA and potential targets for therapy.

In addition to the clinical data, *Drosophila* and murine models have also been crucial to better understanding the neurodegenerative properties of SBMA. *Drosophila* research has examined the survival of photoreceptor neurons when mutant AR is expressed in the eye. Results from one study indicate that receptors with expanded CAG regions but confined to the cytosol do not induce degeneration of photoreceptor neurons. However, a chimeric protein fused to the nuclear localization signal of AR was enough to induce neuron degeneration in the eyes, indicating that translocation of the AR to the nucleus regulates the androgen dependence of

SBMA (Takeyama et al., 2002). Additionally, the SBMA phenotype requires a functional AF-2. AF-2 is a region on AR activated by ligand binding and recruits co-activators in order to initiate androgen signaling (Nedelsky et al., 2010). This suggests some of the native functions of WT AR are still present during SBMA onset and/or progression. Thus, *Drosophila* research has advanced our understanding of the mechanisms associated with AR toxicity to cause neuronal death. Murine models have also added to our understanding of SBMA. Five mouse models of SBMA have been engineered by broadly expressing AR containing the CAG repeat expansions (Chevalier-Larsen et al., 2004; Katsuno et al., 2002; McManamny et al., 2002; Sopher et al., 2004; Yu et al., 2006). Three of the five models (named the 112Q, 97Q, and KI models) have been confirmed to recapitulate the androgen-dependence of the disease observed in humans (Chevalier-Larsen et al., 2004; Katsuno et al., 2002; Monks et al., 2008; Yu et al., 2006). Males are symptomatic, and motor conditions can improve with castration. Conversely, females are asymptomatic until treated with T. More recently, another mouse model was engineered where transgenic (Tg) mice overexpress wild type rat androgen receptors (WT AR) specifically in skeletal muscles. Contrary to expectations, Tg mice exhibit androgen-dependent motor dysfunction similar to what is seen in the other five models; T treatment in females induces disease, and castration ameliorates disease in males (Monks et al., 2007). As the altered genetic expression is confined to the skeletal muscle fibers, data from this model suggest skeletal muscles may be affected primarily, with the disease then spreading to the motoneurons secondarily. Motoneuron function has been shown to be compromised in retrograde axonal trafficking studies in this novel SBMA model (Kemp et al., 2011).

Experiments to determine disease origin

While previous results have suggested the importance of skeletal muscle in SBMA (Monks et al., 2007; Palazzolo et al., 2009), whether motoneuron diseases have a myogenic origin is an area of active research in other conditions, such as ALS and SMA. Thus, while findings relevant to skeletal muscle (dys)function during SBMA will be useful in better characterizing SBMA specifically, that research may also serve to inform mechanisms involved in other so called motoneuron diseases such as ALS and SMA. In several animal models of neurodegenerative diseases, the broad expression of genetic mutations does not allow determination of specific pre- or postsynaptic site(s) of action for disease onset and progression. The lack of a confirmed site of action has led to studies trying to determine the exact origin of the disease by selectively expressing or suppressing the disease-causing genes in either motoneurons or skeletal muscles (Cifuentes-Diaz et al., 2001; Dobrowolny et al., 2005; Johansen et al., 2011; Kieran et al., 2005; Monks et al., 2007; Palazzolo et al., 2009; Perlson et al., 2009; Wong and Martin, 2010; Yu et al., 2006).

A feature reported in one SBMA mouse model is the loss of motoneurons and nuclear inclusions in some of the motoneuron soma (Thomas et al., 2006). However, other data from another model suggest nuclear inclusions and neuronal dysfunction can occur in the absence of cell death (Adachi et al., 2001). This is also seen in ALS models where overexpressing mutant SOD1 specifically in motoneurons does not result in motoneuron pathology or an ALS phenotype (Lino et al., 2002). Moreover, another study using an ALS model where uncoupling protein 1 was specifically overexpressed in skeletal muscles has suggested distal defects in the neuromuscular junction may be caused by early pathology of the skeletal muscle, leading to dysfunction in the motoneuron (Dupuis et al., 2009). Thus, early myogenic factors could contribute to the later disease effects in motoneurons in conditions often thought to be due to a

primary effect directly on motoneurons. One possibility is the loss of neurotrophic factors in muscles that retrogradely promote the viability and function of motoneurons.

Typically, muscle function has been assessed by one of two ways: 1) stimulating the nerve and measuring force production in skeletal muscles, or 2) isolating and field-stimulating skeletal muscles directly with electrodes to induce contractions. While most labs have utilized indirect muscle stimulation via the nerve to trigger muscle contractions in ALS models and SBMA patients (Hegedus et al., 2008; Kieran et al., 2005; Suzuki et al., 2008), this approach does not allow one to determine whether muscle weakness is due defects intrinsic to the muscle or due to defects upstream of the muscle. Thus, the approach I took was to examine muscle function directly in isolation from the nervous system (the latter of the two methods previously mentioned). To better understand skeletal muscle measurements, a description of skeletal muscle architecture and function is necessary.

Anatomy and Physiology of Skeletal Muscle

Skeletal muscles are large organs that comprise about 40% of total body mass in humans. They are organized in descending orders of complexity as a single skeletal muscle is divided into fascicles, bundles within a muscle that contain myocytes or myofibers surrounded by a connective tissue layer known as fascia. The myofibers in fascicles are large multinucleated cells that are the primary components of muscles (Figure 1). Myofibers come in a diverse array of types and several fiber types are usually found within one muscle. Fiber type composition of a muscle determines its contractile speed and the amount of force that it can produce. Myofibers are comprised of myofibrils, which contain repeat structures in series known as sarcomeres, which form the basic contractile unit within a single fiber. Inside the sarcomere are

myofilaments and the organelles necessary for contraction, such as the sarcoplasmic reticulum (SR), T-tubules and mitochondria (Figure 2). The myofilaments are comprised of thick filaments (myosin) and thin filaments (actin) (Figure 3). Actin contains the binding site where myosin heads attach and initiate skeletal muscle contractions. Additionally, troponins are located near the actin filament. Troponin is comprised of troponin C (TnC), troponin I (TnI), and troponin T (TnT) which play regulatory roles in muscle contraction (Szent-Gyorgyi, 2004).

Voluntary *in vivo* contractions are initiated at the motor endplate, where a presynaptic signal is transmitted to the muscle via release of acetylcholine (ACh) from the nerve terminal. Upon binding to its receptors (AChR) postsynaptically, sodium rushes into the muscle to induce a depolarization via the T-tubule. When skeletal muscles are isolated, electrode(s) replace the input from the nervous system and the voltage change in the electrode(s) induce(s) a depolarization within the muscle. T-tubules are invaginations of the sarcolemma that surround myofibrils and are in close contact with the SR. The regions where T-tubules contact the SR are called the terminal cisternae, and the association of the T-tubule to two terminal cisternae form a triad (Figure 3; reviewed in (Al-Qusairi and Laporte, 2011)). Within a skeletal muscle fiber, there are thousands of triads, and this arrangement enables myocytes to overcome the spatial limits of using calcium (Ca) as a second messenger. T-tubules conduct the electrical depolarization to initiate conformational changes in the dihydropyridine receptor (DHPR), a voltage-gated Ca channel. The DHPR is mechanically coupled to the skeletal muscle ryanodine receptor (RyR1), which opens and releases Ca from the sarcoplasmic reticulum (SR) (Figure 4-1). It is this change in intracellular Ca concentration that critically mediates muscle contraction. Upon its release from the SR, Ca binds to TnC, the Ca-sensitive subunit of the troponin complex. TnC binding Ca induces a conformational change in the troponin complex which removes

troponin I, the inhibitory subunit of the troponin complexes, from the actin filament (Figure 4-2; (Ebashi and Endo, 1968)). As TnI moves away from the actin binding sites, tropomyosin is pulled away, allowing myosin heads to bind to actin filaments with TnT linking the other troponins to tropomyosin (Figure 4-3).

Once the myosin heads bind to the binding sites on actin, ATP is hydrolyzed, resulting in ADP and inorganic phosphate. Phosphate is released, turning the myosin head (Figure 4-4). With the release of ADP, the myosin head is turned even further, moving the actin filament, shortening the sarcomere, and resulting in a power stroke to initiate skeletal muscle contraction (Figure 4-5; (Eisenberg and Hill, 1985)). This results in shortening in the sarcomeres and produces the contractile force generated by muscles (Huxley and Niedergerke, 1954). As long as Ca ions and ATP are available, another ATP will bind to the myosin head to release it from the actin filament and return the myosin head to its original position for another power stroke to occur, and the cycle can repeat (Figure 4-6&7). In cases where ATP is depleted, the myosin head remains in the locked position on the actin filament (Figure 4-5). Once the membrane potential returns to resting potential, the DHPR-RyR1 complex closes, and sarcoendoplasmic reticulum ATPases (SERCAs) actively return Ca ions to the SR (Figure 4-8). Consequently, TnC no longer binds Ca, and the troponin-tropomyosin complex returns to its resting state where tropomyosin covers the myosin binding sites on actin (Figure 4-0).

Force output of the skeletal muscle can vary based on fiber properties of skeletal muscles: I, IIA, IIB, IIX, and hybrids (Pette and Staron, 2000). Skeletal muscles containing primarily type IIB/X fast fatigable glycolytic fibers generate higher levels of force over a faster time course. The fast-twitch muscles fatigue over a relatively short time course due to low vascularization and mitochondrial content. In contrast, skeletal muscles with primarily types IIA fast fatigue-

resistant or I slow fatigue-resistant fibers generate lower levels of force over a slower time course. Slow-twitch muscles also fatigue over a relatively long time course due to greater vascularization and mitochondria content (Burke et al., 1971). In addition to differences in force production and fatigability, fast-twitch and slow-twitch muscles exhibit different kinetic properties. Fast-twitch muscles, so named due to the relatively shorter amount of time to contract, have faster acting ryanodine receptors (RYR1) and sarcoendoplasmic reticulum ATPases (SERCA) to release and restore Ca ions from/to the SR, respectively. Additionally, in smaller mammals, fast-twitch muscles contain a Ca-buffering protein, parvalbumin (PV), which shortens the contraction duration (Heizmann et al., 1982). In contrast, slow-twitch muscles have longer contraction times due to slower RYR1 and SERCA subtypes and lack PV (Brandl et al., 1987; Heizmann et al., 1982; Imagawa et al., 1989). Defects in the function of one or more such proteins in skeletal muscles could lead to dysfunction, often observed as motor weakness, without changes in kinetics of muscle contraction.

Overview

Like SBMA in humans, several of the animal models show a male-specific phenotype that depends on male levels of androgens. Male mice present a phenotype, and symptoms can be ameliorated by castration (Chevalier-Larsen et al., 2004; Katsuno et al., 2002). In some models, T can also be given to female Tg mice, and disease can be rapidly induced (Katsuno et al., 2002). Thus, females of SBMA models are critical to understanding the early symptoms and pathology of the disease, whereas males are useful in understanding pathology and weaknesses due to a chronic disease phenotype. For this reason, females and males were tested, and these experiments form the two research chapters to the thesis. Originally, it was uncertain if muscle

weakness would be measured in SBMA mice, and only female mice overexpressing a WT AR transgene only in skeletal muscle fibers were tested and forms the first chapter of the thesis. Once muscle weakness was confirmed in these females, males from the same model were also tested. However, as the expectation of observing muscle weakness was confirmed, the scope of the study was expanded to also include males from two other SBMA models. The so-called “97Q” model is a Tg mouse model in which a full length AR transgene containing 97Qs is broadly expressed in mice. The KI model expresses a humanized AR gene in mice. Exon 1 of mouse AR gene was replaced with exon one of the human AR gene containing 113 CAG repeats. This mutant AR is expressed in all cells that normally express AR because its expression is being driven by native AR promoters. This study indicates that muscle weakness is also likely involved in the disease phenotype of male SBMA mice and forms the second chapter of the thesis.

**CHAPTER 1: Androgen receptors in muscle fibers induce rapid loss of force but not mass:
Implications for SBMA**

Oki, K., Wiseman, R.W., Breedlove, S.M., Jordan, C.L. (2013) “Androgen receptors in muscle fibers induce rapid loss of force but not mass: Implications for SBMA.” Muscle & Nerve **47**(6):823-34.

Abstract

Introduction: Testosterone (T) induces motor dysfunction in transgenic (Tg) mice that overexpress wild type androgen receptor (AR) in skeletal muscles. Since many genes implicated in motor neuron disease are expressed in skeletal muscle, mutant proteins may act in muscle to cause dysfunction in motor neuron disease. *Methods:* We examined contractile properties of the extensor digitorum longus (EDL) and soleus (SOL) muscles *in vitro* after 5 and 3 days of T treatment in motor-impaired Tg female mice. *Results:* Both muscles showed deficits in tetanic force after 5 days of T treatment, without losses in muscle mass, protein content, or fiber number. By 3 days of T treatment, only SOL showed a deficit in tetanic force comparable to that at 5 days of treatment. In both treatments, EDL showed slowed twitch kinetics, whereas SOL showed deficits in the twitch/tetanus ratio. *Conclusions:* These results suggest calcium handling mechanisms in muscle fibers are defective in motor-impaired mice.

Introduction

The long-held assumption that motor dysfunction caused by motoneuron disease is the direct result of motoneuron loss has been challenged recently (Dupuis et al., 2009; Gould et al., 2006). Furthermore, whether motor impairments associated with motoneuron disease are due to defects that originate in the motoneurons, muscles, or both has also come under scrutiny recently. Because genes linked to motoneuron disease are expressed widely, typically in both motoneurons and muscles, deficits in motor performance associated with motoneuron disease could arise from dysfunction in the motoneurons, skeletal muscles, or both. Recent data from muscle-specific mouse models of motoneuron disease suggest that skeletal muscle may indeed be a primary site of action for disease genes, and dysfunction in skeletal muscles may contribute,

if not underlie, motor dysfunction (Braun et al., 1995; Cifuentes-Diaz et al., 2001; Di Giorgio et al., 2007; Dupuis et al., 2009; Monks et al., 2007; Nagai et al., 2007; Wong and Martin, 2010).

The transgenic (Tg) model used here recapitulates a polyglutamine disease called spinal bulbar muscular atrophy (SBMA) (Monks et al., 2007), a late-onset motoneuron disease that affects only men and is linked to a CAG repeat mutation in the androgen receptor (*AR*) gene. While not interfering with masculine development and function, this CAG expansion mutation in *AR* causes men with SBMA to develop progressive loss of strength that greatly impairs their motor function (Fischbeck, 1997). This muscle-specific or “myogenic” Tg model was engineered by inserting a transgene into mice that overexpresses wild type (WT) rat androgen receptors (*AR*) selectively in skeletal muscle fibers using the human skeletal α actin promoter (Monks et al., 2007). Like SBMA in humans and other mouse models of this disease, motor dysfunction in such myogenic Tg mice is triggered by male levels of androgens and can be relieved by lowering circulating androgen levels (Banno et al., 2009; Chevalier-Larsen et al., 2004; Katsuno et al., 2002; Kinirons and Rouleau, 2008; Monks et al., 2007; Yang et al., 2007; Yu et al., 2006). While Tg females in this model also express the *AR* transgene at comparably high levels, they are asymptomatic throughout life. However, when provided with male-typical levels of testosterone, the motor function of Tg females deteriorates rapidly. Motor defects develop in only a few days, comparable to those seen in Tg males, including shortened stride length and deficits in grip strength (Johansen et al., 2009; Monks et al., 2007). Significantly, Tg male mice with a mutation in endogenous *AR*, which eliminates endogenous *AR* function, also show the *same* androgen-dependent loss of motor function (Johansen et al., 2011). This demonstrates that testosterone activates functional transgenic *AR* to impair motor function. While Tg males show several markers of motoneuron disease, including atrophic and angulated

muscle fibers and deficits in the number of axons in ventral roots, acutely diseased Tg females do not (Johansen et al., 2009; Monks et al., 2007). Thus, AR acting directly in muscles can produce profound deficits in motor function without the expected histopathology in muscle, and/or loss of motoneurons, a dissociation that is also evident in other mouse models of SBMA (Chevalier-Larsen et al., 2004; Katsuno et al., 2002; Yu et al., 2006).

To explore whether muscle dysfunction might underlie motor dysfunction in myogenic mice, we directly examined the contractile properties of muscles from diseased and healthy female mice. We chose to study females over males, because unlike Tg males, who are chronically impaired, the disease state can be “turned on” by exposure to androgens in Tg females. Thus, given that the time of disease onset is known, acutely-impaired Tg females offer the potential to distinguish proximal pathogenic mechanisms that underlie motor dysfunction from secondary effects of disease. Muscle mechanics of the fast-twitch extensor digitorum longus (EDL) and slow-twitch soleus (SOL) were examined *in vitro* from adult Tg females and age-matched WT controls following 5 and 3 days of testosterone treatment. We observed a rapid loss of intrinsic force in both the EDL and SOL that occurs independent of muscle mass in this model.

Methods

Animals and hormone treatment. Transgenic (Tg) mice were generated and genotyped using PCR as previously described (Monks et al., 2007). Tg animals from the 141 founding line express a WT rat AR cDNA under the control of the human skeletal α actin promoter. Tg females were mated to C57/B6J mice for several generations to produce progeny for this study. Water and food were provided *ad libitum*. All animal procedures were approved and performed in compliance with the Michigan State University Institutional Animal Care and Use Committee,

in accordance with the standards in the NIH Guide for the Care and Use of Laboratory Animals. Adult (90-120 days) Tg and age-matched wild type (WT) females were deeply anesthetized with isoflurane, and Silastic capsules (1.57 mm i.d. and 3.18 mm o.d., effective release length of 6 mm) containing either crystalline testosterone (T) (~0.15 mg per capsule) or nothing (blank) were implanted subcutaneously just caudal to the scapula, as previously described (Johansen et al., 2009). Incisions were closed with 9 mm surgical staples. All animals received the analgesic ketoprofen (5 mg/kg, sc) immediately following surgery. In the first experiment, mice were treated for 5 days before muscle function was examined. Treatment groups were as follows: blank-treated wild type (B WT), testosterone-treated wildtype (T WT), blank-treated transgenic (B Tg), and testosterone-treated transgenic (T Tg) with n=5–6 mice/group. Separate cohorts of mice were used to examine the EDL and the SOL after 5 days of treatment. In a second experiment, contractile properties of the EDL and SOL harvested from the same set of mice were examined after 3 days of T treatment, comparing muscles from T WT to T Tg mice, n=5-6 mice/group.

Motor function tests. Motor function was assessed using the grip strength and hang tests 1 hour before surgery to establish baseline performance (Day 0) and on each day following surgery (Days 1-3 or 1-5) until the time of sacrifice. Forelimb grip strength was assessed using a grip strength meter (Columbus Instruments) oriented in the horizontal plane (Chevalier-Larsen et al., 2004; Johansen et al., 2009; Yu et al., 2006). Mice were held by the tail and lowered to the apparatus, allowed to grasp the metal grid with their forelimbs only, and were pulled by the tail vertically at a 90° angle away from the grid until their grip was released. Force (g) applied to the bar at the moment of release was recorded as grip strength. Seven consecutive measurements

were done within a single 2-minute session for each subject with the lowest and highest grip values excluded, and the mean of the remaining 5 values recorded as the grip strength for that animal and session. The hang test was conducted by placing mice on a wire grid that was then turned upside-down 40 cm above a counter. Latency to fall (up to 120 seconds) from the wire grid was measured (Monks et al., 2007; Sopher et al., 2004).

In vitro studies to assess muscle mechanics. To determine whether impairments in skeletal muscle function might underlie motor dysfunction, muscle contractile characteristics of the EDL and SOL were examined *in vitro* in motor-impaired Tg females and controls after 3 or 5 days of hormone treatment. These hindlimb muscles were selected, because the EDL and SOL are prototypical fast and slow twitch muscles, respectively, with considerable background information available on their normal contractile properties (Crow and Kushmerick, 1982; Kushmerick et al., 1992). Moreover, we were interested in determining whether the toxic effects of an activated AR in this model system might depend on fiber type, as observed in other diseases (Atkin et al., 2005; Hegedus et al., 2008).

Mice were anesthetized deeply with a single intraperitoneal injection of sodium pentobarbital in saline solution (0.1 mg/g body weight, Abbott Laboratories, North Chicago, IL, USA). We chose sodium pentobarbital as opposed to ketamine/xylazine as our anesthetic, which has little to no residual effect on the contractile properties of muscles assessed *in vitro*, yielding estimates that best fit those reported in the literature (Lapointe and Cote, 1999). Once the muscles were exposed, 5-0 silk sutures were tied to the proximal and distal tendons *in situ*, and muscle resting length was recorded. Muscles were then excised by cutting above the suture knot on the proximal tendon and below the suture knot distally. Excised muscles were incubated in an 8 mL

organ bath containing oxygenated Ringer solution (117.1 mM NaCl, 4.6 mM KCl, 25.3 mM NaHCO₃, 2.5 mM CaCl₂, 1.2 mM MgSO₄, pH 7.4; equilibrated with 95% O₂/5% CO₂) (Dentel et al., 2005; Wiseman et al., 1996). The temperature of the bath was monitored continuously using a K-type thermocouple (Omega Engineering, Stamford, CT) adjacent to the muscle and maintained at 25±0.2° C by circulating water through a glass-jacketed organ bath (Radnoti Glass Technology, Monrovia, CA). Isolated muscles were fixed at their approximate resting length by tying 1 end of the muscle ligature to a glass hook and the other to an isometric force transducer (Astro-Med, West Warwick, RI) fitted with a positioning micrometer. Muscles were initially set to their *in vivo* resting length by using the suture distances between the proximal and distal tendons. The optimal length (L_o) for each muscle was determined precisely using the length-tension relation. Electrical stimulation was delivered via 2 platinum plate electrodes (3-4 mm apart, 25 mm long) parallel to the long axis of the muscle using a Grass S88 Stimulator (Grass Instruments, Quincy, MA). Force output was digitized using an analog-to-digital converter (ADC) (model AT MIO16E; National Instruments, Austin, TX) controlled via commercially available software (LabScribe/NI; iWorx, Dover, NH) operating at a sampling rate of 1 KHz (1 ms time resolution). Muscles were stimulated to produce successive twitches (1 ms duration, 1 Hz) at 10-60 volts (V) to determine the supramaximal stimulation voltage (voltage at which maximal twitch force was elicited X 1.35) used subsequently during the experiment (generally 30-40 V). Although the voltage used to directly stimulate the SOL muscle after 5 days of treatment was slightly higher for diseased mice (T Tg) compared to the other groups, there was no statistical difference in stimulation voltages between treatments and genotypes for the SOL and EDL muscles at either the 5- or 3-day time points. After muscle excision, mice were euthanized.

Muscle function was assessed based on directly evoked twitches and tetani. Stimulation parameters used to evoke muscle twitches were 1 ms duration pulses delivered at rates ranging from 0.2 Hz to 120Hz at supramaximal voltage to generate the full range of function from single twitch to fused tetani. These data were used to generate the force-frequency relation for each preparation. Muscle tetani were evoked by stimulating the muscle directly with 1 ms duration pulses at fusion frequency, defined operationally as the frequency at which ripples in the plateau phase of the tetanic force are $\leq 3\%$ of the peak force (Wiseman et al., 1996). The fusion frequency ranged from 80-100 Hz for the EDL and 30-40 Hz for the SOL. Because the kinetics of force development are slower in the SOL muscles, the length of the stimulus train to induce the plateau phase of a tetanus also differed between muscle fiber types. Tetanic contractions were elicited by delivering a 500 ms train to EDL and a 1 s train to the SOL. In all instances both the twitch and tetanic peak forces were normalized to the tendon-free muscle mass. Resistance to fatigue was assessed by stimulating the EDL and SOL with repeated tetanic stimuli (1 train/s; 330 ms duration, ~80-100 Hz in EDL and 670 ms duration, 30-40 Hz in SOL) until force decreased to approximately 10% of initial force. This was determined experimentally to be 90 s for wild type EDL and 135 s for wild type SOL from start of the fatigue stimulation, and this parameter was used for all treatment groups. Fatigue resistance was measured by determining the duration in seconds it took for maximal tetanic force to drop to half its starting value. Following the experiment, muscles were removed rapidly from the apparatus, dissected free from tendons, blotted of excess media, and weighed to estimate mass and then stored at -80°C.

In a separate series of experiments with other mice (B WT mice and T Tg, 90-120 days old; n=2-4/group), D-tubocurarine was added to bath (100 μ M, Sigma-Aldrich) to test whether the

motor nerve contributed to the force produced (Cairns et al., 2007). Force production was not affected by the addition of curare, indicating that field applied electrodes were not relying on stimulation of neuromuscular junctions to elicit muscle contractions (data not shown).

Histology. In a separate cohort of age-matched WT and Tg females (90 -120 days of age) treated for 5 days with either T or blank capsules, the SOL was dissected, placed in OCT compound (Sakura Japan) in cryomolds (Cryomolds) and snap frozen in liquid nitrogen (n = 5 mice/group). SOL were sectioned on a Leica cryostat at 10 μ m, thaw-mounted onto gelatin-coated slides, and stained with hematoxylin and eosin (H&E) for fiber counting, as previously described for the EDL (Johansen et al., 2009).

Androgen receptor protein expression. Upon completion of force recordings, we assessed total protein content and AR expression in muscles, using previously described methods (Johansen et al., 2007). In brief, the EDL and SOL were homogenized in lysis buffer [14 mM NaCl, 0.268 mM KCl, 0.147 mM KH₂PO₄, 0.802 mM Na₂HPO₄ 1% Nonidet P-40 (v/v), 0.5% sodium deoxycholate (wt/v), 1% sodium dodecyl sulfate (wt/v), 10% protease inhibitor (v/v; Sigma-Aldrich P2714)] using a Bio-Gen PRO 200 homogenizer (PRO Scientific). Samples were centrifuged at 12,000x at room temperature for 5 minutes. Supernatant from each sample was isolated to determine protein concentration using a Pierce BCA protein assay (Thermo Scientific) and a spectrophotometer (Beckman DU 530). Ten μ g of protein was loaded per lane on an 8% Tris-Glycine gel (Invitrogen), run at 125 V for 2 hours, transferred to a nitrocellulose membrane at 45 V for 2 hours, and probed using a rabbit polyclonal antiserum directed at AR (N-20, Santa Cruz Biotechnology; Santa Cruz, CA, USA; dilution 1:500; 0.4 μ g/mL). This was followed by

incubation of the membrane in anti-rabbit goat antiserum labeled with horseradish peroxidase (HRP; Santa Cruz, sc-2004; 0.4 $\mu\text{g}/\text{mL}$) and detected by Luminol (Santa Cruz Biotechnology). Films were exposed and developed using an X-OMAT 1000A Processor (Kodak). After probing for AR, nitrocellulose membranes were stripped and re-probed for actin using goat polyclonal anti-actin antiserum directly conjugated to HRP (I-19 Santa Cruz; 0.4 $\mu\text{g}/\text{mL}$).

Protein gels. Muscle homogenates were prepared as described previously and loaded into 12% SDS gels. Gels were run until the dye front had reached the bottom of the gel (~2 hours at 125 V). Protein bands were visualized by incubating in Coomassie Brilliant Blue R250 (Thermo Scientific Pierce) and destaining (40% methanol, 10% acetic acid v/v in distilled water).

Testosterone levels. Blood was collected via transcardial puncture from deeply anesthetized mice used for studies on muscle mechanics and held on ice for 30 minutes before centrifugation at 3000 rpm for 20 minutes at 8° C (Sorvall Biofuge Fresco, Thermo Scientific, Asheville, NC). After centrifugation of blood samples, plasma was collected and held at -80° C until it was assayed for circulating testosterone levels as described previously (Zuloaga et al., 2008).

Data analysis and statistics. Analysis of mechanical transients was performed using a custom algorithm (Jayaraman et al., 2006) in a MatLab programming environment (Mathworks, Natick, MA). In brief, raw digital signals were passed through a low-pass filter to smooth the data and then analyzed for force output and tension-time integrals. Kinetic parameters for the rise time (time to peak force) and relaxation time (time of return to baseline) were also measured in individual muscle twitches as described previously (Jayaraman et al., 2006). Statistical analysis

of data after 5 days of treatment was performed using two-way analysis of variance with genotype and hormone treatment as independent variables (SPSS Inc., Chicago, IL). Group differences were considered significant at $P < 0.05$, and *post hoc* comparisons were done using the Tukey *post-hoc* test. Independent group *t*-tests were used to evaluate significant differences between muscles from Tg versus WT mice after 3 days of T treatment.

Results

Testosterone (T) treatment impairs motor function without loss of muscle mass

At Day 0, before testosterone treatment, comparisons across treatment groups indicated similar body weights (data not shown) and comparable motor function based on both the hang and grip strength tests (Fig 5A, B). Replicating previous findings (Johansen et al., 2009; Monks et al., 2007), T induced a rapid and progressive decline in motor performance *only* in Tg mice. None of the 3 control groups (B WT, T WT, B Tg) showed any change in motor function. Although T also induced decreases in the body weight of Tg females (Figure 5C), losses in body weight lagged significantly behind the loss of muscle strength, as seen previously (Johansen et al., 2009). For example, a significant deficit in hang time was detected by day 2 of T treatment in Tg females ($P < 0.001$, compared to T WT or B Tg), with performance on this test reaching 0 s by Day 3, whereas a significant loss in body weight did not emerge until 3 days of T treatment ($P < 0.05$ at Days 3-5 in T Tg females versus asymptomatic controls, T WT, or B Tg). These data indicate that a rapid loss of motor function occurs only when T activates transgenic AR in skeletal muscle fibers and that neither the AR transgene nor T alone affect motor performance, replicating previous results (Johansen et al., 2009; Monks et al., 2007).

Although T induced marked losses in both body weight and muscle strength based on the hang and grip strength tests in Tg females, 5 days of T treatment did *not* induce any apparent decrease in muscle mass. Specifically, neither the EDL nor SOL muscle of Tg females showed a significant decrease in mass following T treatment (Table 1).

As expected, circulating T levels were greater in females given T capsules (T WT, T Tg) than those given blanks (B WT, B Tg; Table 1, $P < 0.05$). However, T capsules of the same size and randomly selected from the same stock produced greater levels of circulating T titers in Tg females than WT females, but both averages were within the physiological range of gonadally intact WT male mice. We suspect that this elevated level of T in Tg mice is due to their reduced body weight by 5 days of T treatment, as we have obtained similar findings in rats that differ in body weight (Johnson et al., 2012).

Skeletal muscles from T-treated Tg female mice show striking androgen-dependent loss of force

Five-Day Treatment

Tetanic Force. Tetanic force measurements from WT or Tg mice with normal motor function indicate that the EDL and SOL exhibit the expected characteristics of fast and slow muscle, respectively, with the fast-twitch EDL requiring less time but higher stimulation frequencies than the slow-twitch SOL to attain maximal force production (data not shown). Also as expected, the EDL produces nearly twice as much force per gram of muscle wet weight as the SOL (Fig 6A-D). While these same fiber-type specific differences were also seen in the EDL and SOL muscles of motor-impaired, T-treated mice, both muscles showed striking deficits in maximal tetanic force normalized to muscle mass (Fig 6). T induced a significant decrease in

maximal tetanic force *only* in Tg females, resulting in a significant interaction of genotype with treatment and significant main effects of both genotype and treatment ($P < 0.001$ for both). Both the EDL and SOL muscles of T-treated Tg females showed significantly less tetanic force compared to either T WT or B Tg females ($P < 0.001$ for both). T also induced a greater proportional deficit in tetanic force in the SOL than in the EDL of motor-impaired mice. While tetanic force for the fast-twitch EDL from T-treated Tg mice was approximately half that produced by the EDL from control mice, tetanic force for the slow-twitch SOL was decreased even further in T-treated Tg mice, to about a quarter of that produced by controls. All muscles tested had comparable force production at the end of the experiment as at the beginning (Fig 6C, D), indicating that there was little deterioration of the muscles *in vitro*, and suggesting that the force deficits observed *in vitro* reflect primary muscle dysfunction *in vivo*.

Muscle histology and protein content. The SOL was chosen for detailed histological analysis, because we had previously established that the EDL from motor-impaired Tg mice treated with T for 9 days shows no notable histopathology in H&E stained cross sections (Johansen et al., 2009). Likewise, we found no signs of histopathology in the SOL of motor-impaired, T-treated Tg mice. For example, muscle fibers in the SOL from T-treated Tg mice appear homogeneous in size (Fig 7A), without evidence of atrophy. While centralized nuclei were occasionally observed, they were no more frequent in the impaired SOL than in control SOL (data not shown). Moreover, we found no differences in the number of SOL muscle fibers from motor-impaired versus control mice (Fig 7B).

Because loss of contractile proteins might not be reflected in overall muscle weight, we also measured the total amount of protein in the EDL and SOL muscles of motor-impaired and control mice but we found no evidence for a net loss in total protein in either the EDL or SOL of

motor-impaired Tg mice compared to control Tg and WT mice with normal motor function (Table 1). Moreover, muscle protein gels revealed no consistent differences in specific contractile proteins in either muscle (data not shown).

We also addressed whether the SOL expresses AR at a higher level than the EDL in Tg females, since this could potentially explain the more severe loss of force in the SOL than the EDL following T-treatment (Fig 6). To assess this possibility, AR expression was examined in Western blots of muscle homogenates from Tg mice. As expected, AR expression was higher in both the EDL and SOL of Tg mice compared to the AR-enriched bulbocavernosus/levator ani (BC/LA) muscles of WT mice (Monks et al., 2007), but there were no consistent differences in AR expression between the two muscles (Fig 7C) that might account for the relatively greater loss of tetanic force induced by T in the SOL compared to the EDL from Tg mice (Fig 6).

Skeletal muscles from T-treated Tg females exhibit androgen-dependent changes in twitch force and kinetics

Twitch Force. Peak force of individual twitches (normalized to muscle weight) produced by the EDL and SOL from T-treated Tg females were decreased to about 60% and 7%, respectively, of peak twitch forces produced by these same muscles from blank-treated Tg mice (Table 1; Fig 8A, B). Although the twitch to tetanus ratio did not differ across treatment groups in the EDL (Table 1; $P > 0.05$), SOL from T-treated Tg females had a significantly lower twitch to tetanus ratio than muscles from Tg and WT control mice (Table 1; $P < 0.001$), due to T treatment reducing SOL peak twitch force more than peak tetanic force in Tg mice.

Contraction Kinetics. Analysis of twitch kinetics revealed a slower rise time to peak force and a slower relaxation time to baseline in EDL from motor-impaired T-treated Tg mice

compared to the EDL from control-treated Tg or WT mice (Fig 8C, E; $p \leq 0.001$ for both rise and relaxation in T Tg versus T WT or B Tg). Delays in both the rise and relaxation times suggest the kinetics of calcium release from, and uptake to, the sarcoplasmic reticulum or binding to troponin C of the thin filament are altered in the EDL of T-treated Tg mice. The observed left-ward shift in the force-frequency curves in T-treated EDL also supports this view (data not shown). However, neither the times to peak force nor relaxation time of the twitch were altered significantly by T in the SOL of Tg mice (Fig 8D, F).

Tetanic force production is reduced in the SOL but not EDL of Tg mice after three days of T treatment

Deficits in motor function are observed as early as 2 days after the initiation of treatment. T-treated Tg mice were unable to perform the hang test by Day 3, raising the question of whether changes in muscle function are also evident this early. Thus, we measured muscle mechanics in a separate cohort of Tg and WT females given T for 3 days.

We found the same time course of motor dysfunction after 3 days of T treatment as seen in the previous cohort (data not shown). *In vitro* measures of contractile properties after 3 days of T treatment revealed that both peak tetanic and twitch forces were reduced significantly in the slow-twitch SOL of Tg mice compared to the SOL of WT mice ($P < 0.05$, Fig 5A, B) but that only peak twitch force was significantly decreased in the EDL from the same Tg mice at this timepoint ($P < 0.05$, Fig 5B). Maximum tetanic force produced by the EDL in Tg mice was slightly but not significantly less than in WT controls ($P=0.07$, Fig 5A). Only the SOL muscle of Tg mice showed a significant deficit in the twitch-to-tetanus ratio after 3 days of T exposure ($P < 0.01$, Table 1), comparable to the effects of T after 5 days of treatment. Twitch kinetics for

the SOL of Tg mice were unaffected by T after 3 days of treatment, as expected. However, for the EDL of Tg mice, in which both speed to contract and relax were prolonged after 5 days of T, only relaxation was significantly slowed after 3 days of T treatment ($P < 0.05$, Fig 5D), with no effect of T on rise time to peak force (Fig 5C). In sum, the same pattern of deficits was seen in the SOL after both 3 and 5 days of T treatment whereas only some deficits, namely peak twitch force and relaxation time, were seen in the EDL after both 5 and 3 days of T treatment, suggesting that deficits in the SOL generally emerge sooner than in the EDL.

Only the EDL from motor-impaired mice show deficits in fatigue resistance

The only effects on fatigue resistance were seen in the EDL after 5 days of T treatment. The EDL from Tg mice treated with T for 5 days fatigued significantly faster, dropping to half maximal tetanic force sooner than the EDL from either blank-treated Tgs or T-treated WTs (Fig 10A, $P < 0.01$). Interestingly, the EDL from blank-treated Tg mice showed a greater resistance to fatigue than the EDL from blank-treated WT mice ($P < 0.05$), indicating that the transgene alone *enhanced* fatigue resistance in the EDL (Fig 10A). We found no effect of T on fatigue resistance in the SOL from motor-impaired Tg mice after either 3 or 5 days of T treatment (Fig 10 B, D) nor did we find an effect of T on fatigue resistances in the EDL of Tg mice after 3 days of treatment (Fig 10D). That deficits in both maximal tetanic force and fatigue resistance in the EDL emerge later than other defects in this muscle suggests that the same mechanism, perhaps involving mitochondrial dysfunction, may underlie both.

Discussion

This study shows that male levels of androgens not only trigger a pronounced and rapid loss of motor function in female Tg mice, but they also trigger a concomitant loss of contractile function in skeletal muscle in such mice; maximal force production of both the fast twitch EDL and slow twitch SOL plummeted to about half that of WT controls. This marked loss in contractile strength develops within a few days, in step with the emergence of motor dysfunction, and occurs *without* detectable losses in muscle mass or protein. Given that the AR transgene is expressed only in skeletal muscle fibers in the Tg mice (Monks et al., 2007), our data show that androgens can act directly on muscle fibers to reduce their contractile strength. Because ARs are normally expressed in skeletal muscle (Johansen et al., 2007; Monks et al., 2004; Sinha-Hikim et al., 2004), mutant AR may act directly in muscle, independent of the motoneurons, to cause muscle weakness in SBMA. Importantly, the deleterious effects of transgenic AR on both motor and muscle function were evident *only* when Tg mice were exposed to male-like levels of androgens, in line with the androgen-dependence of SBMA in humans.

We have confirmed that the loss in force production reflects neither a loss in muscle mass nor a disproportionate decay in muscle function *in vitro*. While force production of muscles from all four treatment groups declined somewhat during the course of the experiment, this decline was no greater in muscles from T-treated Tg mice than in muscles from control mice (Fig 6), indicating that the reduced force exhibited by the EDL and SOL muscles of motor-impaired mice cannot be attributed to a more rapid demise of muscle function *in vitro*. Moreover, while muscle mass generally correlates with the amount of force produced, the robust loss of maximal tetanic force to less than half that of normal was not accompanied by reduced muscle mass in motor-impaired mice. This was surprising, particularly because the mice lose nearly 20% of their body weight during the 5-day treatment period. This weight loss likely reflects the increased

metabolic rate and loss of fat stores triggered by androgen activation of transgenic AR in muscle, which is known to occur in such myogenic rodent models (Fernando et al., 2010). Indeed, at the end of the 5-day treatment, fat pads in T-treated Tg females are negligible in size (unpublished observation). Measures of twitch and tetanic force were normalized to the wet weight of each muscle, which takes into account any change in mass that might contribute to changes in force. We also saw no change in muscle mass *per se*, based either on their weight or total protein content (Table 1). Neither did we see any apparent histological changes. The impaired SOL contained a normal number of fibers, and those fibers appeared intact, with no signs of atrophy ordinarily associated with deficits in muscle strength (Fig 7). Our results in the SOL also agree well with prior results from the EDL of similarly treated mice (Johansen et al., 2009). Given that myosin and actin make up most of the bulk in muscle fibers, these data suggest that AR perturbs the contractile capacity of skeletal muscles in motor-impaired mice, not by inducing protein loss, but by perturbing the function of critical proteins that mediate muscle contraction either directly or through modulation of calcium handling properties.

Contractile strength was more severely and more rapidly affected in the SOL than in the EDL in T-treated Tgs; it declined by about 75% of force after only 3 days of androgen exposure, a time when effects on the EDL are negligible (Fig 5). This finding raised the question of whether transgenic AR is expressed at appreciably higher levels in the SOL than in the EDL. However, AR Western blots revealed no consistent difference in AR content between the EDL and SOL of Tg mice. It is also noteworthy that the EDL of Tg mice showed other androgen-dependent defects in contractile properties that the Tg SOL did not. These results also indicate that differences in AR expression cannot readily explain the more severe effects of T on force in the SOL.

While deficits in contractile *force* favored the SOL, the kinetics of force development showed the opposite pattern. Only the EDL of Tg mice affected by T showed significant slowing in both the rise and relaxation times compared to control-treated mice (Fig 8). We also found that fatigue resistance was reduced in the EDL, but not in the SOL, after 5 days of T treatment in Tg mice, with no effects on fatigability at 3 days (Fig 10). Interestingly, other investigators who have studied the same model report that the number and size of mitochondria in the EDL increases significantly after a week of T exposure (Musa et al., 2011), suggestive of mitochondrial dysfunction. While the EDL normally derives much of its ATP from glycolytic metabolism, the EDL from female Tgs after 9 days of T has shifted to a more oxidative metabolism based on NADH staining (Johansen et al., 2009). This apparent shift toward oxidative metabolism in the face of possibly impaired mitochondrial function could explain why fatigue resistance is reduced in the EDL after 5 days of T. In sum, these findings suggest that there are other inherent differences between these muscles, perhaps related to their fast- versus slow-twitch fiber type composition (Crow and Kushmerick, 1982), that predispose them to respond differentially to the toxic effects of an activated AR.

The overall profile of defects in both the EDL and SOL of motor-impaired mice suggest that mechanisms controlling intracellular calcium fluxes in muscle fibers may be perturbed. For example, the prolonged rise time to peak twitch force in the EDL of T-treated Tg mice suggests that the function of the ryanodine receptor (RyR1) may be impaired. This receptor controls the release of intracellular calcium from the sarcoplasmic reticulum to trigger muscle contraction. Likewise, the decreased twitch to tetanus ratio seen in SOL after both 3 and 5 days of T treatment, as well as the loss of tetanic force, suggests inefficient or impaired release of calcium from the sarcoplasmic reticulum controlled by the RyR1. Moreover, the prolonged relaxation

times seen at both 3 and 5 days of T treatment in the EDL of Tg mice suggest that the sarcoplasmic reticulum calcium ATPases (SERCA), which pump calcium back into the sarcoplasmic reticulum to allow muscles to relax, may also be impaired (Berchtold et al., 2000).

While it is possible that other mechanisms involved in the initiation of muscle contraction may be impaired, such as troponin C which binds calcium to trigger contraction, compelling evidence suggests that post-translational modifications to the RyR1 may have a role in the contractile defects we find. Recent studies of the mechanisms behind a loss of contractile strength in both aging and dystrophic muscles indicates that the RyR1 becomes modified by reactive oxygen and nitrogen species, causing the receptor to become leaky and leading to a deficit in muscle force (Andersson et al., 2011; Bellinger et al., 2009; Bellinger et al., 2008). Moreover, mitochondria likely play a key role in these maladaptive changes in the RyR1. In our model, loss of muscle function is associated with both an increase in mitochondrial number and activity of complexes I, II, and IV in the respiratory chain of mitochondria (Musa et al., 2011). These mitochondrial complexes are the primary source of reactive nitrogen and oxygen. Paradoxically, the production of ATP may at the same time be decreasing, as suggested by the reduced resistance to fatigue in the EDL and a deficit in citric synthase activity found in the fast twitch anterior tibialis muscle of these same T-treated Tg mice (unpublished observation). Together, these data are consistent with the idea that excessive amounts of reactive oxygen and nitrogen species produced by dysfunctional mitochondria in muscles of T-treated Tg mice may modify the RyR1, impairing its function. Such modifications of the RyR1 could explain many, if not all, the defects in muscle contraction that we observe. It is also noteworthy that such changes in the RyR1 can occur quite rapidly. A bout of intense exercise has been shown to induce such

changes in the RyR1 in less than 24 hours (Bellinger et al., 2008), consistent with the rapid decline in muscle force that we observe, particularly in the slow twitch SOL.

These data from our Tg mouse model may be relevant to human disease, particularly SBMA, an androgen-dependent motoneuron disease that affects only men (Fischbeck, 1997; Kinirons and Rouleau, 2008; La Spada et al., 1991; Schmidt et al., 2002). Several different mouse models of SBMA have been developed that broadly express a full length human AR harboring the disease-causing CAG repeat expansion. Such SBMA models show androgen-dependent loss of motor function (Chevalier-Larsen et al., 2004; Katsuno et al., 2002; Yu et al., 2006). However, because the mutated AR is expressed in both skeletal muscle and motoneuron in these various models, whether mutant AR acts in 1 or both of these cell types or in some other cell population is unknown. While androgen-dependent motor dysfunction in this model is triggered by WT AR acting exclusively in muscle fibers, such mice show a disease phenotype remarkably similar to that of other SBMA mouse models, indicating that AR may act in muscle to directly cause muscle weakness. Consistent with this view, humans with SBMA show elevated levels of serum creatine kinase (CK), indicative of skeletal muscle damage (Chahin and Sorenson, 2009). Such elevations are observed in patients with primary myopathies, such as muscular dystrophy but not in patients who have primary neuropathies (Pearce et al., 1964). Evidence from a knock-in (KI) mouse model of SBMA also suggests that primary myopathy is caused by muscle AR (Yu et al., 2006). Significantly, muscles from KI males show signs of pathology before motoneurons. Affected muscles in those males also have decreased expression of the ClCN1 chloride channel, and show abnormal spontaneous activity, like muscles affected by myotonic dystrophy, a primary myopathy. Finally, given that WT AR and the polyglutamine-expanded AR can exert toxicity through common mechanisms (Nedelsky et al., 2010), it is possible that the pathogenesis

of SBMA originates through different pathways of which mutant AR is only one such route. This is not unlike other neurodegenerative diseases, where known genetic mutations account for only a minority of the cases. Recognizing that an apparently normal AR protein can cause disease by a failure of mechanisms which ordinarily limit its inherent toxic potential could explain why some individuals diagnosed with SBMA due to muscle weakness *and* reduced androgen sensitivity, nonetheless lack the CAG expansion in their *AR* gene (Mariotti et al., 2000). In short, SBMA could be caused by different pathogenic events that perturb normal AR function in comparable ways, triggering the same disease. Because the *AR* transgene is expressed exclusively in muscle fibers of our myogenic model but nonetheless leads to expression of an SBMA phenotype, these findings are consistent with the possibility that AR acts directly in muscle fibers to cause or substantively contribute to SBMA pathogenesis.

CHAPTER 2: Muscle dysfunction may underlie androgen-dependent motor dysfunction in mouse models of SBMA

Oki, K., Katsuno, M., Adachi, H., Sobue, G., Wiseman, R.W., Breedlove, S.M., Jordan, C.L (submitted). “Muscle dysfunction may underlie androgen-dependent motor dysfunction in mouse models of SBMA.”

Abstract

Spinal and bulbar muscular atrophy (SBMA) is a late-onset motoneuron disease associated with the progressive loss of muscle strength. This disease is linked to a CAG/polyglutamine (polyQ) repeat expansion in the androgen receptor (AR) gene. Current views about SBMA suggest that cell dysfunction rather than cell death triggers motor dysfunction and that muscle dysfunction *per se* may underlie or contribute to the loss of motor function in this disease. Using a myogenic transgenic (Tg) mouse model in which androgen exposure can acutely induce a motor phenotype recapitulating SBMA in female Tg mice, both fast and slow twitch muscles from such mice show a precipitous drop in specific force that is independent of muscle mass. In the current study, we set out to determine whether muscle contractile function was similarly perturbed in chronically diseased *males* of three different SBMA mouse models: a Tg model that broadly expresses a full length human AR with 97 CAGs (97Q), a knock-in (KI) model that expresses a ‘humanized’ AR containing a disease-causing CAG expansion, and a Tg myogenic model that overexpresses wildtype AR only in skeletal muscle fibers. Significant deficits were found in muscle contractile strength independent of muscle mass, twitch/tetanic ratio and in the fatigue resistance of muscles, although the pattern of results was not uniform across models. These results raise the possibility that primary muscle dysfunction may be a key underlying feature of SBMA, and implicates skeletal muscle as a prime target for SBMA therapeutics.

Introduction

Whether functional deficits in motoneurons or muscles or both underlie motor dysfunction in motoneuron disease is not clear. Current evidence on amyotrophic lateral sclerosis (ALS), for example, indicates that dysfunction likely exists in both presynaptic and postsynaptic elements of

the neuromuscular system (Dekkers et al., 2004; Diaz-Amarilla et al., 2011; Dobrowolny et al., 2008a; Dobrowolny et al., 2008b; Gifondorwa et al., 2007; Kaspar et al., 2003; Li et al., 2007; Miller et al., 2006). Thus, functional impairments in one or both parts of the system may underlie the loss of motor function in motoneuron disease.

Spinal and bulbar muscular atrophy (SBMA), another motoneuron disease, is distinct from ALS in its strict male bias and apparent dependence on male levels of androgens. SBMA is linked to a CAG expansion mutation in exon one of the *androgen receptor (AR)* gene (Fischbeck et al., 1991; La Spada et al., 1991). This polyglutamine (polyQ) expansion in AR triggers a slowly progressing neurodegenerative phenotype that typically emerges in middle aged men. Female carriers of the mutated AR allele are largely unaffected (Soraru et al., 2008), even in those rare cases where females have two copies of the disease allele (Schmidt et al., 2002). Symptoms of SBMA include difficulties in ambulation due to limb weakness, and problems with speech and swallowing due to weakness in bulbar and facial muscles (Soraru et al., 2008). Findings from studies on SBMA mouse models indicate that the loss of motor function depends critically on male levels of androgens, with castration rescuing males from disease (Chevalier-Larsen et al., 2004; Katsuno et al., 2002; Yu et al., 2006) and testosterone (T) inducing disease in otherwise asymptomatic females (Katsuno et al., 2002; Monks et al., 2007). Because T reversibly exacerbates SBMA symptoms in a male patient (Kinirons and Rouleau, 2008), it is likely that T also plays a role in promoting SBMA in humans.

Data from animal models of SBMA suggest that cell dysfunction is a critical mediator of motor dysfunction with cell death being a rather late, end-stage event (Chevalier-Larsen et al., 2004; Johansen et al., 2009; Yu et al., 2006). Perturbations in axonal transport may be one hallmark feature of cellular dysfunction in neurodegenerative disease (Chevalier-Larsen and

Holzbaaur, 2006). For example, retrograde axonal transport in motoneurons of affected males is impaired in three different mouse models of SBMA, an impairment which emerges early and is androgen-dependent (Katsuno et al., 2006; Kemp et al., 2011). Surprisingly, while muscles of SBMA patients exhibit marked histopathology, little is known about the effects of disease on muscle function.

Whether muscles are dysfunctional in SBMA has recently been addressed using a muscle-specific transgenic (Tg) mouse model of SBMA. This so-called “myogenic” model shows an androgen-dependent loss in motor function (Monks et al., 2007), in step with other SBMA mouse models. Exposing asymptomatic females to male levels of androgens triggers a precipitous loss in motor function. Using an *in vitro* approach, muscles from impaired female mice were found to produce 50 – 75% less contractile force after five days of treatment (Oki et al., 2013). On the other hand, muscle mass did not decrease over the five days of T treatment, suggesting that the loss of contractile force reflects changes in function rather than net losses of contractile machinery.

These data beg the question of whether comparable deficits exist in muscles of diseased SBMA *male* mice. Thus, we used the same *in vitro* approach of stimulating isolated muscles attached to a strain gauge to examine the contractile properties of skeletal muscles in affected male mice of three different SBMA models, a myogenic Tg model in which rat wildtype (WT) AR is expressed *only* in skeletal muscle fibers, the ‘97Q’ Tg model in which a full length 97 polyQ AR is globally expressed, and a KI model in which a humanized polyQ-expanded mouse allele of AR is broadly expressed. Our results show that muscle force is compromised independent of muscle atrophy in two of the three models, suggesting that primary impairments in the contractile properties of skeletal muscles may contribute to motor dysfunction in SBMA.

Methods

Animals and treatment. The contractile properties of the fast twitch extensor digitorum longus (EDL) and the slow twitch soleus (SOL) muscles of affected male mice from three different models of SBMA were examined. Myogenic' transgenic (Tg) mice express under the control of the human skeletal α -actin (HSA) promoter a wildtype AR allele only in skeletal muscle fibers (Monks et al., 2007). Mice of the 97Q Tg model globally express under the control of a CMV promoter/chicken β -actin enhancer a full length human AR transgene harboring 97 CAGs (Katsuno et al., 2002). KI mice express a humanized CAG-expanded mouse AR allele under the control of native AR promoters (Yu et al., 2006). Heterozygous female carriers in each model were mated to C57/B6J male mice for several generations to produce progeny for this study. Animals were group housed and had access to water and food *ad libitum*. All animal procedures were approved and performed in compliance with the Michigan State University Institutional Animal Care and Use Committee, in accordance with the standards in the NIH Guide for the Care and Use of Laboratory Animals.

97Q males. Because disease onset is highly variable in transgenic males of the 97Q model, we attempted to synchronize disease onset and progression by exposing castrated juvenile males to adult levels of testosterone (T). Age-matched (30-32 days old) WT and Tg male mice (n=5-6 mice/group) were deeply anesthetized with isoflurane, castrated, and implanted subcutaneously just caudal to the scapula with Silastic capsules (1.57 mm i.d. and 3.18 mm o.d., effective release length of 6 mm) containing crystalline T (~0.15 mg per capsule), as previously described (Johansen et al., 2009). Incisions were closed with 9 mm surgical staples. All animals received ketoprofen analgesic (5 mg/kg, sc) immediately following surgery. One T capsule was used

throughout the duration of the study for each mouse and treatment was continued until Tg mice developed motor impairments.

Motor function was assessed using the grip strength and hang tests as described below one hour before surgery to establish baseline performance (Day 0) and twice weekly following surgery up to the time of sacrifice when end-stage motor function was reached. End-stage motor function was defined as hang times < 24 s or 20% of the latency to fall in WT mice and grip strengths around 16 g force, roughly half of WT control values. On average, this level of dysfunction was reached by around 50 days of age and only in Tg mice. Mice were sacrificed at this point, and muscles were removed under a surgical plane of anesthesia for in vitro muscle testing as previously described (Oki et al., 2013).

141 males. Normally, most males in the myogenic model carrying the HSA-AR transgene of the 141 line die on the day of birth (Monks et al., 2007). However, such Tg males can be rescued from perinatal death by blocking the effects of prenatal T with the AR antagonist, flutamide (Johansen et al., 2011; Monks et al., 2007). Thus, timed pregnant Tg dams were given daily sc injections of flutamide (5 mg flutamide dissolved in 100 μ l in propylene glycol) on gestational days 14-18. Flutamide-rescued Tg males show the same androgen-dependent disease phenotype as Tg male mice that survived without the aid of prenatal flutamide (Johansen et al., 2011). The motor function of Tg and age-matched WT male mice (90-135 days old, n=5-6 mice/group) was assessed based on grip strength and hang test. Since Tg males in this model are chronically impaired, motor function was assessed three times: three days before harvest, the day before harvest, and on the day of harvest.

KI males. The length of CAG repeat in the AR gene of the KI model tends to contract across generations, necessitating sequencing the first exon to determine the length of the repeat and

thus, potential for toxicity. KI males used in this study had a repeat length ranging from 84-93. Motor function of KI male mice and yoked WT controls (n=5-7/group) was measured starting at 30 days of age and tested twice weekly using the grip strength and hang tests until a $\geq 30\%$ decline was seen on one or both tests in KI males, at which point muscles were harvested from the KI male and its yoked WT control for *in vitro* examination.

Motor function tests. In the 97Q and 141 lines, forelimb grip strength was assessed using a grip strength meter (Columbus Instruments) oriented in the horizontal plane (Chevalier-Larsen et al., 2004; Johansen et al., 2009; Katsuno et al., 2002). Mice were held by their tails and lowered to the apparatus, allowed to grasp the metal grid with their forelimbs only, and were pulled by their tail vertically at a 90° angle away from the grid until their grip was released. Force (g) applied to the bar at the moment of release was recorded as grip strength. Six consecutive measurements were done within a single two minute session for each subject with the lowest and highest grip values excluded, and the mean of the remaining four values recorded as the grip strength for that animal and session. In the KI line, consistent with previously used methods (Kemp et al., 2011; Yu et al., 2006), a triangle gauge was used to measure grip strength as deficits in these mice are more easily detected with the triangle. Out of five values, the lowest and highest was dropped and the middle three values were used to estimate average grip strength for that mouse on that day. We saw no evidence of a consistent drop in grip strength over the five bouts of this test.

The hang test was conducted by placing mice on a wire grid that was then turned upside-down 40 cm above a counter. Latency to fall (up to 120 seconds) from the wire grid was measured (Monks et al., 2007; Sopher et al., 2004).

The number of rears (i.e. number of vertical movements) was also assessed in an open field (16 × 16 inch Plexiglas chamber) for five minutes using the Versamax activity monitor (AccuScan Instruments, Columbus, Ohio, USA). The chamber was cleaned with 70% ethanol between tests, and data were analyzed using the Versamax software (Johansen et al., 2009). Rearing behavior is an indirect readout of hindlimb muscle strength and was conducted in the 97Q and 141 models.

In vitro studies to assess muscle mechanics. To determine whether impairments in skeletal muscle function might underlie motor dysfunction, muscle contractile characteristics of the fast-twitch EDL and the slow-twitch SOL were examined *in vitro* in motor-impaired Tg/KI males and their respective WT controls using freshly excised preparations. These hindlimb muscles were selected because the EDL and SOL are the prototypical fast- and slow-twitch muscles, respectively, with considerable background information available on their normal contractile properties (Crow and Kushmerick, 1982; Kushmerick et al., 1992). Moreover, the toxic effects of an activated AR in SBMA might depend on fiber type, as we have previously seen in diseased females of the myogenic model (Oki et al., 2013) and as observed in other diseases (Atkin et al., 2005; Hegedus et al., 2008).

Mice were deeply anesthetized with a single intraperitoneal injection of sodium pentobarbital in sterile saline (0.1 mg/g body weight, Abbott Laboratories, North Chicago, IL, USA). Once muscles were exposed, 5-0 silk suture was tied to the proximal and distal tendons *in situ* and their resting length approximated by recording the intersuture distance prior to excision. Muscles were then removed by cutting above the suture knot on the proximal tendon and below the suture knot distally. After muscles were excised, mice were euthanized. Excised muscles

were incubated in an 8 mL organ bath containing oxygenated Ringer's (117.1 mM NaCl, 4.6 mM KCl, 25.3 mM NaHCO₃, 2.5 mM CaCl₂, 1.2 mM MgSO₄; pH 7.4; equilibrated with 95% O₂/5% CO₂) (Dentel et al., 2005; Oki et al., 2013). Temperature of the bath was continuously monitored using a K-type thermocouple (Omega Engineering, Stamford, CT) adjacent to the muscle and maintained at 25±0.2°C by circulating water through a glass-jacketed organ bath (Radnoti Glass Technology, Monrovia, CA). Isolated muscles were fixed by tying one end of the muscle ligature to a glass hook and the other to an isometric force transducer (Astro-Med, West Warwick, RI) fitted with a positioning micrometer. Muscles were then set to their *in situ* resting length using the length-tension relation.

Electrical stimulation was delivered via two platinum plate electrodes (3-4 mm apart, 25 mm long) parallel to the long axis of the muscle using a Grass S88 Stimulator (Grass Instruments, Quincy, MA). Force was recorded using an analog-to-digital converter (model AT MIO16E; National Instruments, Austin, TX) controlled via commercially available software (LabScribe/NI; iWorx, Dover, NH). Muscles were stimulated with successive twitches (1 ms duration, 1 Hz) at 10-60 volts (V) to determine the supramaximal voltage (generally 30-40 V).

Muscle function was assessed based on directly evoked twitches and tetani. Stimulation parameters used to evoke muscle twitches were 1 ms duration pulses delivered at a rate of 0.2 Hz for 3 seconds at supramaximal voltage. Muscle tetani were evoked by stimulating the muscle directly with 1 ms pulses at the fusion frequency which was operationally defined as the frequency at which ripples in force on the tetanic plateau are ≤ 3% of the total peak force. The fusion frequency ranged from 80-100 Hz for the EDL and 30-40 Hz for the SOL in WT animals. Length of the stimulus train to induce tetanus also differed between muscle fiber types, with a

500 ms train and 1 s train used for EDL and SOL, respectively. Absolute force was recorded in grams and converted to Newtons (N) using the conversion

$$1 \text{ gram of force} = 9.80665 \times 10^{-3} \text{ N.}$$

This force value was then normalized to the grams tendon-free muscle mass (N/g). While muscle atrophy could contribute to motor dysfunction via a loss in strength, normalizing force to mass reveals changes in force that are independent of mass. Contraction kinetics were also measured using the trace of individual twitches. Time to peak force in the twitch (rise time) and time to return to baseline (relaxation time) were measured in all muscles using customized software (details below).

Resistance to fatigue was assessed in the EDL by stimulating with tetani at ~80-100 Hz, each train lasting 330 ms, repeated every 1 second (Burke et al., 1971). This was done until the final tetanus was ~10% of initial force, determined to be 90 s in EDL. A similar protocol was used for the SOL. Each SOL was stimulated with tetani at ~30-50 Hz repeated every 1 second. However, due to a higher percentage of slow-twitch, fatigue resistant fibers being present, the SOL fatigues much slower than the EDL, and the protocol was adjusted to induce fatigue (final tetanus decreased to ~10% of initial) in a shorter window of time. The train duration was increased to 670 ms in duration, and the tetani were repeated for 135 s in the SOL. Fatigue profile was determined by generating a curve that calculated the amount of force relative to muscle mass produced at each stimulus pulse. Following the experiment, muscles were rapidly removed from the apparatus, dissected free from tendons, blotted of excess media, weighed to estimate mass, and then stored at -80° C.

Histology. The contralateral SOL was dissected from the same mice of the 141 line that were used for the mechanical studies, placed in OCT compound (Sakura Japan) in cryomolds (Cryomolds) and snap frozen in liquid nitrogen (n = 5 mice/group). Unlike the EDL, the SOL had not been previously examined in this model for histopathology (Johansen et al., 2009). The SOL were sectioned on a Leica cryostat at 10 μ m, thaw-mounted onto gel-subbed slides, and stained with hematoxylin and eosin (H&E). Both the EDL and SOL from 97Q males and WT controls were prepared in a similar fashion for histological analyses. Because we did not find any significant deficits in the contractile properties of either the EDL or SOL of KI males, we did not conduct similar morphological analyses of muscles in this model.

Testosterone levels. Blood was collected via a transcardial puncture from deeply anesthetized mice used for studies on muscle mechanics, and held on ice for 30 minutes before centrifuging at 3000 rpm for 20 minutes at 8 $^{\circ}$ C (Sorvall Biofuge Fresco, Thermo Scientific, Asheville, NC). After centrifugation of blood samples, plasma was collected and held at -80 $^{\circ}$ C until assayed for circulating testosterone levels as previously described (Zuloaga et al., 2008).

Data analysis and statistics. Analysis of mechanical transients was performed using a custom algorithm created for the MatLab programming environment (Mathworks, Natick, MA). In brief, raw digital signals were passed through a low-pass filter to smooth the data and then analyzed for force output and tension-time integrals. Kinetic parameters for the rise time (time to peak force) and relaxation time (time of return to baseline) were also measured in individual muscle twitches as previously described (Jayaraman et al., 2006). Briefly, a point for peak force was determined in the digitally acquired twitch traces. The ascending portion of the twitch trace up to the peak

force was defined as the rise time, and the descending portion of the trace from the peak force back to baseline was defined as the relaxation time. Independent groups T-tests were used to evaluate significant differences between muscles from affected Tg or KI males versus their WT controls.

Results

Motor dysfunction correlates with muscle dysfunction in 97Q Tg mice.

Motor tests confirmed that castrated 97Q Tg males treated with T show the same androgen-dependent motor dysfunction as previously reported for gonadally intact 97Q Tg males (Katsuno et al., 2002). All three indices of motor function—number of rears in an open field (Fig 11A), frontpaw grip strength (Fig 11B), and hang times (Fig 11C) indicate that the motor function of 97Q Tg males was significantly impaired compared to WT controls (p-values ≤ 0.002). Serum T levels were comparable between Tg mice and their respective controls, suggesting these functional changes were not due to differences in circulating T (Table 2). 97Q Tg and WT males did have higher T levels than gonadally intact males of either the 141 myogenic or KI models (data not shown for KI model) as expected because of the exogenous T treatment. Relatively severe motor deficits emerged in Tg males by 50 days of age (age range: 40–57 days). At the time of testing, all symptomatic Tg mice had lower body weights than their WT controls (Table 2), although deficits in body weight lagged behind deficits in motor function by ~3 days.

Both the isolated EDL and SOL from 97Q males showed significant deficits in force that were evident for both raw and normalized force measures (Fig 12). With one exception (raw tetanic force in SOL, Fig 12J), raw twitch and tetanic force were significantly decreased in

muscles of Tg males compared to WT males (p-values ≤ 0.007 for raw EDL twitch and tetanus and raw SOL twitch). However, once force measures for individual muscles were normalized to their mass, all force measures showed significant and robust deficits in both EDL and SOL muscles of Tg males (p-values ≤ 0.002 for all measurements), indicating a loss of force in both fast and slow twitch muscles in diseased 97Q males that occurred *independent* of the losses in muscle mass. Notably, the EDL from Tg males exhibited a greater loss in both normalized twitch and tetanic force than did the Tg SOL, producing less than 20% of the normal WT force whereas the Tg SOL exhibited more than 50% of WT force. These data are consistent with the idea that a loss of motor function may be due to a loss in contractile force of muscles, some of which reflects muscle atrophy, but much of which seems to occur independent of losses in muscle mass. We found no evidence of a drop in force production from the first to the last recording of peak tetanic tension (Fig 16) prior to stimulating the muscle to induce fatigue. This apparent stability of muscle performance *in vitro* strongly argues that the force deficits reflect genuine deficits *in vivo*.

Although force was more affected in the Tg EDL, only the Tg SOL showed significant changes in the twitch/tetanus ratio (Fig 12L), with significant decreases in this ratio compared to WT (p < 0.02). The diseased EDL did however show a similar trend (Fig 12F) raising the possibility that with a larger sample size, the decreased twitch/tetanus ratio may be significant. These data suggest impairments in calcium handling mechanisms in the SOL and possibly the EDL of motor-impaired 97Q Tg males.

Twitch traces (Fig 12C, I) were subjected to a kinetics analysis to assess whether time to peak force (rise time) and time to baseline (relaxation time) was also affected by disease.

Although both contraction and relaxation times were consistently longer in Tg muscles compared to WT controls, such differences fell short of significance (Table 3).

Initial fatigue analysis examining the percentage of force lost over the entire stimulation period suggested the EDL from 97Q Tg males were less fatigable than WT controls (Fig 13A), that is, losing less force over a given period of time (45% force loss in Tg vs. 92% force loss in WT). We also determined the time it took for muscles to lose 50% of their original force (i.e., time to half maximal force loss). Based on this measure, the EDL from Tg males fatigued faster, reaching a 50% drop in force twice as fast as WT EDL (Tg versus WT: 14.3 ± 3.0 s versus 25.8 ± 0.9 s, Fig 13B, $p < 0.05$). The SOL from Tg males showed a similar decrease in fatigue susceptibility, losing 50% of its original force significantly sooner than WT SOL (Tg versus WT: 38.6 ± 3.2 s versus 46.9 ± 1.8 s, $p < 0.05$) but the effect of disease on fatigability in the SOL seems much less marked than in the EDL (Fig 12C, D).

Motor dysfunction correlates with muscle dysfunction in myogenic Tg males.

As expected, 141 Tg mice also exhibited profoundly compromised motor function, showing deficits on all three measures – rearing, grip strength, and hang times (Fig 11D, E and F; p -values < 0.001 for all tests). These data confirm findings from previous studies (Monks et al., 2007). Body and muscle weights were also decreased in Tg males compared to WTs but serum T levels were comparable (Table 2), indicating that abnormal T levels do not explain the motor phenotype in 141 Tg male mice.

The EDL and SOL of motor-impaired 141 Tg males showed similar functional deficits as muscles from diseased 97Q males (Fig 14), with both the EDL and SOL showing significant deficits in both raw twitch and tetanic force production compared to WT EDL and SOL muscles

(p -values < 0.001). Significant deficits were also evident once muscle mass was taken into account (Fig 14B, H and K), with the one exception that tetanic force in the Tg EDL was no longer less than WT controls (Fig 14D vs. 4E). Given that the EDL from chronically impaired 141 Tg males contains about 30% fewer fibers than normal (Johansen et al., 2011; Monks et al., 2007), we suspect that this deficit in fiber number in Tg EDL underlies the deficit in raw tetanic force and that the maximal contractile force produced by each fiber is comparable to that of WT fibers. However, because the Tg EDL showed deficits (compared to normal) in normalized twitch but not tetanic force, the twitch/tetanus ratio in this muscle was also significantly reduced ($p < 0.005$) to about half that of WT muscle (Fig 14F). The twitch/tetanus ratio for Tg SOL was also significantly decreased compared to WT controls although the magnitude of the effect was less (Fig 14L). In short, both EDL and SOL muscles in diseased myogenic males show primary dysfunction that is independent of muscle mass, sharing similar defects as muscles of diseased 97Q males. We again found no evidence of a drop in force production from the first to the last recording of peak tetanic tension (Fig 16) prior to fatiguing stimulation.

Our analysis of twitch kinetics reveals that rise time of twitches in the myogenic EDL was significantly prolonged compared to normal (Table 3; $p < 0.001$). However, relaxation time in the EDL was not affected by disease nor was contraction or relaxation time affected in the SOL of myogenic Tg males.

During fatiguing stimulation, the EDL from myogenic motor-impaired males lost less force overall than the WT EDL (71% force loss in Tg versus 95% in WT; Fig 15A), suggesting that the Tg EDL had greater endurance than the WT EDL, consistent with an apparent shift toward a more oxidative phenotype in diseased EDL (Monks et al., 2007). However, the time it took to reach a 50% drop in force was the same for Tg and WT EDL muscles (Fig 15B). The fatigue

profile in the SOL of diseased myogenic Tg males was similar to that of the 97Q EDL, with little apparent loss in force overall during the period of fatiguing stimulation. Nonetheless, the diseased SOL in myogenic Tg males fatigued faster, at least initially, since it took significantly less time to reach a 50% drop in force compared to WT SOL (Tg versus WT: 9.8 ± 0.9 s versus 42.1 ± 2.4 s, $p < 0.05$).

Histology.

Finding similar muscle dysfunction in both the 97Q and myogenic Tg models prompted us to examine muscles directly in histological sections stained with hematoxylin and eosin to evaluate whether dysfunction correlates with any known histological markers of disease. We counted the number of muscle fibers in each muscle and the number of fibers with centralized nuclei, excepting the EDL from 141 myogenic males, which have been analyzed previously (Johansen et al., 2011).

97Q model. Even though the EDL muscles from diseased 97Q males were about half the mass of those from age-matched WT males (Table 2), the number of EDL fibers did not differ between diseased 97Q Tg males and healthy WTs. These data suggest that EDL fibers from diseased 97Q Tg males are on average significantly smaller. Consistent with this speculation, some fibers in cross section of EDL are visibly atrophic (Fig 17). Regardless, even when differences in muscle mass are taken into account, force capacity of the diseased EDL of 97Q males is ~6 times less than that of WT EDL during both twitch and tetanus contractions, indicating that fiber size alone cannot explain the loss of intrinsic strength. The SOL of diseased 97Q males also contained a normal number of fibers (Table 4), in this case paralleling its normal mass (Table 2). The percentage of SOL fibers with centralized nuclei was also the same as

normal. Cross sections of stained SOL also look remarkably normal (Fig 17). On the other hand, the 97Q EDL contains significantly more fibers with centralized nuclei than normal (Table 4), paralleling the greater force deficit in the EDL of the 97Q model.

141 myogenic model. Previous work shows that the EDL of myogenic males contains about a third fewer fibers than WT EDL (Johansen et al., 2011). In contrast, the SOL of 141 diseased males shows no change in total fiber number even though its mass is significantly less than WT SOL. While variability in fiber size appears relatively normal, fibers in general appear smaller in size but otherwise remarkably normal (Fig 17). However, diseased SOL of 141 males contains a significantly higher proportion of fibers with centralized nuclei compared to WT SOL (Table 4). This pattern of differences is similar to that in the 97Q model, where the incidence of centralized nuclei correlates with the most severe force deficit, with decreases in muscle mass but no change in overall fiber number (EDL in the 97Q model and SOL in the myogenic 141 model).

Knock-in model.

Although motor dysfunction was observed in KI mice relative to WT controls, with both forelimb grip strength and hang times significantly less (Fig 6A, B; grip $p < 0.002$; hang $p < 0.03$), we found no significant deficits in the contractile properties of the EDL or SOL of these KI males (Fig 6C – N). Still, the EDL of KIs produced consistently less force than did the WT EDL (Fig 6C-G). Neither did we find significant deficits in the twitch kinetics of either muscle from KI males (data not shown).

Discussion

We set out to determine whether skeletal muscle dysfunction could underlie motor dysfunction in spinal and bulbar muscular atrophy (SBMA). To this end, the contractile properties of isolated fast twitch EDL and slow twitch SOL were examined *in vitro* from motor-impaired male mice of three different mouse models of SBMA. The KI and 97Q Tg models each broadly express a CAG expanded AR allele linked to SBMA (Katsuno et al., 2002; Yu et al., 2006) while the third ‘myogenic’ (141) model expresses a rat WT AR transgene only in skeletal muscle fibers but nonetheless, recapitulates the same androgen-dependent loss of motor function as seen in the other two models (Monks et al., 2007). *In vitro* studies of muscle function using acutely diseased Tg females in the myogenic model indicate that muscles of diseased mice undergo profound losses in contractile strength that are independent of muscle mass (Oki et al., 2013), suggesting that primary muscle dysfunction may contribute to the loss of motor function in SBMA. These data led us to ask whether similar muscle defects are evident in affected SBMA *male* mice. We find that the EDL and SOL of motor-impaired 97Q and myogenic male mice generally show striking deficits in their ability to produce contractile force and resist fatigue. While KI males show motor impairments, albeit less severe than in the other two models, only subtle deficits in force production were detected in the EDL, suggesting that other mechanisms underlie motor impairments in this model. We are the first to directly examine the function of skeletal muscles isolated from the nervous system in any SBMA model. Consistent with other reported findings implicating skeletal muscle in motoneuron disease (Dobrowolny et al., 2005; Johansen et al., 2011; Kieran et al., 2005; Monks et al., 2007; Palazzolo et al., 2009; Perlson et al., 2009; Wong and Martin, 2010; Yu et al., 2006), these data suggest that therapies that target skeletal muscle may be effective in protecting or rescuing motor function in SBMA.

There are several possible reasons why KI males did not show defects in contractile properties of muscle despite impaired motor function. The most obvious possibility is that the motor tests used, hang and grip strength, reflect defects in muscles other than the EDL and SOL. Since grip strength was based on forepaw grip, it tests the function of only forelimb and not hindlimb muscles. Moreover, disease susceptibility seems to vary in the KI model depending on the specific muscle (Yu et al., 2006). Because perineal muscles are enriched for AR (Johansen et al., 2007; Monks et al., 2004), these muscles are affected first and more severely in KI males than limb muscles. Hence, it is possible that marked dysfunction would have been detected if perineal muscles had been studied rather than the EDL and SOL. Another possibility is that presynaptic dysfunction underlies the loss in motor function in KI males with the muscle themselves functionally intact. Retrograde axonal transport is severely impaired in diseased KI males (Kemp et al., 2011), indicating that motoneurons are indeed dysfunctional in KI males. Since defects in axonal transport are often associated with defects in nerve terminal function (Pigino et al., 2009), it seems likely that KI males have impairments in synaptic function. Finally, the apparent deficits in muscle strength suggested by shortened hang times and reduced grip strengths may reflect nonspecific effects of disease in KI males. Dysfunction of the perineal muscles in KI males leads to occlusion of the urethra, uremia and early morbidity (Yu et al., 2006). Poor motor performance could reflect effects of this condition rather than direct toxic effects of AR on limb neuromuscular. Regardless, these data underscore the fact that defects in motor function do not always translate to defects in muscle contractile properties in SBMA models.

Muscle atrophy triggered by the loss of innervation has long been assumed to underlie the progressive loss of muscle strength in SBMA. Current data does not support this view. While

muscles from both 97Q and 141 male mice generally have less mass and produce less absolute force than muscles from WT controls, significant deficits in twitch and tetanic force remain even once force measures are normalized to muscle weight (Figs 2 and 4). The one exception is the myogenic (141) EDL in which a deficit in raw tetanic force drops out once muscle mass is taken into account. However, the myogenic EDL is also the only muscle among the two models that contains significantly fewer muscle fibers (Johansen et al., 2011), suggesting that the deficit in raw tetanic force in the myogenic EDL reflects the deficit in fiber number. For the EDL and SOL of 97Q males and the SOL of myogenic males, most of the deficit before normalization is also evident after normalization, indicating that muscle atrophy accounts for only a small portion of the deficit in contractile strength. These data point to other mechanisms besides the loss of actin and myosin contractile proteins that contribute to the loss of muscle strength in SBMA perhaps mediated by altered function of calcium-handling proteins. Changes in the twitch/tetanus ratio in the two Tg models supports this view and implicates mechanisms that release, bind and/or sequester calcium.

How toxic AR causes a loss in contractile force is not known and warrants future studies. However, recent microarray results assessing changes in gene expression in hindlimb muscle from males of these three SBMA models suggests possible candidate molecules (Mo et al., 2010). For example, calpain 2 is upregulated in hindlimb muscles of both 97Q and 141 Tg males but not KI males. Calpain 2 is a calcium-dependent protease which resides in the sarcoplasm of muscle fibers (Vermaelen et al., 2007). Calpain activity is thought to be an important player in promoting muscle atrophy (Talbert et al., 2013). While enhanced calpain activity may account for loss of muscle strength due to atrophy, it may also be involved in regulating muscle strength independent of mass. Calpain promotes the activity of caspase 3 (Talbert et al., 2013), with

caspase 3 activity during sepsis implicated in the rapid loss of force without mass (Supinski and Callahan, 2006).

Another possibility is that toxic AR causes muscle weakness by impairing the function of the ryanodine receptor (RyR1), a critical player in the excitation-contraction pathway. The RyR1 opens in response to activity, releasing calcium from intracellular stores to bind troponin-C which triggers muscle contraction. While this receptor is ordinarily closed during inactivity, in some pathological states such as muscular dystrophy or aging, the RyR1 stays partially open (Bellinger et al., 2009), leaking calcium into the cytosol of muscle fibers in the absence of action potentials. This slow and constant leak of calcium leads to an elevated concentration of cytosolic calcium and is thought to underlie muscle weakness in both muscular dystrophy and aging (Andersson et al., 2011; Bellinger et al., 2009). Importantly, this defect in RyR1 function involves post-translational modifications which can develop within hours and is readily reversible (Bellinger et al., 2008). Recent evidence from acutely diseased Tg 141 females also points to leaky RyR1 underlying the loss of muscle strength in SBMA (Oki et al., 2013).

Trophic factors may also be involved in regulating the strength of muscles. One molecule of particular interest is insulin like growth factor-1(IGF-1). In addition to IGF-1 likely being a main mediator of the anabolic effects of androgens on skeletal muscle (Gentile et al., 2010), IGF-1 has also been implicated in SBMA. When overexpressed exclusively in skeletal muscle, IGF-1 rescues 97Q mice from disease (Palazzolo et al., 2009). IGF-1 expression is also lower in muscles of affected KI males (Yu et al., 2006). While studies often focus on the effects of muscle-derived trophic factors on motoneurons, the role of such factors in regulating muscle function in disease merits further attention, particularly because skeletal muscles express the receptors for many muscle-derived trophic factors (Chevrel et al., 2006).

One significant aspect of these data is that losses in force occur *without evidence of histopathology*. For example, the SOL in the 97Q males appears largely protected from disease based on morphological attributes: its mass is unaffected (Table 2), the number and apparent size and uniformity of muscles fibers is normal (Table 3, Fig 17), and the frequency of fibers with centralized nuclei is also normal (Table 3). Despite the lack of histopathology, its function is significantly impaired. It exerts significantly less twitch and tetanic force (Fig 2H, K), has a significantly reduced twitch/tetanus ratio (Fig 2L) and fatigues more rapidly, losing 50% of its starting force sooner than normal SOL (Fig 13D). The SOL muscle in myogenic males presents a similar picture. While stained cross sections of SOL look remarkably normal, with fibers appearing relatively uniform in size, albeit smaller, and fiber number normal (Table 4), the diseased SOL produces considerably less force (~65–70% less) than the WT SOL (Fig 14H, K). The only apparent morphological correlate of muscle dysfunction that we found was the incidence of fibers containing centralized nuclei but this relationship is not strict. Only muscles that lost the most amount of force in each model (EDL in the 97Q males and SOL in the myogenic males) contained a significantly higher percentage of fibers with centralized nuclei compared to their respective WT controls. However, the 97Q SOL and 141 EDL also both show significant force deficits, albeit not as severe. The marked absence of muscle histopathology in motor-impaired mice is reminiscent of reports for another mouse model of SBMA (Chevalier-Larsen et al., 2004) and reinforces the likelihood that cellular dysfunction well precedes disease-related changes in cell morphology.

While motor function appears comparably affected in the two different SBMA Tg mouse models, the severity of the deficit in muscle force differed for each model. The EDL was more severely affected in the 97Q model while the SOL was more severely affected in the myogenic

141 model. Given that the EDL is a fast twitch muscle while the SOL is slow, these results suggest that the toxic potential of AR in each model depends on the fiber type composition of the muscle although the factors behind this fiber-type dependence are not clear. Fiber-type differences have also been found to play a role in ALS models where fast-twitch motor units are more severely affected (Atkin et al., 2005; Hegedus et al., 2008). One possible explanation for the differing susceptibilities to disease is that AR expression levels also vary, paralleling the more toxic effects in select muscles. We think this explanation is unlikely. In the myogenic model, for example, we find the same pattern of deficits in acutely diseased Tg females, with force being more severely affected in the SOL than in the EDL (Oki et al., 2013). However, AR expression appears comparable in the EDL and SOL muscles of 141 Tg females (Oki et al., 2013). While enhanced AR expression might explain the greater force deficits in the 97Q EDL compared to the SOL, it does not readily account for the deficit in the twitch/tetanus ratio that occurs only in the 97Q SOL. Microarray data also offer a possible explanation, indicating that the slow isoform of troponin-C, which binds calcium to trigger skeletal muscle contractions, is downregulated in limb muscle of 141 males. Slow troponin-C is found primarily in slow-twitch and cardiac muscles, and its downregulation could potentially contribute to the more severe loss of force in 141 Tg SOL. However, the fact that the force deficit is fully established within three days of disease onset in the SOL of acutely diseased 141 Tg females but the half life of slow troponin-C is more than five days (Martin, 1981) challenges this idea.

Contraction kinetics were largely normal in diseased muscles with the exception of the EDL from myogenic 141 Tg males where twitch rise time was significantly prolonged (Table 3). These data in addition to deficits in the twitch/tetanus ratios also implicate calcium handling mechanisms, particularly the RyR1. Both defects could readily be explained by altered channel

properties in RyR1 that lead to inefficient or reduced calcium efflux from the sarcoplasmic reticulum. Parvalbumin also represents a candidate molecule that may underlie the selective effects on contractions kinetics in the 141 EDL. This protein is expressed only in fast-twitch muscles where it buffers calcium upon its release from the sarcoplasmic reticulum to regulate twitch kinetics. For example, parvalbumin overexpression has been shown to shorten twitch rise time in the SOL (Chin et al., 2003) while reducing its expression in the EDL leads to prolonged rise times (Schwaller et al., 1999). Microarray data indicate that parvalbumin mRNA level is downregulated ~17-fold in hindlimb muscle of affected myogenic male mice, whereas it is only modestly downregulated (3-4 fold) in hindlimb muscles of 97Q males and it is normal in KI males (Mo et al., 2010). Thus, the large decrease in parvalbumin expression seen only in the EDL of myogenic males may explain the prolonged rise time of the twitch in this muscle. However, reduced parvalbumin also predicts prolonged relaxation time (Schwaller et al., 1999) which we do not find (Table 3). Moreover, decreased parvalbumin also increases the force of the twitch (Schwaller et al., 1999), just the opposite of how disease affects twitch force. Thus, changes in parvalbumin expression in the myogenic EDL are unlikely to explain the prolonged rise time seen in this muscle.

Skeletal muscles of affected 97Q and myogenic 141 Tg males may also have altered metabolic properties as suggested by the fatigue data. The EDL of myogenic Tg males exhibited greater resistance to fatigue than WT controls, losing less total force over the course of the experiment (Fig 15A). These data are consistent with previous findings of a more oxidative profile (Fernando et al., 2010; Monks et al., 2007). The SOL of myogenic males, on the other hand, exhibited little drop in force output with repeated stimulation, but we suspect this is because force output was near basement to begin with (Fig 14H, K). Nonetheless, what force was

lost, occurred at a faster rate, with the SOL from 141 Tgs losing 50% of their original force ~4 times faster than WT EDL. Both the EDL and SOL muscles of 97Q males show less resistance to fatigue compared to WT controls (Fig 13). While mitochondrial function in muscles of 97Q mice have not been studied, the effects of the 97Q AR transgene in neuron-like cell cultures suggest that mitochondria are defective in 97Q muscles (Ranganathan et al., 2009).

The current work suggests that primary defects in muscle function may underlie the loss of motor function in SBMA. Finding elevated levels of serum creatine kinase consistently in SBMA patients also implicates muscle as a primary site of AR action in this disease (Battaglia et al., 2003; Chahin and Sorenson, 2009; Soraru et al., 2008; Sorenson and Klein, 2007). In summary, data from isolated fast and slow twitch muscles indicate that defects in skeletal muscle function may contribute to deficits in motor function in two different mouse models of SBMA. While muscle strength may well be reduced by reductions in mass, significant losses in strength occur independent of muscle mass. Muscles from SBMA models affected by disease are also generally more susceptible to fatigue. Future studies aimed at developing therapies that block the toxic effects of AR in skeletal muscle may offer significant benefits to SBMA patients.

GENERAL DISCUSSION

General Findings

The current findings confirm that skeletal muscles exhibit androgen-dependent dysfunction in models of spinal and bulbar muscular atrophy (SBMA). In general, force loss or inability to produce normal force in skeletal muscles may underlie the motor dysfunction observed in diseased mice modeling SBMA. This was demonstrated in testosterone (T)-treated transgenic (Tg) female mice of a myogenic (141) model and in male Tg mice of the 141 and the CAG-expanded 97Q model that exhibit androgen-dependent motor dysfunction. The current data add to clinical data suggesting primary skeletal muscle involvement in SBMA. Previous reports find elevated serum creatine kinase levels in SBMA patients comparable to what are seen in patients suffering from primary myopathies, such as Duchenne's muscular dystrophy or myotonic dystrophy (Arenas et al., 1988; Ebashi et al., 1959; Heatwole et al., 2006; Vassella et al., 1965) but notably, not in patients who have amyotrophic lateral sclerosis (ALS) (Chahin and Sorenson, 2009). However, this is the first line of research that examines directly the *function* of skeletal muscles in diseased SBMA mice compared to healthy controls using an isolated *in vitro* preparation that is separated from the nervous system.

Overview of findings

In vitro muscle mechanics in all tested muscles measured force, kinetics, and fatigue. Muscle force was measured by inducing twitch and tetanus in the predominantly fast-twitch extensor digitorum longus (EDL) and predominantly slow-twitch soleus (SOL). All measurements were normalized to skeletal muscle mass, and the deficits in muscle force still remained, suggesting mechanisms aside from atrophy likely mediate muscle dysfunction. Force

production of skeletal muscles at the beginning and end of experiments suggest force loss was not due to decay of the preparations *in vitro*. Although previous studies suggest atrophy genes are upregulated in muscles of SBMA mice (Mo et al., 2010), the current physiological data, particularly from female SBMA mice, indicate cell dysfunction precedes cell atrophy or death (Oki et al., 2013) and likely underlies the expression of early disease symptoms. Thus, atrophy and death of skeletal muscle fibers and, possibly, motoneurons are likely when symptoms are advanced in SBMA rather than being the underlying cause of the disease.

Although muscle weakness was present in both sexes of the 141 model and in males of the 97Q model, the force loss in skeletal muscles was different between sexes within the 141 model and between males across Tg models. The different muscle weakness was based on fiber-type composition between the fast-twitch EDL and the slow-twitch SOL. Differences in motor unit vulnerability has been observed in other disease models as fast motor units tend to be more affected in ALS models (Atkin et al., 2005; Hegedus et al., 2007; Hegedus et al., 2008) while slow motor units may be more vulnerable in SMA models (Murray et al., 2008). In the current SBMA studies, females 141 Tg mice treated with T exhibited loss of force and endurance in both the EDL and SOL, but the SOL showed a more severe force loss than the EDL. Like diseased Tg females, male 141 Tg mice exhibited loss of force and endurance in SOL, which was more severe than what was measured in the EDL. However, male 141 Tg mice did not exhibit loss of tetanus force in the EDL and showed higher endurance in the Tg EDL compared to WT EDL. It is uncertain if the difference in males versus females in the 141 model occurs due to the time period of disease symptoms or due to differences in development. It is possible that genetic adaptations in skeletal muscles may have occurred in male mice surviving longer with chronic disease symptoms and is reinforced by microarrays showing a different gene expression profile

in male 141 Tg mice compared to male WT mice (Mo et al., 2010). Alternatively, because the disease is present in male 141 Tg mice from a prenatal stage, skeletal muscle and motor unit development could have been altered in these mice. In cell cultures, myoblasts expressing AR with a reduced or expanded CAG region had abnormal muscle development, suggesting this could occur with muscles in SBMA subjects during early development (Sheppard et al., 2011). Although the 141 Tg mice have a normal CAG repeat numbers, they overexpress the protein and have a similar phenotype to the CAG-expanded SBMA models. Thus, it is possible that the disease phenotype compromises muscle development in male 141 Tg mice compared to WT mice. In contrast, acutely diseased females were treated with T in adulthood and likely did not have altered development. The period of T treatment (3-5 days) and subsequent muscle weakness is likely too short of duration to induce significant genetic changes or adaptations in skeletal muscles and could have contributed to the differences seen between the sexes in Tg mice of the 141 model. In male mice of the 97Q model, the EDL and SOL exhibited weakness during twitch and tetanus, but unlike the 141 model, the EDL was more severely weakened rather than the SOL. Although differences in muscle weakness between fiber types could be due to different *in vivo* functions of the EDL and SOL in the animals (i.e. sporadically activated for movement vs. chronically activated for posture), such an effect would likely result in a similar pattern of muscle weakness across SBMA models. As this was not observed, it is likely that different effects are due to AR toxicity having different effects due to fiber-specific properties of the EDL and SOL across the two Tg models.

Examination of skeletal muscle histology during the disease phenotype suggests pathological markers in the skeletal muscles were not always accurate predictors for muscle dysfunction. Although the frequency of fibers with internalized nuclei was correlated with the severity of

force loss in the 97Q and 141 myogenic models, the SOL from T-treated female 141 Tg mice had little to no pathological markers in skeletal muscle cross sections but exhibited severe force loss. Conversely, EDL from male 141 Tg mice had greater loss of mass and a greater presence of internalized nuclei than WT controls but exhibited the same output of normalized maximal force as EDL's from male WT control. This suggests that standard histological markers of disease are not very informative about the mechanisms underlying functional deficits in disease.

Although mice from two of the investigated models exhibited skeletal muscle dysfunction, intact male mice in the third model, the knock-in's (KI) with the diseased exon 1 allele containing 113 repeats of the codon CAG, similar to humans (Thomas et al., 2005; Yu et al., 2006), did not exhibit differences in skeletal muscle function between KI and WT controls in spite of motor dysfunction in KI mice. The loss of motor function could be due to non-specific effects due to an inability to evacuate their bladders, presynaptic rather than postsynaptic effects underlying disease symptoms in this particular model (Kemp et al., 2011), or skeletal muscle dysfunction not being present in the particular muscles investigated because they are not androgen-responsive in rodents (Souccar et al., 1982). In fact, the muscle effects observed in the KI model in a previous study were in the androgen-dependent bulbocavernosus/levator ani muscles, suggesting mechanics may be affected based on androgen-dependence of skeletal muscles.

In addition to force measurements, kinetic measurements were recorded during the time to peak force (rise time) and time to return to baseline (relaxation time) during a twitch stimulation. Rise time is dependent on the release of Ca from the sarcoplasmic reticulum (SR) initiated by dihydropyridine receptors and ryanodine receptor 1 (RyR1), and relaxation time is dependent on Ca reuptake into the SR by sarcoendoplasmic reticulum ATPase (SERCA). Alterations to either

measurement suggest impaired Ca handling in the skeletal muscles and would warrant further investigation into the level and function of the main proteins during the separate contraction events. Only the 141 model exhibited differences in the rise and relaxation measurements. Delays in rise and relaxation times were recorded in T-treated female Tg mice, and delayed rise time was recorded in male Tg mice.

Finally, fatigue measurements were induced by repetitive tetanic stimulation in the EDL and SOL. This test indicates whether the disease phenotype could be due to differences between susceptibility to fatigue in muscles of symptomatic and asymptomatic mice. Based on the susceptibility to fatigue, inferences can also be made on the fiber type composition of each muscle as done in Burke et al. (1971). Histochemical staining, particularly stains for myosin types, mitochondrial complexes, and periodic acid Schiff could be done on sections tested during the fatigue protocol to validate speculation on alterations to muscle fiber composition in these mice. This would be relevant as some disease conditions result in changes to motor units that affect their endurance (Kieran et al., 2005).

Mechanisms of Muscle Dysfunction

It is still unclear what mechanisms are involved in underlying the skeletal muscle dysfunction. The heterogeneity of the muscle weakness across fiber types in spite of similar androgen-dependent disease phenotypes suggests there may be more than one universal mechanism underlying skeletal muscle dysfunction in the different groups. However, several lines of evidence suggest that examining calcium (Ca) as handling mechanisms, trophic factors, and metabolic pathways in muscle could provide insight into the mechanisms causes skeletal muscles to become dysfunctional.

Calcium Mechanisms

Ionic concentrations in general may underlie the motor and skeletal muscle dysfunction observed in the SBMA mice. Yu et al (2006) noted that in the KI model of SBMA, chloride (Cl) channel expression was decreased in the skeletal muscles of the perineum. This is in line with features in myotonic dystrophy where decreased Cl channels are thought to underlie the hyperexcitability and myotonia in skeletal muscles. One would predict that this would require a lower stimulating voltage to initiate muscle contractions in diseased EDL and SOL as decreased Cl channels would raise the resting membrane potential of muscles closer to the threshold for activation. Differences in stimulation voltages were not observed in the current studies, but this may be due to the method involving parallel electrodes where the distance between the electrodes has a greater influence on the stimulation voltage rather than inherent properties of the skeletal muscle. Future experiments could examine Cl channel expression levels in weaker skeletal muscles and the voltage required to elicit a muscle response during direct stimulation on the surface of the muscle membrane. This could determine whether Cl channel loss/dysfunction is a possible mechanism of muscle weakness.

Possible involvement of Ca mechanisms has been indicated by the current and previous research into mice with weaker muscles. Nearly all Tg muscles in the 97Q and 141 models had lower twitch to tetanus ratios compared to WT controls, indicating a greater deficit in twitch force compared to tetanic force in diseased muscles. These findings are suggestive of abnormalities in Ca handling mechanisms during contractions. The delays in rise and relaxation times in T-treated female Tg mice and rise time in male Tg mice of the 141 model also suggest impaired Ca handling.

Previous microarrays in the 141 model indicate decreased parvalbumin (PV) gene (17-fold downregulation) in muscles from Tg compared to WT controls (Mo et al., 2010). This also suggests protein levels for PV could be decreased in diseased muscles. PV buffers Ca levels during muscle contractions and shortens rise and relaxation times in rodent muscles with a greater proportion of fast-twitch muscle fibers (Heizmann et al., 1982). PV decreases could lead to the delay in rise and relaxation times in EDL's from T-treated 141 Tg females and the delay in rise time of the 141 Tg male EDL's, but there were no effects on relaxation times in 141 Tg male EDL's. Additionally, aside from the kinetic effects, the decline in PV expression in muscle would not explain the loss of force (Schwaller et al., 1999). Thus, if Ca handling mechanisms are affected, it would likely occur during the phases when Ca acts as the messenger during contraction: 1) release from the sarcoplasmic reticulum, which is mediated by dihydropyridine receptors (DHPR) and ryanodine receptor 1 (RyR1), 2) Ca binding of troponin C (TnC) to remove tropomyosin from actin binding sites, and 3) relaxation with sarcoendoplasmic reticulum ATPases (SERCA's) returning Ca back into the sarcoplasmic reticulum (SR). Each of these specific mechanisms could be impaired and contribute the deficits in contractile function of diseased muscles.

Involvement of RyR1 was implicated by the severe force loss concomitant with delay in kinetics, specifically in the 141 Tg EDL's. Although their studies did not exhibit changes in rise time, Bellinger et al. (2008, 2009) suggest leaks in RyR1 may underlie the disease phenotype in Duchenne muscular dystrophy (DMD). As Ca leaks out of the SR, it is hypothesized that protein degradation and cell death occur, leading to aberrant skeletal muscle morphology and function. Additionally, leaks may activate Ca-dependent proteases, such as calpains (Spencer et al., 1995), that lead to the muscle pathology seen in the EDL of 141 Tg mice (Johansen et al., 2011). The

hypothesis for RyR1 leaks leading to muscle damage and weakness was reinforced when S107, a compound that prevents RyR1 leaks, was given to mice modeling DMD and resulted in overall improvement in motor function and skeletal muscle structure as well as decreased calpain activity compared to mice receiving vehicle (Bellinger et al., 2009). In the SBMA models, defective RyR1 would likely lead to increased basal tension, a measurement not tested in the mechanics studies but important to find in future studies, and would likely manifest as hypertonia or rigidity in mice. This is observed in humans and pigs with cases of malignant hyperthermia (MH). The underlying genetic basis for MH is a mutation on the RyR1 gene in skeletal muscles, and the condition is triggered by certain anesthetics and/or nondepolarizing muscle relaxants. The binding of the compounds results in a continuous release of Ca ions, leading to rigidity, and increased metabolic activity leading to higher body temperatures (Mickelson and Louis, 1996). Although 141 Tg mice may exhibit muscle rigidity, they did not exhibit differences in body temperatures compared to WT controls (data not shown). One way of testing whether RyR1-related Ca leaks underlie the weakness would be to treat diseased 141 Tg mice with S107, a compound that prevents RyR1 leaks (Bellinger et al., 2008), and measure whether that leads to motor improvements (at the behavioral level) and return of muscle function. However, this would only explain the results in the fast-twitch EDL's of the 141 Tg mice. The greatest force deficits seen in the EDL's of 97Q mice and SOL's of 141 Tg mice occur in the absence of any kinetic changes and may be due to other Ca-related mechanisms.

Evidence for the involvement of TnC is inferred from microarrays showing that expression of the slow TnC gene is downregulated in limb muscles from male 141 Tg mice. Slow TnC is primarily found in slow-twitch and cardiac muscles, and its decrease could explain the force loss in the SOL of myogenic 141 Tg mice. To assess this possibility, one could estimate the amount

of TnC protein in muscle by Western blotting (Hartner and Pette, 1990). However, loss of protein may not explain the loss of force in T-treated 141 Tg females due to the rapid onset of weakness: after 3 days of T exposure, force is maximally reduced in the SOL but the TnC half life (Martin, 1981) is much longer. Moreover, the fast TnC isoform found in fast-twitch skeletal muscles was not reported to be decreased in male 97Q Tg mice (Mo et al., 2010) but nonetheless, it was the EDL that showed the most severe loss in force in this model. However, before TnC is ruled out as a possible mechanism underlying muscle weakness, in T-treated 141 Tg females and 97Q males, it would be necessary to examine not just TnC levels but also its function. TnC is pH-sensitive and has decreased affinity to bind Ca at lower pH during conditions such as acidosis (Parsons et al., 1997). Thus, function can be affected without changes in protein levels. If TnC does not properly bind Ca, it is likely that less binding sites on actin are available for myosins, leading to decreased force. A way to investigate whether TnC binding affinity is affected is to examine skeletal muscle function using skinned fiber experiments. In brief, this method involves either chemically or mechanically “skinning” the fibers to remove their plasma membrane and then image Ca binding using Ca-sensitive dyes. After the initial imaging, TnC can be extracted to deplete muscle fibers of TnC. Comparisons of the initial and final images indicate whether TnC was functional in the skeletal muscles (Patel et al., 1997). This approach could be done in conjunction with Western blots or ELISAs to estimate the amount of specific TnC isoforms in diseased and healthy muscle.

Finally, SERCA involvement with RyR1 dysfunction may also result in muscle weakness. Slowed relaxation was observed in T-treated female 141 Tg mice also suggesting possible SERCA defects in those mice. Due to the rapid occurrence of the phenotype, it may be possible that part of the initial onset of disease is due to SERCA dysfunction. Apart from the continuous

contraction leading to ATP hydrolysis in the actin-myosin interactions due to a RyR1 leak, SERCA also utilizes ATP during reuptake of Ca against the Ca gradient (MacLennan et al., 1997). With SERCA constantly activated by Ca presence due to RyR1 leaks, it may be possible that SERCA function is compromised due to the metabolic stress. To determine whether this is an issue of SERCA downregulation vs. dysfunction, SERCA Western blots could be run to indicate or eliminate quantity as the underlying issue (Chami et al., 2001). Additionally, missplicing of SERCA and RyR1 has been observed in mice modeling myotonic dystrophy (Kimura et al., 2005) and may be worth investigating if alterations to protein structure lead to functional deficits in the current SBMA models. This could be done using the RT-PCR analysis described by Kimura et al. (2005) to determine splice variants within EDL and SOL of SBMA mice.

Trophic Factors

Several muscle-derived trophic factors have been found to be decreased in skeletal muscle of diseased SBMA mice. In addition to Ca mechanisms, it is of interest to investigate whether trophic factors in skeletal muscles may alter the disease phenotype. One trophic factor, insulin-like growth factor I (IGF-1) has been shown to improve motor function and increase survival in ALS and SMA models when given directly to skeletal muscles (Bosch-Marce et al., 2011; Dobrowolny et al., 2005). Those results have been replicated in SBMA models by crossing mice with skeletal muscle-restricted IGF-1 overexpression with 97Q mice (Palazzolo et al., 2009) or by injecting 97Q mice with IGF-1 (Rinaldi et al., 2012). It is currently unknown what would occur if IGF-1 were overexpressed by crossing in the 141 Tg mice or were injected into the 141 Tg mice. Another trophic factor, glial cell line-derived neurotrophic factor (GDNF) has also

produced improvement in neurodegenerative mouse models. Grafting myoblasts modified to secrete GDNF into hindlimb muscles of mice modeling ALS with a SOD1 mutation resulted in improvement of motor function and motoneuron survival (Mohajeri et al., 1999). Furthermore, similar to the IGF-1 study, crossing mice with muscle-specific GDNF overexpression with G93A ALS mice improves disease phenotype in the resulting offspring (Li et al., 2007). Vascular endothelial growth factor (VEGF) has also been shown to be consistently decreased in skeletal muscles from diseased mice (Monks et al., 2007). However, VEGF levels are still decreased upon recovery of motor function and may proceed from, rather than underlie, muscle weakness (Johansen et al., 2009). Thus, experiments manipulating trophic factor levels in diseased mice could lead to a better understanding of their roles during disease and improvement. Additionally, recovery experiments in Tg mice could be used to examine trophic factor levels in skeletal muscles during disease phenotype and at several different timepoints during recovery.

Metabolic Mechanisms

Data from the 141 model have consistently shown that metabolic properties are altered in rodents overexpressing WT AR in skeletal muscle fibers. The EDL of male Tg mice consistently exhibit a more oxidative profile with NADH-TR staining (Johansen et al., 2011; Monks et al., 2007). This is in line with functional alterations observed in the isolated EDL from 141 Tg males showing greater endurance during the fatigue stimulation protocol. Additionally, mice and rats overexpressing WT AR in muscles have decreased fat pads and increased mitochondrial complex activities (Monks, unpublished observations; (Fernando et al., 2010; Musa et al., 2011)). However, it is unknown whether the shift in metabolic properties precedes or proceeds from alterations in muscle function as metabolic mechanisms may also be related to Ca-related

mechanisms. Increased PV expression has been shown to decrease activity of succinate dehydrogenase, a mitochondrial marker enzyme (Chin et al., 2003) while mice with decreased PV have increased cytochrome C oxidase activity and mitochondrial volume (Chen et al., 2001). This is relevant to the current studies as male 141 Tg mice exhibited PV gene downregulation in microarrays (Mo et al., 2010). Overexpressing activated calcineurin, a Ca-dependent phosphatase, leads to higher levels of slow-twitch fibers and lower PV levels (Chin, 2004; Naya et al., 2000; Wu et al., 2001). Increased Ca levels also activate calcium/calmodulin-dependent kinases leading to mitochondrial biogenesis (Fluck et al., 2000; Wu et al., 2002) and a slow-twitch phenotype. Thus, while metabolic alterations may underlie the muscle weakness and motor dysfunction, metabolic alterations may also be a consequence of Ca handling issues in the skeletal muscles. Aside from possible mechanisms inducing changes in muscle phenotype, if Ca is unable to bind TnC in 141 Tg SOL, as stated previously, it is possible that muscles are not producing enough force to induce fatigue during testing, another line of reasoning that suggests deficits in Ca handling may underlie some of the metabolic alterations seen in skeletal muscles.

Future Directions

Given all of the data, it would be prudent to investigate Ca mechanisms using an initial immunoblot of relevant Ca handling proteins and proceeding to examine function of the proteins of interest. Trophic factor experiments focusing on IGF-1 and GDNF could be conducted by manipulating levels in diseased mice, or by monitoring their levels during different stages of disease and recovery. Finally, metabolic mechanisms should also be investigated by examining mitochondrial activity and levels in muscles. However, such experiments should be done in

conjunction with Ca-related experiments to determine the extent of or to rule out overlap between the two mechanisms.

Conclusions

While previous studies have suggested skeletal muscle involvement in SBMA, the current findings indicate unequivocally that primary skeletal muscle dysfunction is an important event during the loss of motor function in SBMA. While it is still unclear what mechanisms may underlie the disease phenotype, several experiments have been suggested that target potential mechanism(s) that cause the loss of muscle strength. Because contraction kinetics were not uniformly affected across muscles from the different SBMA models, it is not clear whether to expect slower contraction kinetics in muscles of SBMA patients. Nonetheless, it seems likely that mutant AR exerts direct toxic effects in muscle that impair its function independent of regressive changes in the strength and viability of its motoneuronal inputs.

APPENDIX

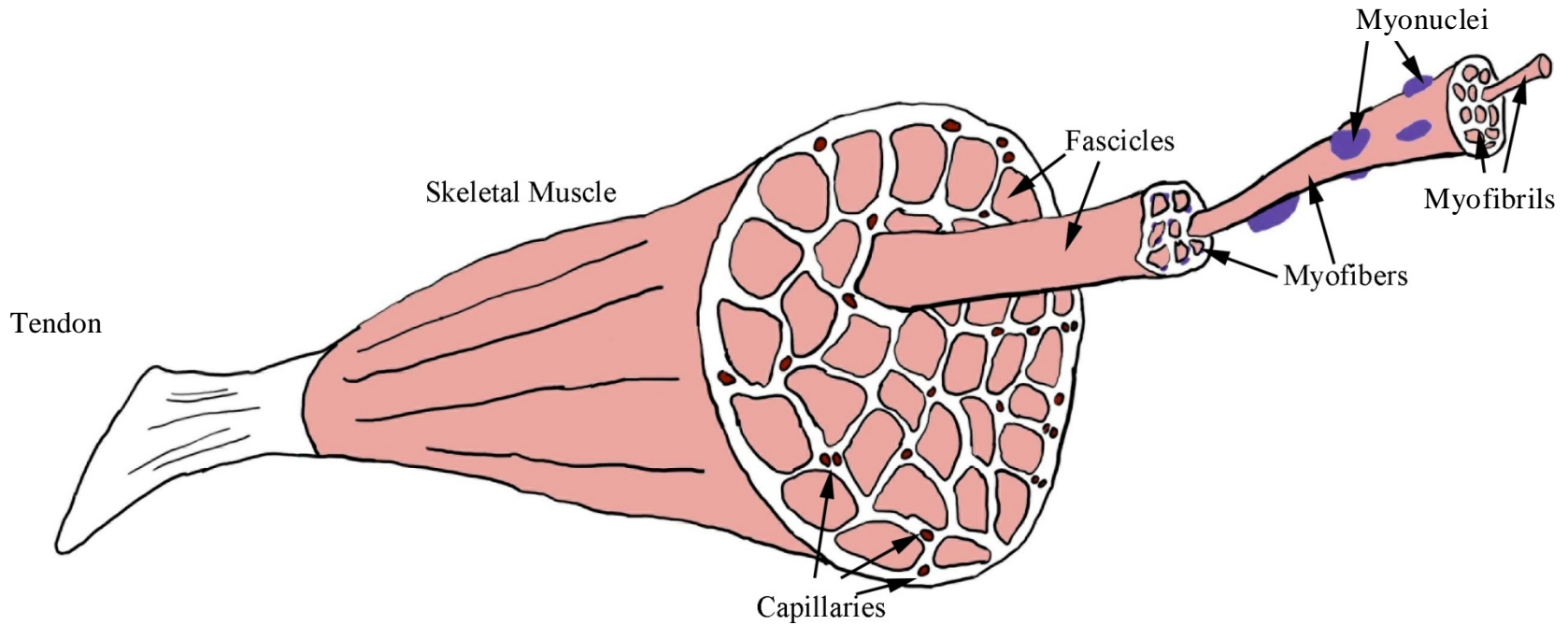


Figure 1. For interpretation of the references to color in this and all other figures, the reader is referred to the electronic version of this dissertation. The whole skeletal muscle is comprised of multiple fascicles with capillaries between fascicles providing a blood supply. Fascicles are then comprised of multiple myofibers. Myofibers are large, multinucleated individual cells of a skeletal muscle and are comprised of myofibrils.

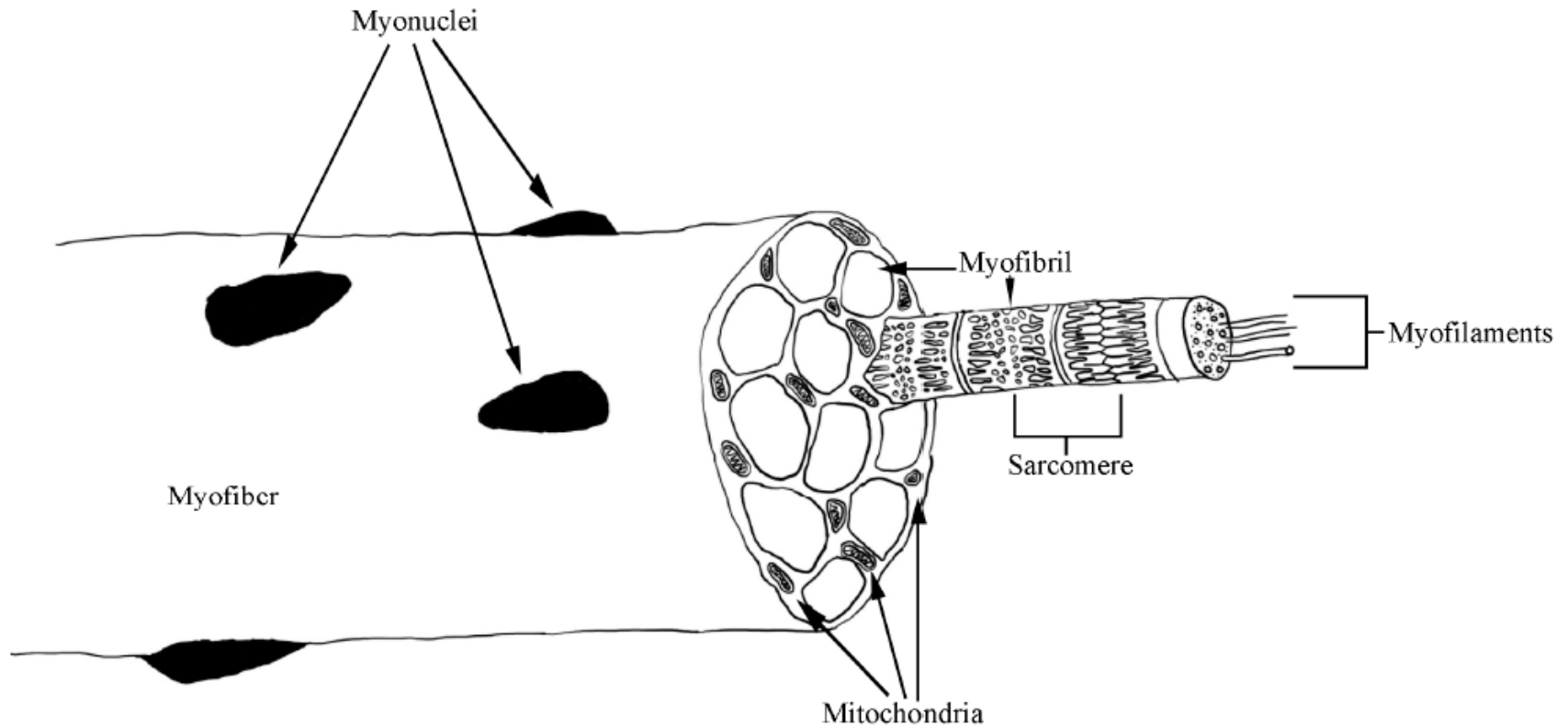


Figure 2. Large multinucleated myofibers contain the mitochondria on the muscle periphery to aid in muscle energetic. Myofibrils comprise the myofiber and are, in turn, comprised of myofilaments. Along myofibrils are sarcomeres, the most basic unit of a skeletal muscle that allows for a contraction. Upon electrical stimulation, multiple sarcomeres shorten within a muscle resulting in whole muscle shortening to produce a contraction.

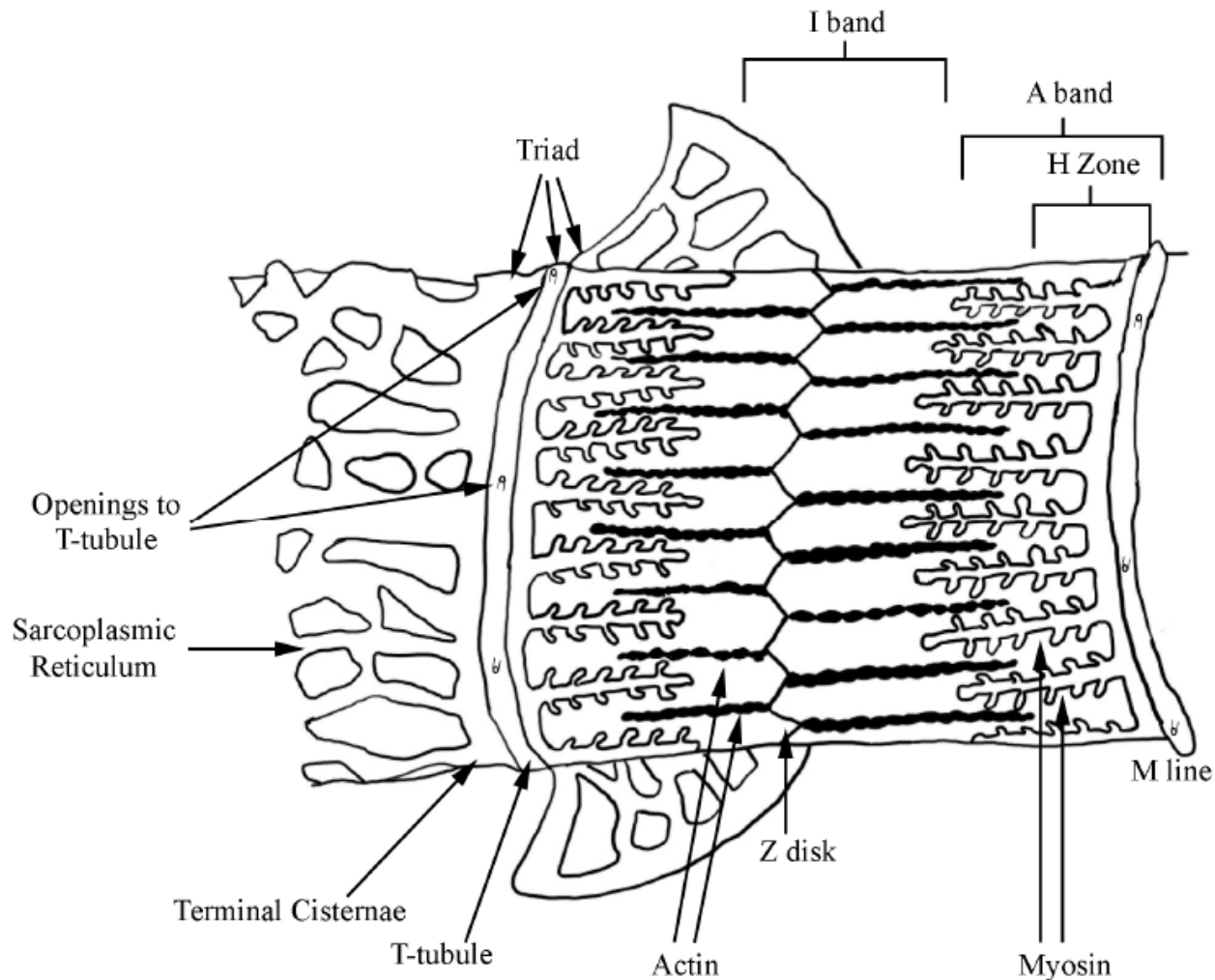
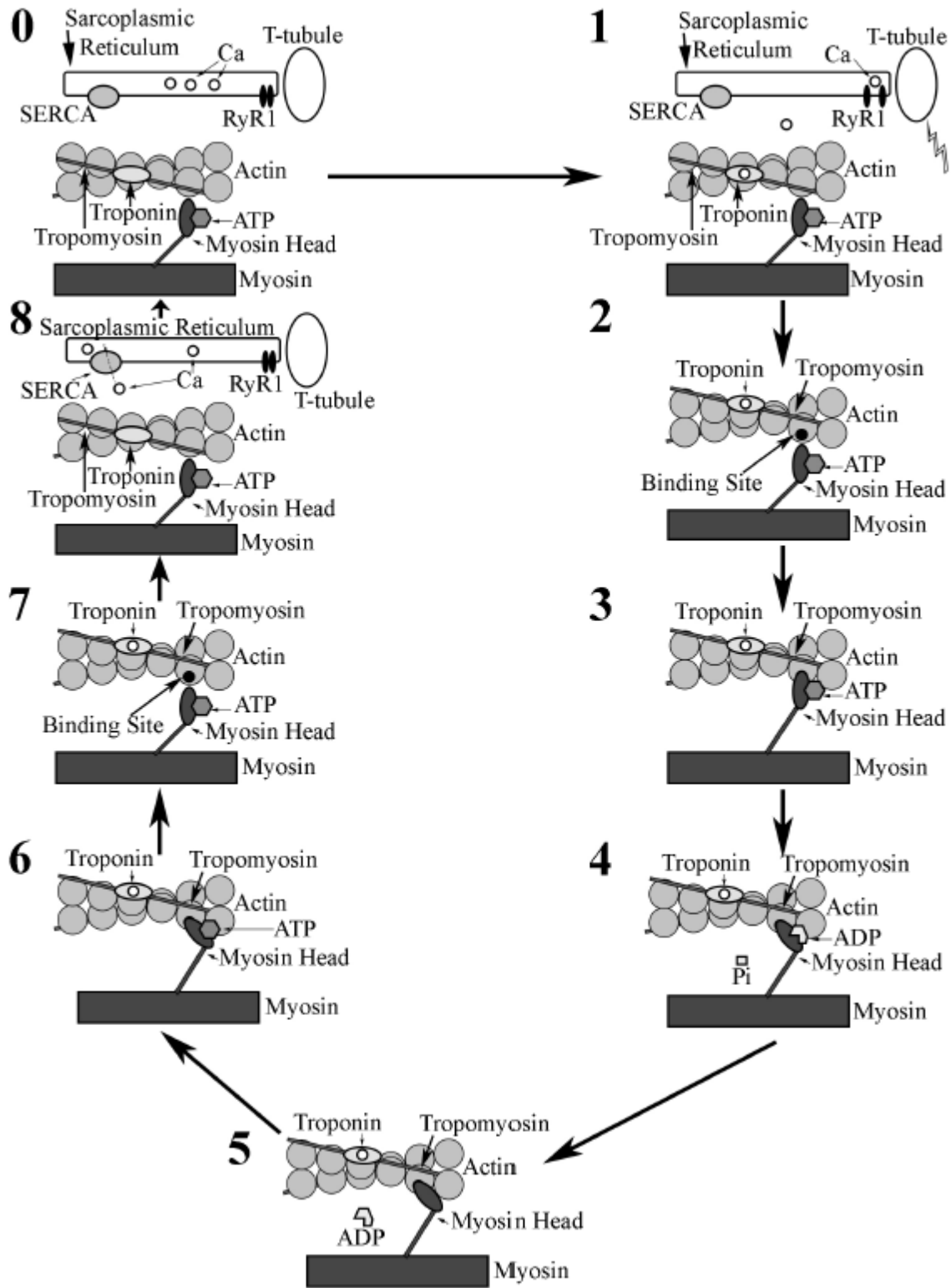


Figure 3. The myofilaments that comprise myofibrils and sarcomeres are shown when the overlying sarcoplasmic reticulum (SR) is removed from the myofibril. Myosin and actin form an interdigitating pattern throughout the myofibril to allow contractions. Myosin are anchored at the M line while actin is anchored by Z disks. Regions of the SR closer to the T tubules are termed the terminal cisternae. T-tubules that run on either side of the interdigitating region contain openings that form a triad with the terminal cisternae. These regions are where the electrical stimulus initiates muscle contractions.

Figure 4. 0) The first image at the top right lists the key proteins involved during a skeletal muscle contraction. A T-tubule is in contact with the sarcoplasmic reticulum (SR) containing calcium (Ca) ions that will initiate contraction. Ryanodine receptor 1 (RyR1) is closed, and sarcoendoplasmic reticulum Ca ATPase (SERCA) is inactive while Ca is within the SR. On the actin filament, tropomyosin covers the binding site preventing myosin heads from binding to actin. 1) With a voltage change, T-tubules conduct the electrical depolarization to initiate the opening of RyR1, releasing Ca from the SR. Upon Ca release from the SR, it binds to the Ca-sensitive subunit of the troponin complex. This also initiates SERCA function, but the large release of Ca into the cytosol is greater than the rate at which Ca is replaced into the SR. 2) Ca binding of troponin induces a conformational change in troponin removes the troponin-tropomyosin complex away from the actin filament, exposing the actin binding sites. 3) A myosin head binds to the actin binding site, and 4) ATP is hydrolyzed, resulting in ADP and inorganic phosphate. Once phosphate is released, the myosin head turns. 5) With the release of ADP, the myosin head is turned even further, moving the actin filament, shortening the sarcomere, and resulting in a power stroke to initiate skeletal muscle contraction. This shortening in the sarcomeres produces the contractile force generated by muscles. In cases where ATP is depleted, the myosin head remains in this locked position on the actin filament. 6) As long as ATP is available, another ATP binds to the myosin head. 7) This releases the myosin head from the actin filament, returning the myosin head to its original position (same as step 2). 8) Once the skeletal muscle returns to resting potential, RyR1 closes, and SERCA, its function initiated when Ca entered the cytosol, is able to return Ca back to the SR against the Ca concentration gradient (dashed arrow). Consequently, TnC no longer binds Ca, and the troponin-tropomyosin complex returns to its resting state where tropomyosin covers the myosin binding sites on actin. 0) With Ca return to the SR, the entire region is ready for another contraction.

Figure 4 (cont'd)



		Treatment Groups			
		Wild Type		Transgenic	
		B	T	B	T
Muscle Weights (mg)	EDL	8.0±0.4	8.6±0.2	9.5±0.3	8.6±0.3
	SOL	7.6±0.2	8.3±0.6	9.3±0.4	9.4±0.4
Plasma T Levels (nmol/L)		1.4±0.3	29.3±1.8	1.2±0.1	49.5±5.9
Normalized Peak					
Twitch Force (N/g)	EDL	6.67±0.73	7.48±0.42	7.20±0.47	4.21±0.40*
	SOL	3.22±0.20	3.38±0.23	3.25±0.19	0.45±0.04*
Twitch/Tetanus					
Ratio (5 Day T)	EDL	0.21±0.01	0.24±0.01	0.21±0.01	0.24±0.01
	SOL	0.17±0.01	0.18±0.01	0.21±0.00	0.12±0.01*
(3 Day T)	EDL	NA	0.27±0.02	NA	0.23±0.02
	SOL	NA	0.21±0.02	NA	0.13±0.02*
Protein					
Content(mg)/Muscle weight(g)	EDL	47.6±8.8	66.0±14.8	53.1±7.4	41.5±6.6
	SOL	52.2±18.5	66.9±12.1	43.5±13.2	55.9±10.1

Table 1. Biometric data for female 141 mice. T, testosterone; mg, milligrams; nmol/L, nanomolar per liter; N/g, newtons/gram. Values are means ± standard error of means. * $P < 0.05$.

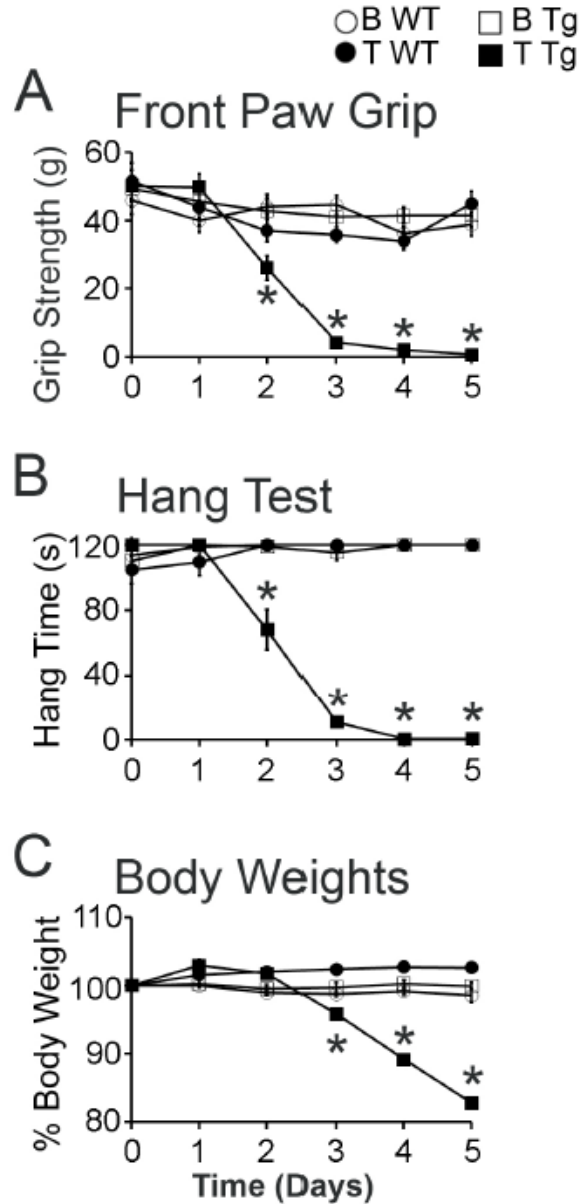


Figure 5. Motor function declines rapidly in testosterone (T)-treated adult female transgenic (Tg) mice that express a wild-type androgen receptor (AR) transgene only in skeletal muscle fibers. Baseline performance at Day 0 before hormone treatment did not differ across treatment groups. T treatment induced a rapid decline in grip strength (A), hang time (B), and body weight (C) only in Tg females. By Day 5, motor performance on both tests was decreased significantly for T-treated Tg (T Tg) females compared to baseline or compared to the other groups, including asymptomatic females that were blank-treated wild-type (B WT), testosterone-treated wild-type (T WT), and blank-treated transgenic (B Tg). Each asymptomatic group maintained pre-treatment performance levels on both the grip strength and hang tests across the 5 days of treatment, indicating that only the combination of AR transgene expression in muscle fibers and male levels of androgens instigates motor dysfunction. Values are means \pm standard errors of means based on N = 5-6 mice/muscle and group. * $P \leq 0.05$, T Tg versus B Tg or T WT.

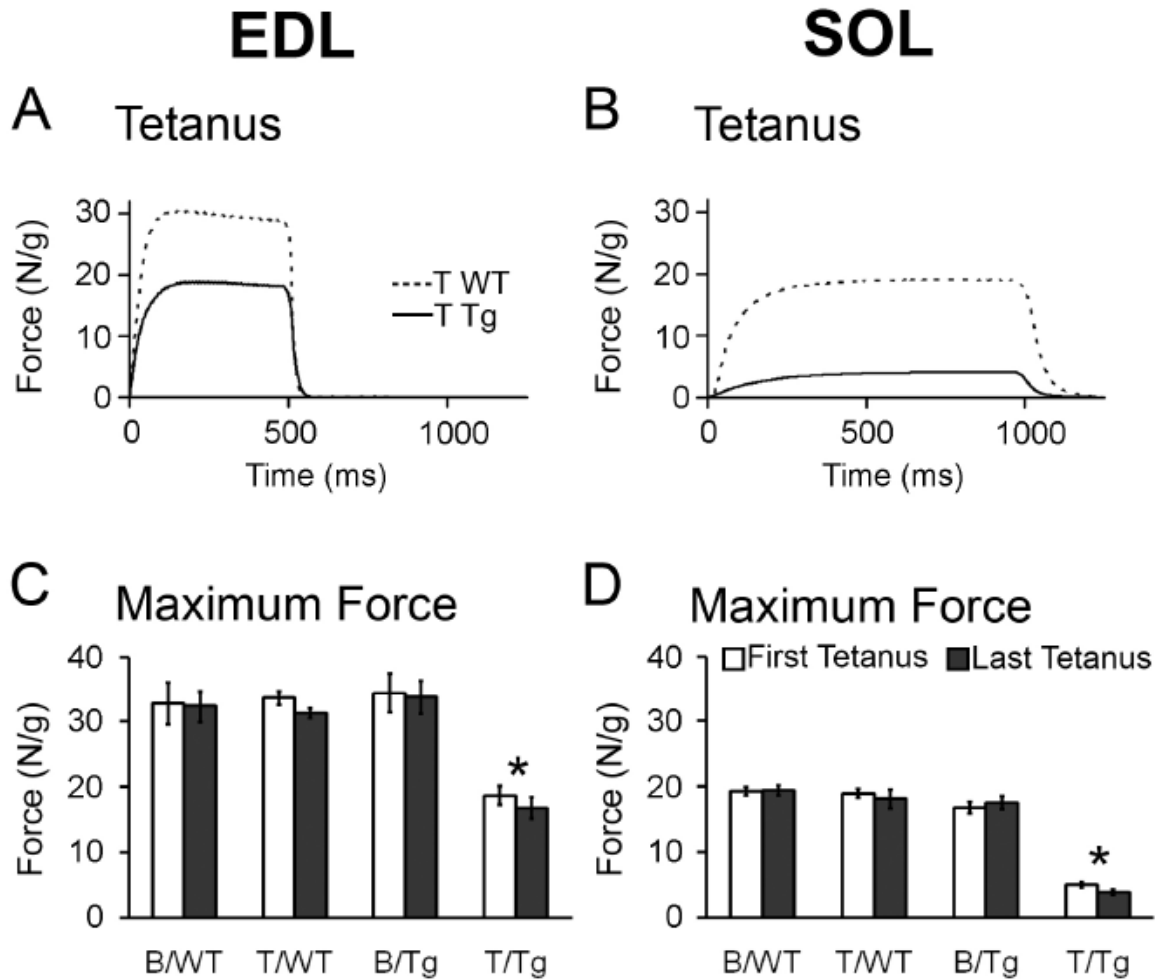


Figure 6. Tetanic force produced by both EDL and SOL of motor-impaired female mice is reduced significantly compared to tetanic force produced by corresponding muscles of asymptomatic controls after 5 days of testosterone (T) treatment. Representative traces for T WT muscles and T-treated transgenic (T Tg) muscles are shown (A, B). Tetanic force produced by the EDL of T Tgs is about half of control females (C), whereas tetanic force produced by the SOL of T Tg females is about a quarter of T WT controls (D). Tetanic force produced by muscles of control-treated Tg females (B/Tg) is equivalent to that of WT, indicating that AR transgene expression *per se* does not impair muscle strength. Comparable force deficits are observed at the beginning and end of experiments (indicated as first and last tetanus) for both EDL and SOL of T Tg mice, suggesting that force deficit is present *in vivo* and is not due to a more rapid deterioration of these muscles *in vitro*. Force (in Newtons-N) was normalized to muscle wet weight (grams-g). Values in histogram are means \pm standard errors of means, N = 5-6 mice/group. * $P < 0.001$, T Tg versus B Tg or T WT.

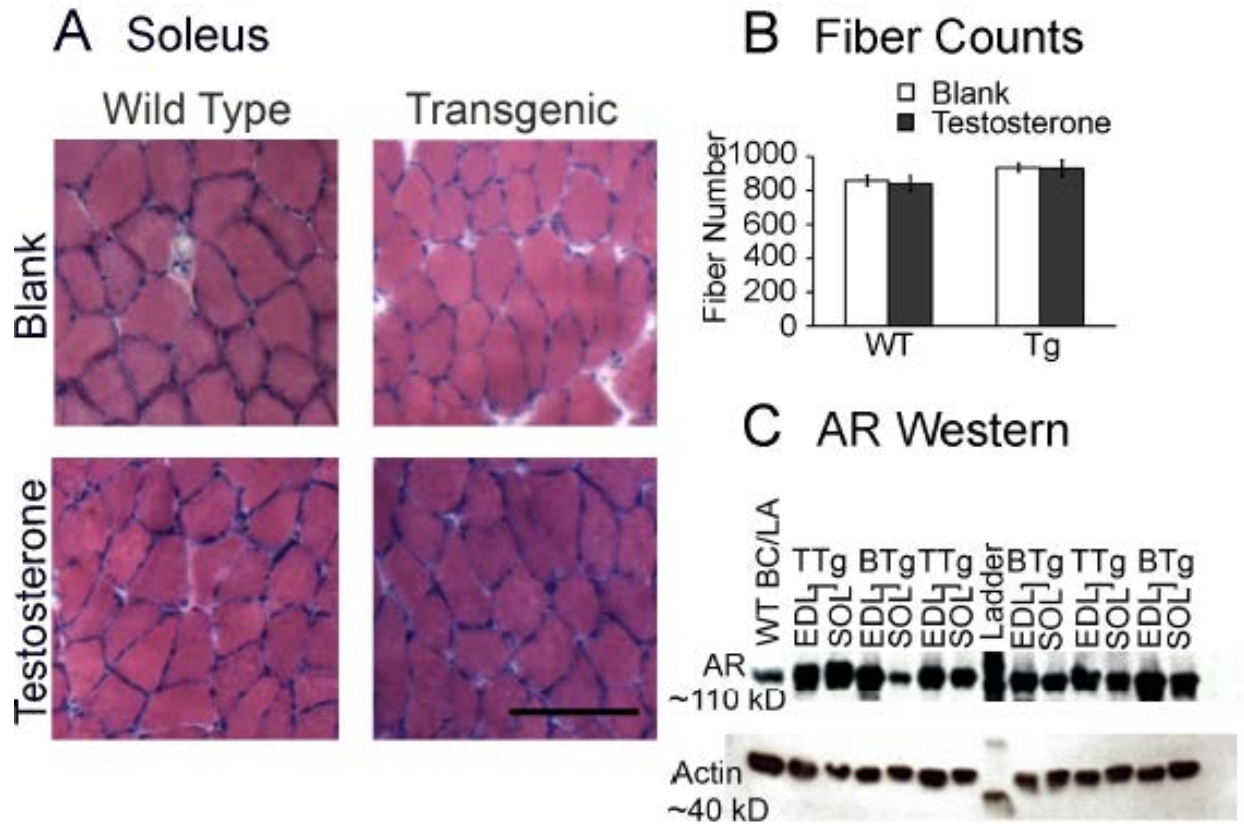


Figure 7. Neither histopathology nor expression of the AR transgene explains the severe deficit in SOL force production of T-treated Tg mice. Cross sections of SOL muscle (scale bar = 500 μ m) from Tg females after 5 days of T treatment stained with H&E exhibit no signs of abnormal morphology (e.g. fiber atrophy/hypertrophy, centralized nuclei, A), nor alterations in fiber number (B) compared to the SOL from other treatment groups (N = 4-5 mice/group). Bars represent means \pm standard errors of means. AR immunoblot (C) shows AR expression levels in the EDL and SOL from asymptomatic (B Tg) versus symptomatic (T Tg) mice. We find no consistent differences in AR expression (~110 kD) between EDL and SOL muscles, indicating that a difference in AR protein content between the EDL and SOL is not likely to underlie the relatively greater force deficit in the SOL compared to the EDL in T-treated Tg mice. Actin (~40 kD) loading control shows no consistent differences in protein loading between the EDL and SOL of Tg mice.

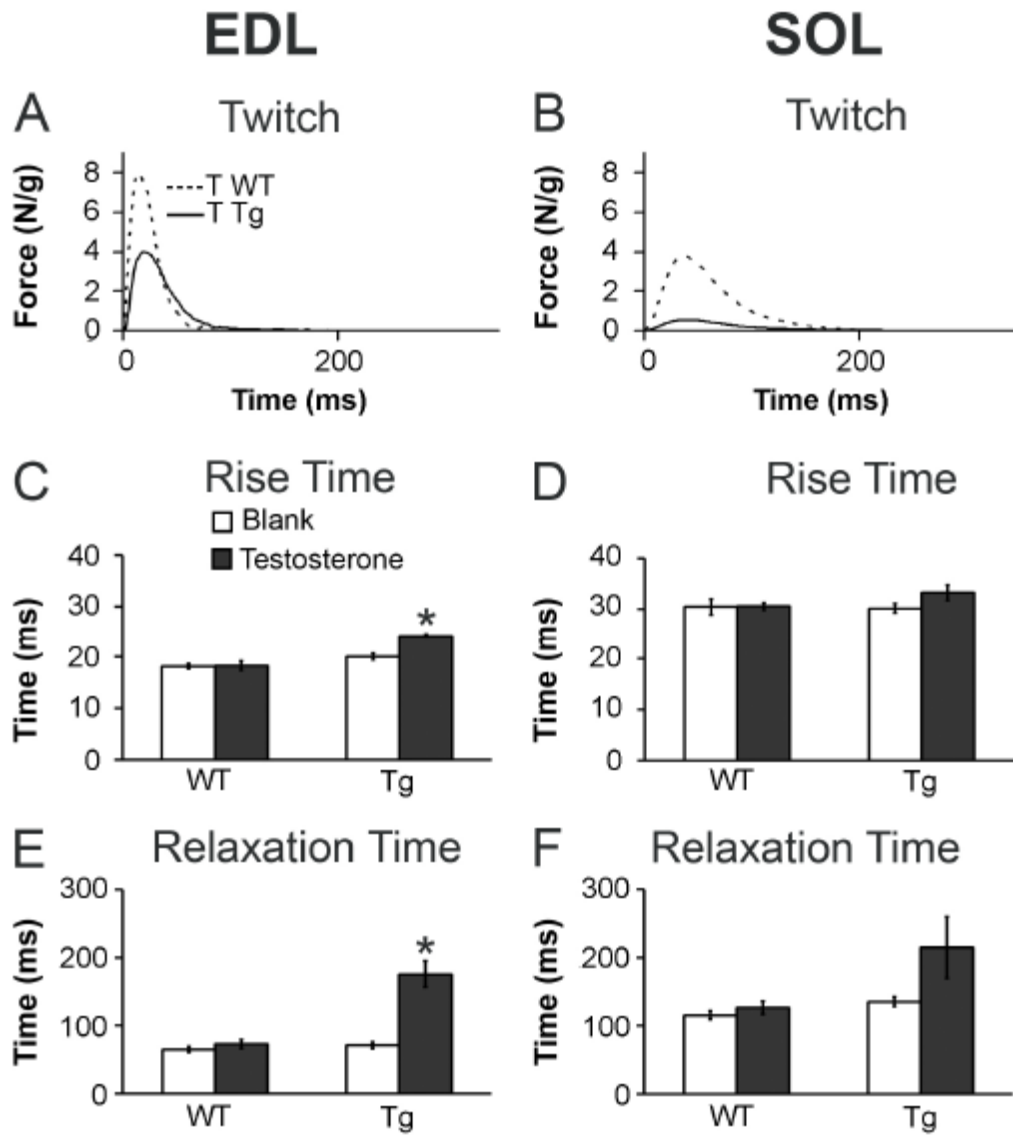


Figure 8. Twitch kinetics are slowed only in the EDL of motor-impaired Tg mice after 5 days of T treatment. Representative twitches from the fast-twitch EDL and the slow-twitch SOL (A, B) reveal decreased peak twitch force for both muscles of T-treated Tg mice (see Table 1 for mean values) but altered twitch kinetics only for the EDL. Quantitative analysis of individual twitches (C – F) confirms a significant prolongation in the time it takes to reach peak twitch force (C) and to relax (E) in EDL, but neither parameter is significantly altered by T in the SOL muscle of Tg mice (D, F). Plotted values are means \pm standard errors of means, with N = 5-6 mice/group. * $P < 0.001$ T Tg versus B Tg or T WT.

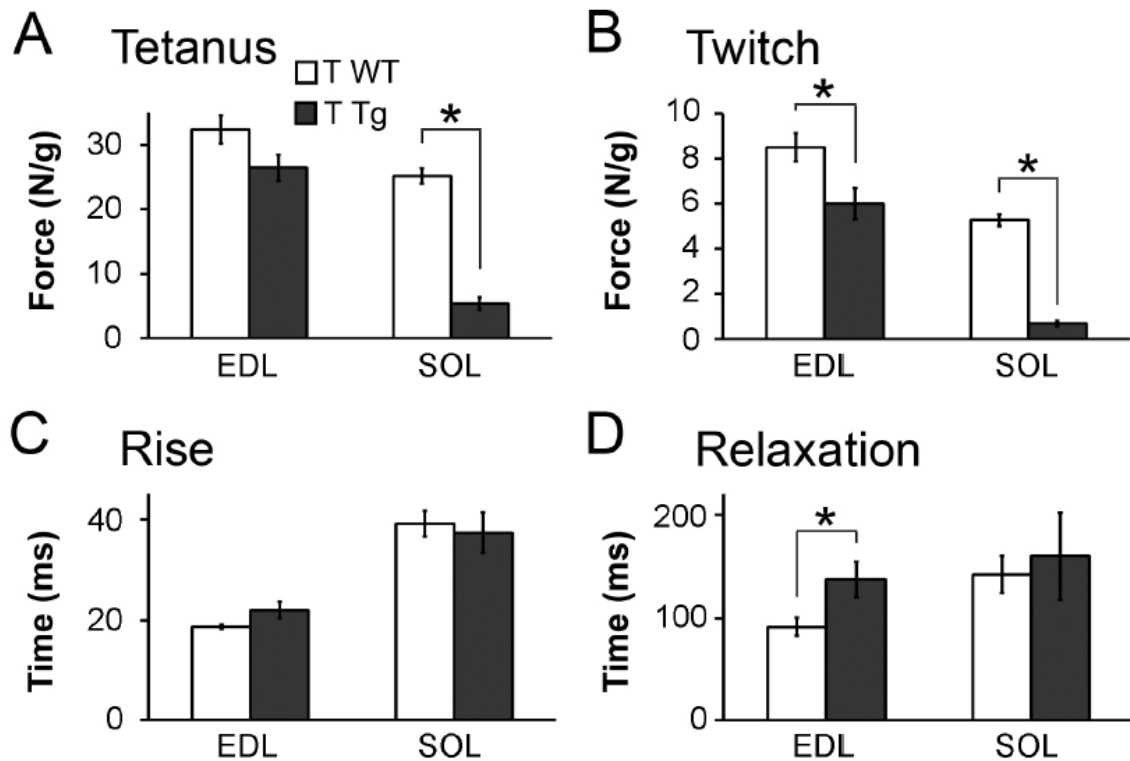


Figure 9. The SOL but not the EDL of motor-impaired mice shows the same deficit in peak tetanic force after 3 days of T treatment. Tetanic force in the slow-twitch SOL from T Tg mice was significantly decreased after 3 days of T treatment (A), comparable to the magnitude of the effect of 5 days of treatment (Fig 6). A subtle, but not significant difference was seen in EDL from the same motor-impaired mice (T Tg versus T WT mice, $p = 0.07$). However, peak twitch force in both muscles was significantly reduced in T Tg mice compared to T WT mice (B). Twitch kinetics were largely unaffected in T-treated Tg mice after 3 days of treatment (C, D) except that relaxation time was slowed significantly in EDL, consonant with the effect of T on this parameter after 5 days of treatment (Fig 8). $N = 5-7/\text{group}$. $*P < 0.05$.

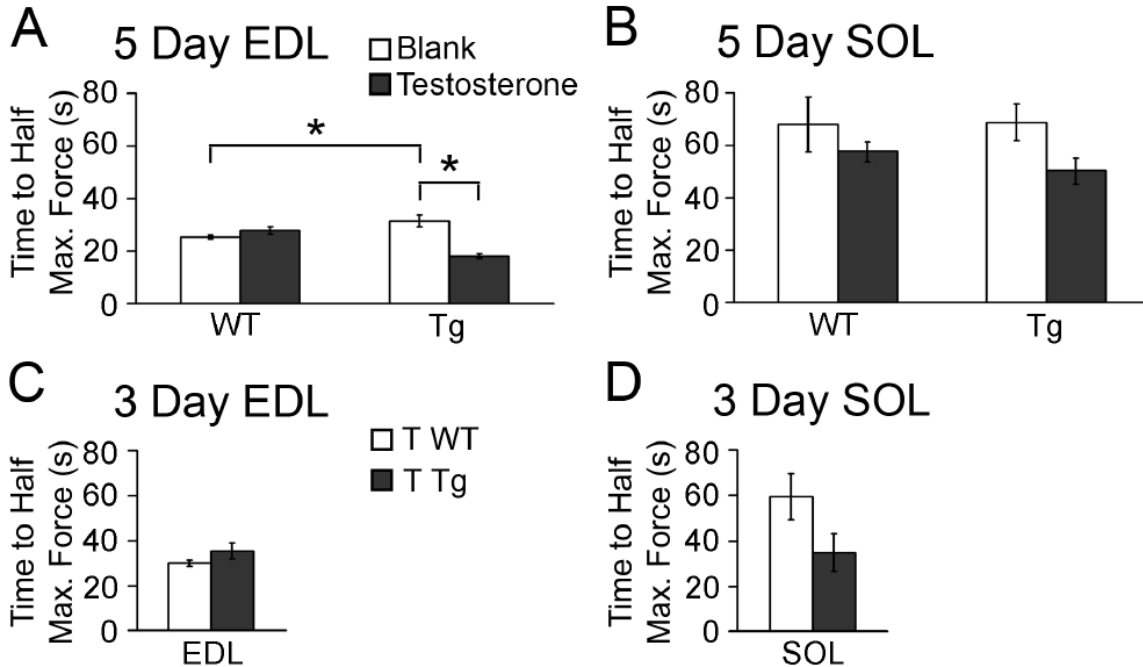


Figure 10. The EDL but not the SOL from motor-impaired Tg mice showed compromised resistance to fatigue after 5, but not 3, days of T treatment. Fatigue resistance was measured as time in seconds from onset of tetanizing stimulation to when the muscles decreased in force by 50% of maximal tetanic force. The EDL from Tg mice after 5 days of T treatment fatigued significantly faster, dropping to half maximal force several seconds sooner than the EDL from either T-treated WT or blank-treated Tg mice (A). Interestingly, the EDL from blank-treated Tg mice showed a *greater* resistance to fatigue than the EDL from blank-treated WT (B Tg versus B WT), indicating a *beneficial* effect of the transgene itself on resistance to fatigue in the EDL. Five days of T treatment had no effect on fatigue resistance in SOL (B), and there was no effect of T on fatigue resistance after 3 days of treatment in either muscle from Tg mice (C and D). 5-day EDL: N = 5-6 mice/group; 5-day SOL, N = 5-6 mice/group; 3-day EDL, N = 6 mice/group; 3-day SOL, N = 4-7 mice/group. * $P \leq 0.05$.

Biometric Table for male SBMA mice

	Body Mass (g)	EDL (mg)	SOL (mg)	T (nmol/L)
WT	21.6 ± 1.0	9.3 ± 0.6	7.2 ± 0.5	26.1±2.4
97Q Tg	16.5 ± 1.2*	4.7 ± 0.7*	8.0 ± 0.6	31.0±3.6
WT	26.8 ± 0.9	12.0 ± 0.7	9.8 ± 0.7	2.7±1.2
141 Tg	16.8 ± 0.6*	6.7 ± 0.3*	7.8 ± 0.4*	2.2±0.9

Table 2. Body weight, muscle mass and plasma testosterone (T) levels at end stage. Motor-impaired Tg male mice in each SBMA model show significantly decreased body weights compared to their respective WT controls. All but the soleus (SOL) muscle in 97Q males had significantly less mass. Circulating T levels were comparable between Tg and WT males within each line but notably higher for Tg and WT males in the 97Q model because these animals were castrated and given exogenous T starting at puberty. *P≤0.05 difference between transgenic mice and their respective WT controls, values = mean ± standard error of mean

	Rise time (ms)		Relaxation Time (ms)	
	EDL	SOL	EDL	SOL
WT	18±0	33±2	65±4	115±12
97Q Tg	21±1	38±3	85±10	121±8
WT	19±1	36±3	78±7	118±6
141 Tg	27±1*	39±2	77±9	103±38

Table 3. Kinetics analysis of individual twitch traces for motor-impaired Tg males and their WT controls. Analyses revealed few significant effects of disease on twitch kinetic; only rise time (time to peak force) in the EDL muscle of 141 Tg males was significantly prolonged compared to WT controls. Note however a consistent trend toward slower twitch kinetics in diseased muscles of both models. * $P \leq 0.05$, values = mean \pm standard error of mean

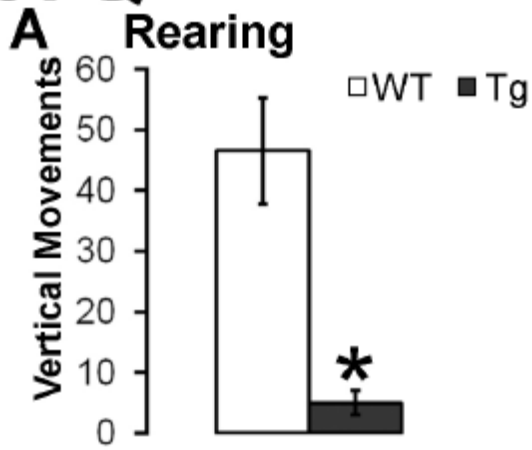
Muscle Morphology				
	EDL		SOL	
	Fibers	Cent Nuclei	Fibers	Cent Nuclei
WT	1169±94	0.003±0.001	976±24	0.003±0.001
97Q Tg	979±80	0.023±0.007*	988±36	0.004±0.002
WT	¹ 1055±75	² 0.005±0.002	869±43	0.003±0.001
141 Tg	753±72	0.013±0.003	922±59	0.017±0.004*

Table 4. Muscle morphology for male mouse muscles. Total number of muscle fibers and percent of total number of fibers containing centralized (cent) nuclei for EDL and SOL of the two Tg SBMA models (141 myogenic and 97Q). Only the EDL from myogenic males had significantly fewer fibers than WT controls. Fiber number was unaffected in both the EDL and SOL of 97Q Tg males and also in the SOL of 141 Tg males. The EDL of 97Q males and the SOL of 141 males contain a higher percentage of fibers with centralized nuclei, indicative of an abnormal muscle state. Note that these two muscles also showed the severest loss in force (Figs 2, 4). n=5/group in all except 141 EDL (n=3) *P≤0.05, values = mean ± standard error of mean. ¹ values from (Johansen et al., 2011); ² unpublished data (Johansen and Jordan).

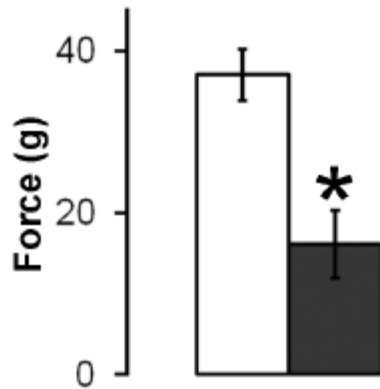
Figure 11. Transgenic (Tg) males in both the 97Q and 141 ‘myogenic’ models of SBMA show the expected impairment in motor function. Mean number of rearings in an open field, taken as an indirect measure of hindlimb strength, was decreased significantly in Tg males of both the 97Q (A) and myogenic 141 (D) models of SBMA compared to their respective WT controls. Similar significant deficits were also found in mean frontpaw grip strength (B, E) and hang times (C, F). These measures indicate that Tg males in both models show the expected SBMA phenotype. * $p \leq 0.05$ compared to WT controls. Error bars represent standard error of the mean, with $n = 6-7$ mice/group.

Figure 11 (cont'd)

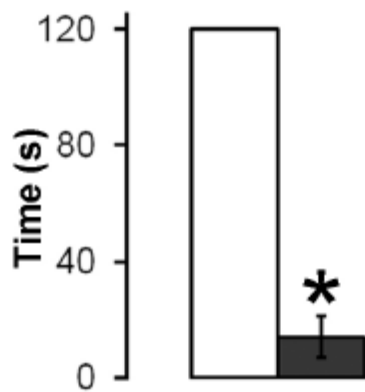
97Q



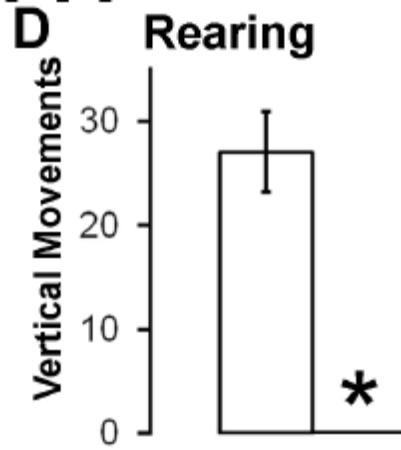
B Grip Strength



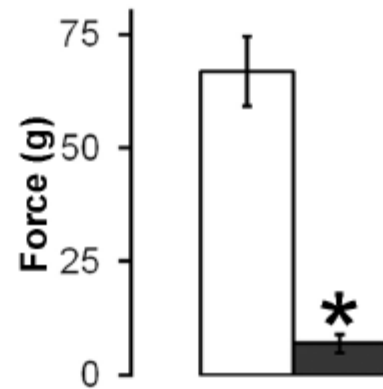
C Hang Test



141



E Grip Strength



F Hang Test

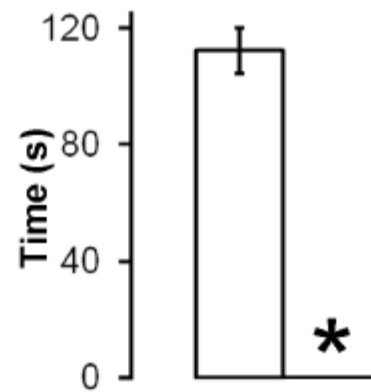
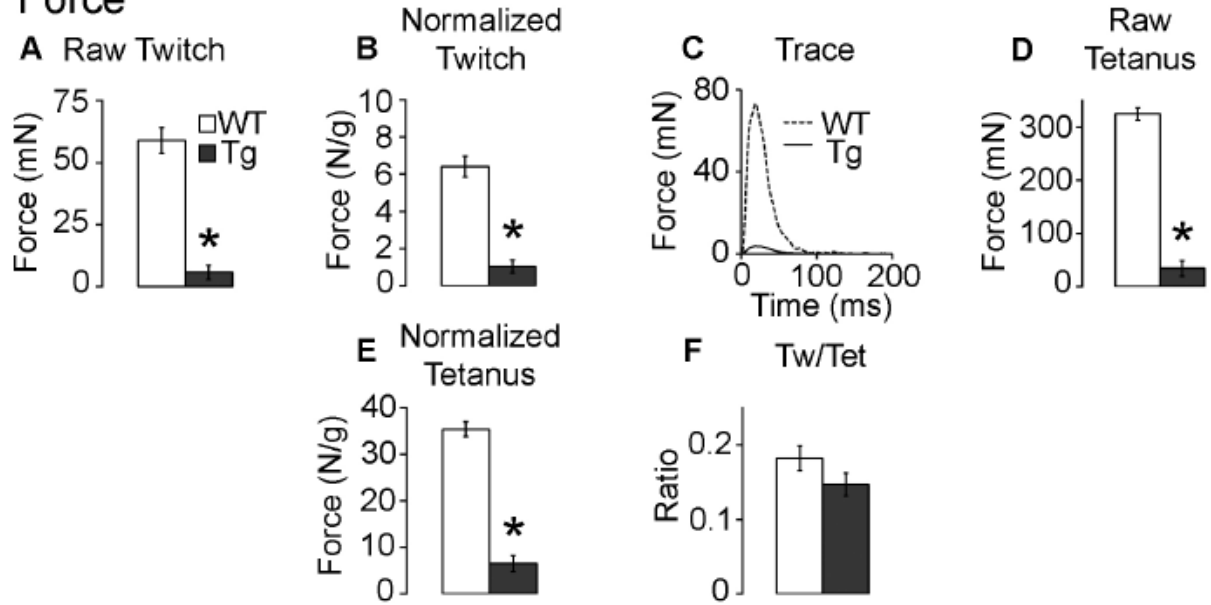


Figure 12. Both the fast twitch extensor digitorum longus (EDL) and slow twitch soleus (SOL) muscles from motor-impaired 97Q Tg males show deficits in contractile force. Raw twitch and tetanic force (A,D, and G) were significantly reduced, with the one exception that raw tetanic force was unaffected in the SOL (J). However, twitch and tetanic forces once normalized to muscle mass were significantly decreased in both muscles, including tetanic force produced by the SOL (B, E, H, and K), indicating primary defects in contractile function of muscles of diseased 97Q Tg males that are independent of their mass. The force deficit is also readily apparent in examples of individual traces of EDL (C) and SOL (I) twitches. Although somewhat reduced, the twitch/tetanus (Tw/Tet) ratio in the diseased EDL was not significantly different than WT (F). In contrast, the Tw/Tet ratio in the SOL of diseased males was significantly reduced (L), suggesting defects in calcium handling mechanisms. Such defects in muscle function may contribute to if not underlie defects in motor function. * $p \leq 0.05$ compared to WT controls. Error bars represent the standard error of the mean, with $n = 4-7$ mice/group.

Figure 12 (cont'd)

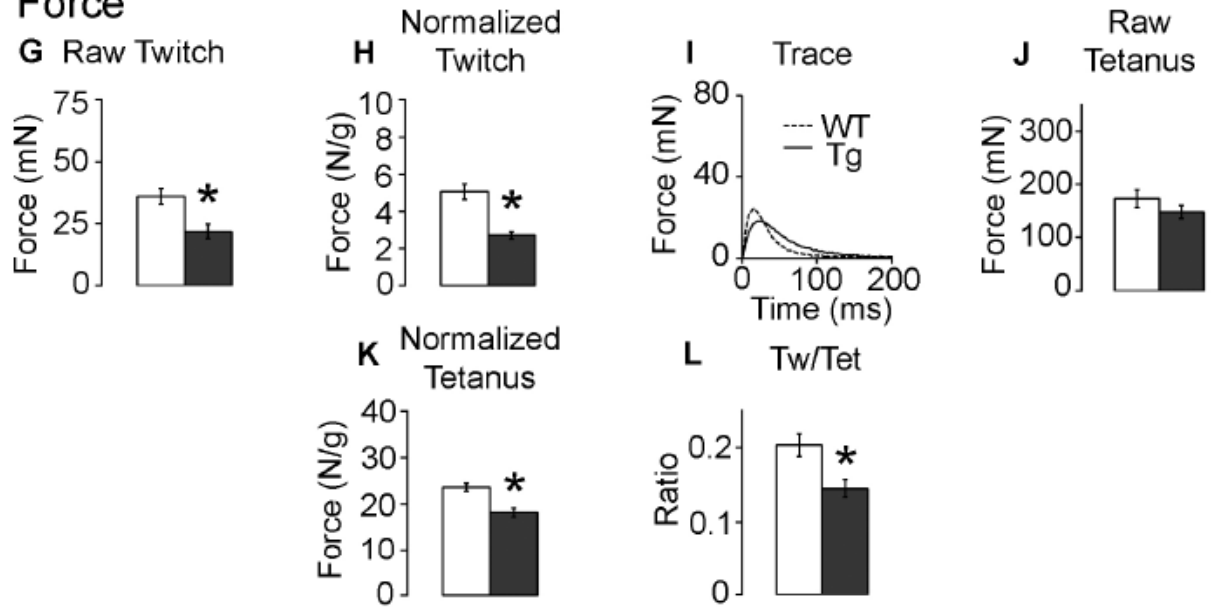
97Q EDL

Force

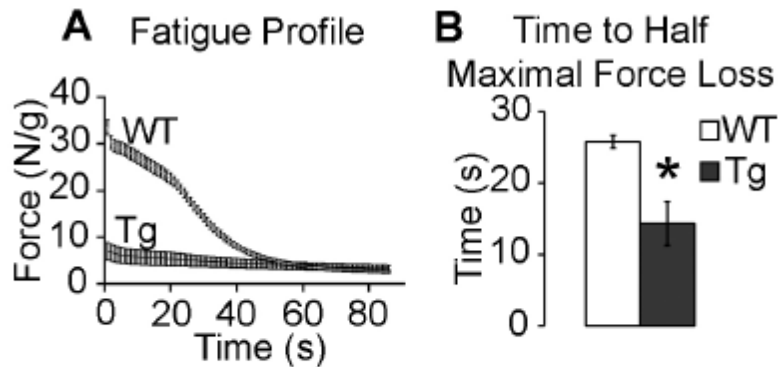


97Q SOL

Force



97Q EDL Fatigue



97Q SOL Fatigue

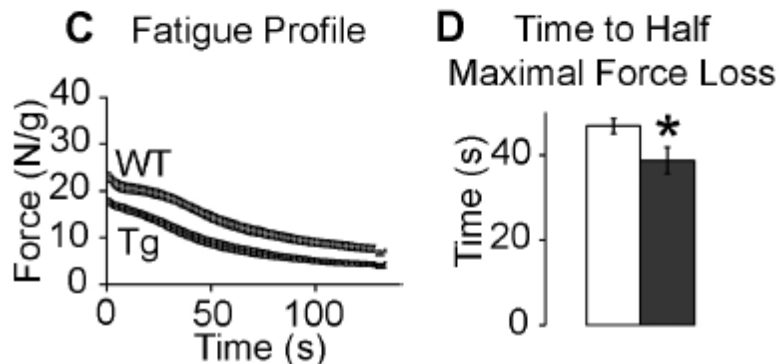


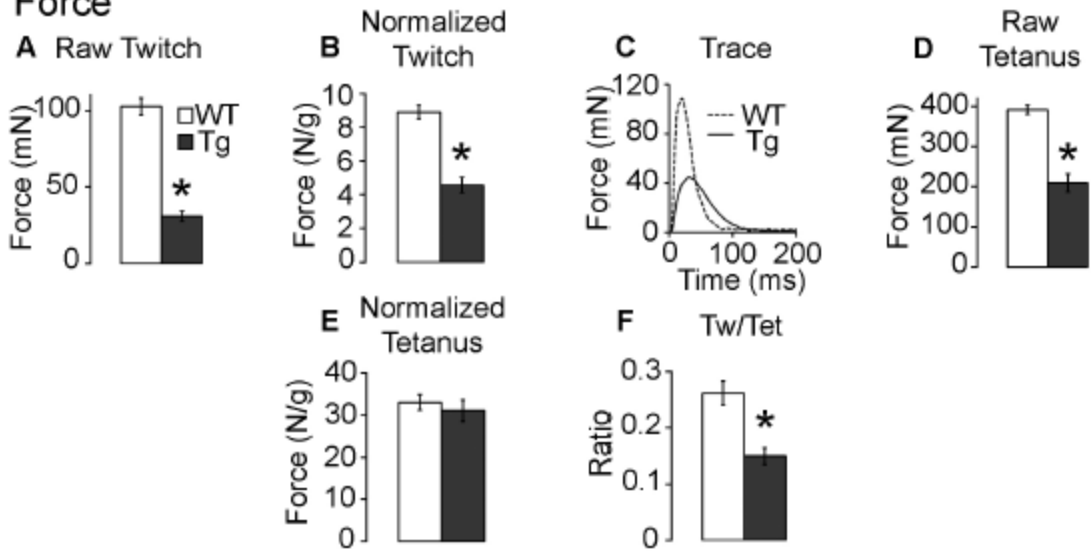
Figure 13. Both the EDL and SOL from motor-impaired 97Q Tg males fatigue more rapidly. The fatigue profile for both the EDL and SOL indicates that both muscles in Tg males produce less force per gram muscle at the start of stimulation (A, C) followed by a drop in force for all muscles indicating muscle fatigue during tetanizing stimulation. While the Tg EDL loses less of its original force than the WT EDL over the stimulation period (A), the Tg EDL appears to fatigue faster, losing 50% of its original force (time to half of maximal force loss) significantly sooner than WT EDL (B). The Tg SOL also appears to have a faster time course of fatigue than WT SOL, losing 50% of its original force significantly sooner than WT SOL (D). * $p \leq 0.05$ compared to WT controls. Plotted values are means \pm standard error of the mean, with $n = 4-7$ mice/group.

Figure 14. Both the fast twitch EDL and slow twitch SOL muscles from motor-impaired myogenic (141) Tg males show deficits in contractile force. Raw and normalized twitch and tetanic force were significantly reduced in both the EDL and SOL of motor-impaired males (A, B, D, G, H, J and K) with the exception of normalized tetanic force in Tg EDL (E). On the other hand, the deficit in raw tetanic force in the EDL probably is due to the deficit in fiber number in this muscle (Table 4). Samples of twitch traces reveal such deficits in twitch force (C, I). The Tw/Tet ratio is also significantly reduced in both the Tg EDL (F) and SOL (L), also suggesting that calcium mobilization from intracellular stores may be perturbed. Muscles of myogenic 141 males show similar defects in contractile properties as 97Q males, although disease affects force most in the SOL of 141 males while affecting most the EDL in 97Q males. Nonetheless, these results suggest that motor dysfunction likely involves primary defects in muscle function. * $p \leq 0.05$ compared to WT controls. Error bars represent the standard error of the mean, with $n = 4-7$ mice/group.

Figure 14 (cont'd)

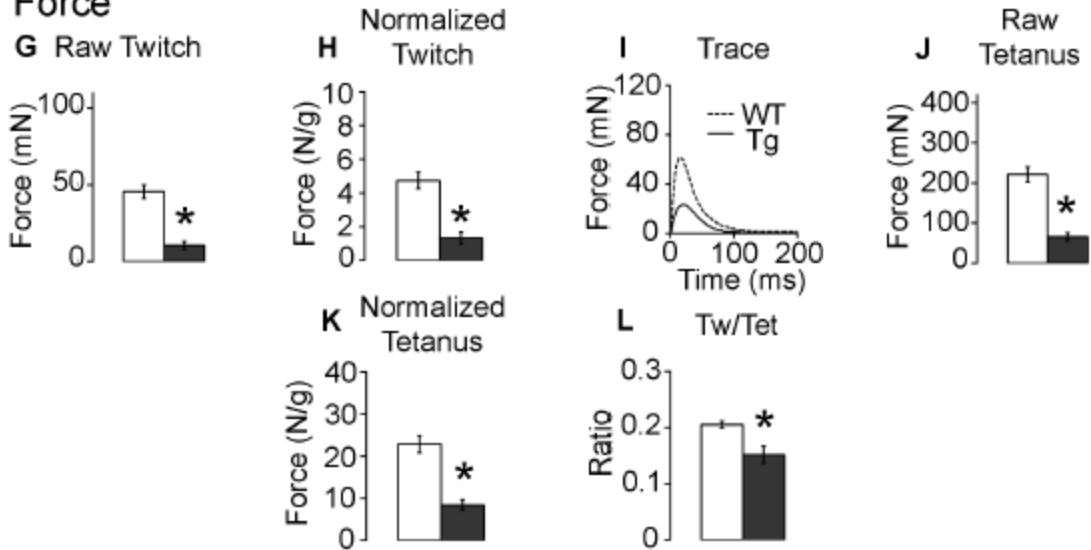
141 EDL

Force

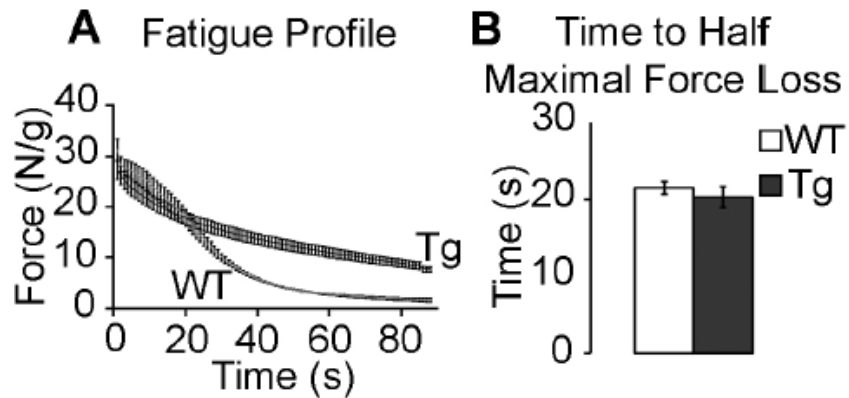


141 SOL

Force



141 EDL Fatigue



141 SOL Fatigue

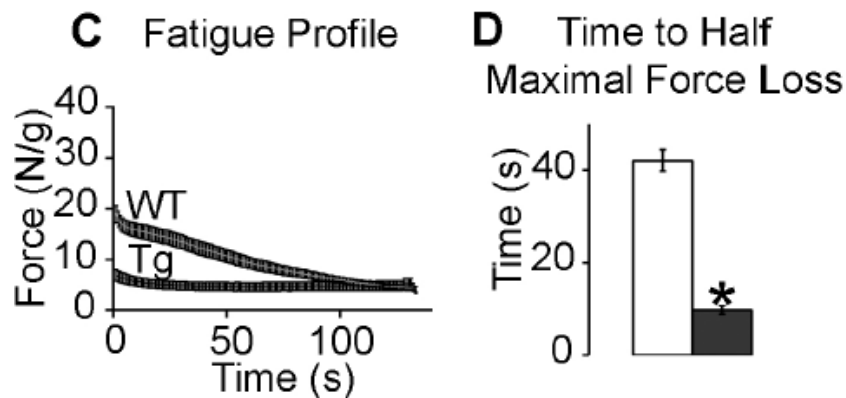
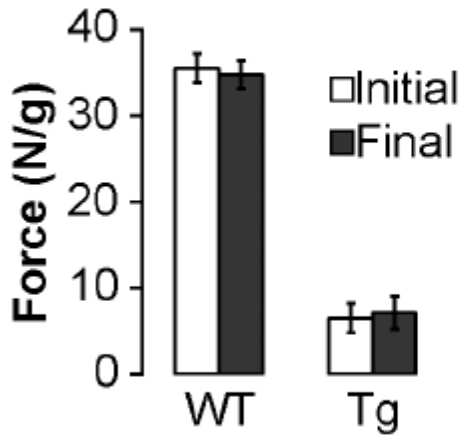
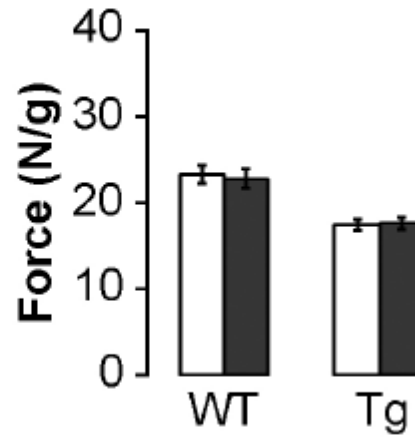


Figure 15. Only the SOL from motor-impaired 141 Tg males fatigues more rapidly. The fatigue profile indicates that the Tg EDL shows increased resistance to fatigue, losing less total force than WT EDL overall (A). However, both Tg and WT EDL appeared to fatigue at about the same rate, reaching a 50% drop at about the same time (B). The apparent increase in oxidative metabolism in the diseased EDL (Johansen et al., 2011; Monks et al., 2007) may help stave off some of the later losses in force exhibited by WT EDL. The SOL of diseased 141 Tg males on the other hand fatigues rapidly, losing 50% of its starting force in less than 9.8 ± 0.9 s compared to 42.1 ± 2.4 s in WT SOL. The marked increase in fatigue susceptibility of the SOL muscle in 141 Tg males also likely contributes to motor dysfunction in this model. * $p \leq 0.05$ compared to WT controls. Plotted values are means \pm standard error of the mean, with $n = 4-6$ mice/group.

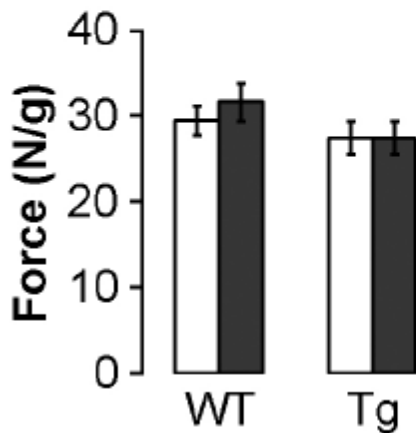
97Q EDL



97Q SOL



141 EDL



141 SOL

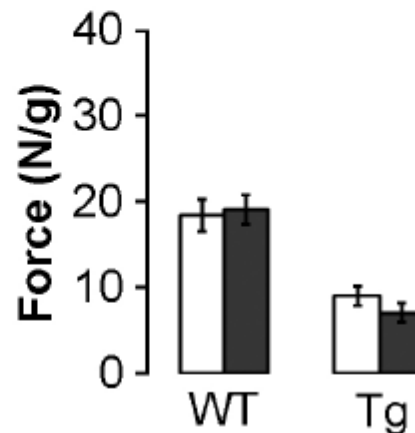


Figure 16. Muscles from diseased and healthy mice remain stable *in vitro* during the course of the experiment. Viability of each skeletal muscle was monitored with tetanus stimulations throughout an experiment. Force produced by tetani at the beginning of the experiment (open bar) was comparable to force produced at the end (filled bar). These data suggest that the force deficits found *in vitro* in diseased muscles likely reflect a genuine force deficit *in vivo*, rather than a defect that emerges *in vitro*. *In vitro* measurements were taken during a 2-3 hour window. Plotted values are mean \pm standard error of the mean.

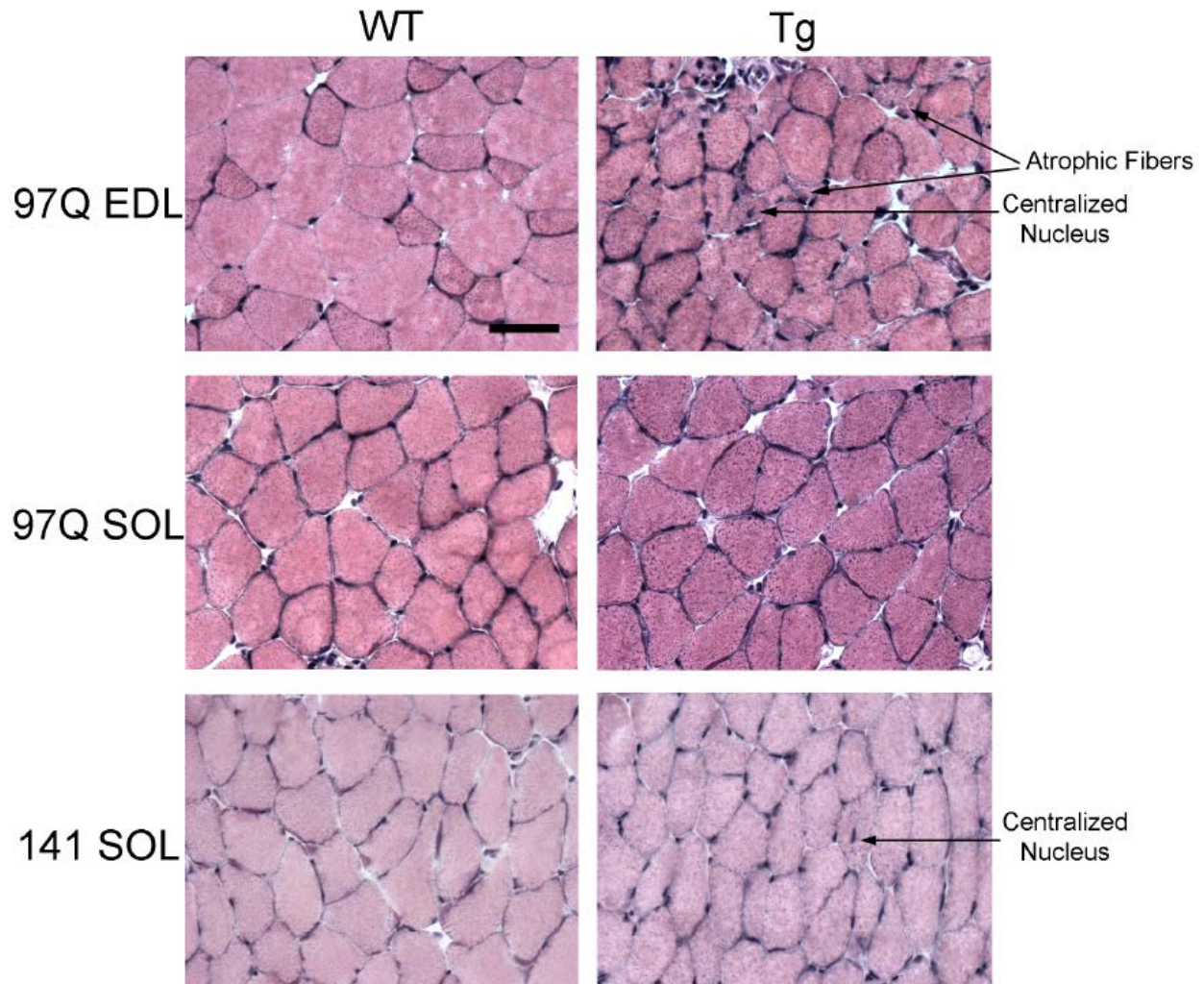
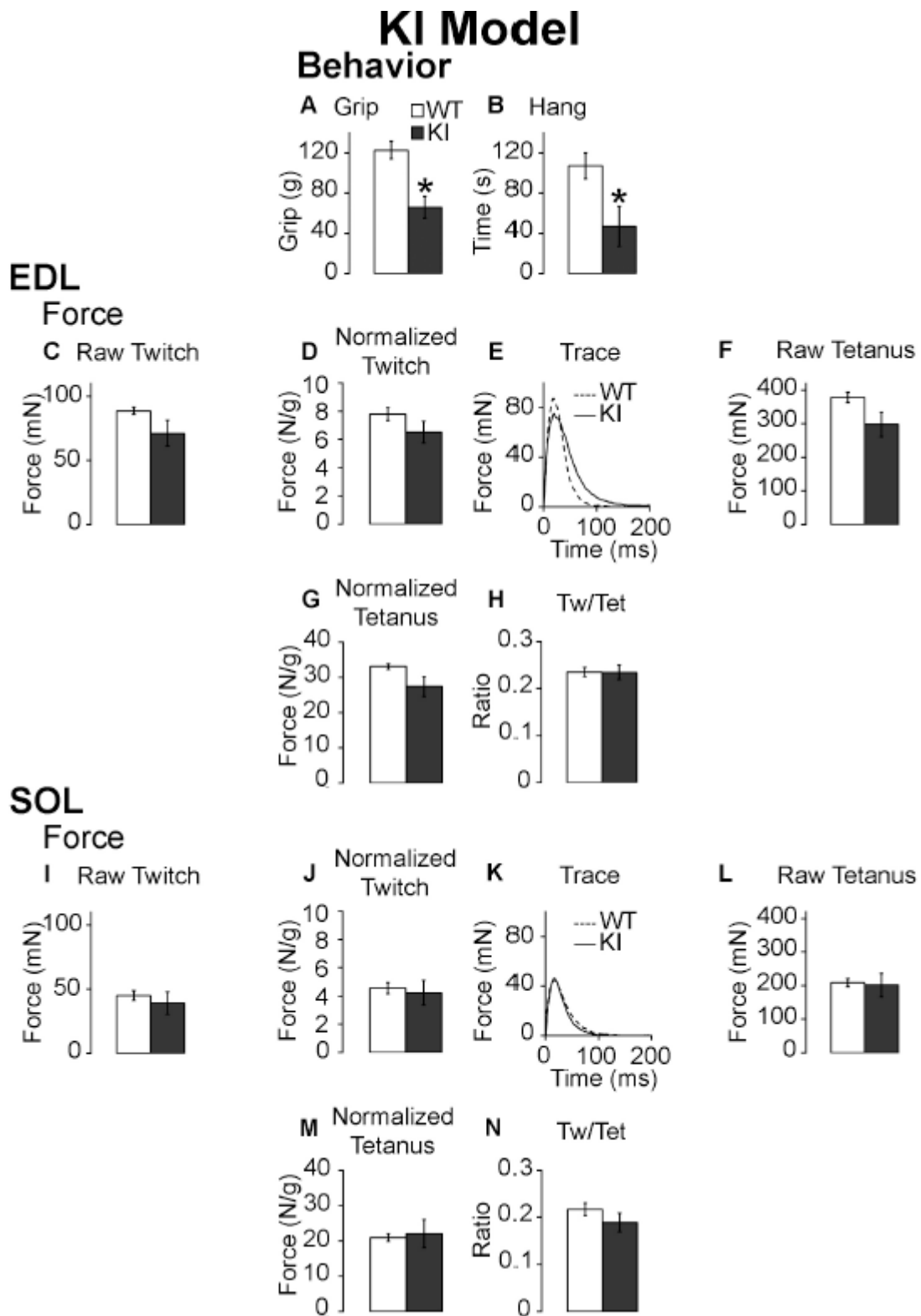


Figure 17. Representative photomicrographs of cross sections of muscle used for fiber counts. The EDL from the myogenic model was previously characterized (Johansen et al., 2011) and therefore not included. EDL muscle fibers in diseased 97Q Tg males are markedly heterogeneous in size, with some fibers notably smaller than the rest (arrow). EDL fibers from 97Q males also contain centralized nuclei (arrow). Since mass of the EDL from diseased 97Q males is reduced by half (Table 2) without loss of fibers (Table 4), it is likely that atrophy of individual fibers underlies the deficit in EDL mass. Note however that decreases in muscle mass contribute little to the deficits in twitch and tetanic force (Fig 2A, B, D and E) since a large proportion of the deficit persists once force measures are normalized to muscle mass. No major histological changes were observed in cross section of SOL from either 97Q males (middle panels) or myogenic (141) males (bottom panels) except for centralized nuclei which were more frequent in the SOL of 141 Tg males compared to WT SOL. Despite the lack of striking histopathology, SOL function is impaired in both models, but particularly in the 141 myogenic males, which show a three-fold loss of normalized force (Fig 14H, K). These data indicate that impairments in muscle function need not be accompanied by marked histopathology. Scale bar = 50 μm .

Figure 18. KI males with mild motor deficits show negligible deficits in muscle function. Measurements of forepaw grip strength and hang times are significantly decreased in KI males relative to WT controls (A, B), showing the expected impaired motor function in KI males. While force measures in the KI EDL suggest small deficits in twitch and tetanic force consistent with the mild motor phenotype in this model, these apparent deficits are not significant (C – H). Likewise, we found no significant deficits in twitch and tetanic forces produced by the SOL from KI males (I - N). These data raise the possibility that motor deficits in KI males may reflect synaptic defects upstream to the skeletal muscles. * $p \leq 0.05$ compared to WT controls. Plotted values are mean \pm standard error of the mean, with $n = 5-7$ mice/group.

Figure 18 (cont'd)



REFERENCES

REFERENCES

- Adachi, H., Kume, A., Li, M., Nakagomi, Y., Niwa, H., Do, J., Sang, C., Kobayashi, Y., Doyu, M., and Sobue, G. (2001). Transgenic mice with an expanded CAG repeat controlled by the human AR promoter show polyglutamine nuclear inclusions and neuronal dysfunction without neuronal cell death. *Hum Mol Genet* *10*, 1039-1048.
- Al-Qusairi, L., and Laporte, J. (2011). T-tubule biogenesis and triad formation in skeletal muscle and implication in human diseases. *Skelet Muscle* *1*, 26.
- Andersson, D.C., Betzenhauser, M.J., Reiken, S., Meli, A.C., Umanskaya, A., Xie, W., Shiomi, T., Zalk, R., Lacampagne, A., and Marks, A.R. (2011). Ryanodine receptor oxidation causes intracellular calcium leak and muscle weakness in aging. *Cell Metab* *14*, 196-207.
- Arbizu, T., Santamaria, J., Gomez, J.M., Quilez, A., and Serra, J.P. (1983). A family with adult spinal and bulbar muscular atrophy, X-linked inheritance and associated testicular failure. *J Neurol Sci* *59*, 371-382.
- Arenas, J., Diaz, V., Liras, G., Gutierrez, E., Santos, I., Martinez, A., and Culebras, J.M. (1988). Activities of creatine kinase and its isoenzymes in serum in various skeletal muscle disorders. *Clin Chem* *34*, 2460-2462.
- Atkin, J.D., Scott, R.L., West, J.M., Lopes, E., Quah, A.K., and Cheema, S.S. (2005). Properties of slow- and fast-twitch muscle fibres in a mouse model of amyotrophic lateral sclerosis. *Neuromuscul Disord* *15*, 377-388.
- Banno, H., Katsuno, M., Suzuki, K., Takeuchi, Y., Kawashima, M., Suga, N., Takamori, M., Ito, M., Nakamura, T., Matsuo, K., *et al.* (2009). Phase 2 trial of leuprorelin in patients with spinal and bulbar muscular atrophy. *Ann Neurol* *65*, 140-150.
- Battaglia, F., Le Galudec, V., Cossee, M., Tranchant, C., Warter, J.M., and Echaniz-Laguna, A. (2003). Kennedy's Disease Initially Manifesting as an Endocrine Disorder. *J Clin Neuromuscul Dis* *4*, 165-167.
- Bawa, P., Binder, M.D., Ruenzel, P., and Henneman, E. (1984). Recruitment order of motoneurons in stretch reflexes is highly correlated with their axonal conduction velocity. *J Neurophysiol* *52*, 410-420.

Bellinger, A.M., Reiken, S., Carlson, C., Mongillo, M., Liu, X., Rothman, L., Matecki, S., Lacampagne, A., and Marks, A.R. (2009). Hypernitrosylated ryanodine receptor calcium release channels are leaky in dystrophic muscle. *Nat Med* *15*, 325-330.

Bellinger, A.M., Reiken, S., Dura, M., Murphy, P.W., Deng, S.X., Landry, D.W., Nieman, D., Lehnart, S.E., Samaru, M., LaCampagne, A., *et al.* (2008). Remodeling of ryanodine receptor complex causes "leaky" channels: a molecular mechanism for decreased exercise capacity. *Proc Natl Acad Sci U S A* *105*, 2198-2202.

Berchtold, M.W., Brinkmeier, H., and Muntener, M. (2000). Calcium ion in skeletal muscle: its crucial role for muscle function, plasticity, and disease. *Physiol Rev* *80*, 1215-1265.

Bertorini, T.E., Bhattacharya, S.K., Palmieri, G.M., Chesney, C.M., Pifer, D., and Baker, B. (1982). Muscle calcium and magnesium content in Duchenne muscular dystrophy. *Neurology* *32*, 1088-1092.

Bosch-Marce, M., Wee, C.D., Martinez, T.L., Lipkes, C.E., Choe, D.W., Kong, L., Van Meerbeke, J.P., Musaro, A., and Sumner, C.J. (2011). Increased IGF-1 in muscle modulates the phenotype of severe SMA mice. *Hum Mol Genet* *20*, 1844-1853.

Brandl, C.J., deLeon, S., Martin, D.R., and MacLennan, D.H. (1987). Adult forms of the Ca²⁺ATPase of sarcoplasmic reticulum. Expression in developing skeletal muscle. *J Biol Chem* *262*, 3768-3774.

Braun, S., Croizat, B., Lagrange, M.C., Warter, J.M., and Poindron, P. (1995). Constitutive muscular abnormalities in culture in spinal muscular atrophy. *Lancet* *345*, 694-695.

Brook, J.D., McCurrach, M.E., Harley, H.G., Buckler, A.J., Church, D., Aburatani, H., Hunter, K., Stanton, V.P., Thirion, J.P., Hudson, T., *et al.* (1992). Molecular basis of myotonic dystrophy: expansion of a trinucleotide (CTG) repeat at the 3' end of a transcript encoding a protein kinase family member. *Cell* *69*, 385.

Bruijn, L.I., Becher, M.W., Lee, M.K., Anderson, K.L., Jenkins, N.A., Copeland, N.G., Sisodia, S.S., Rothstein, J.D., Borchelt, D.R., Price, D.L., *et al.* (1997). ALS-linked SOD1 mutant G85R mediates damage to astrocytes and promotes rapidly progressive disease with SOD1-containing inclusions. *Neuron* *18*, 327-338.

Burglen, L., Lefebvre, S., Clermont, O., Burlet, P., Viollet, L., Cruaud, C., Munnich, A., and Melki, J. (1996). Structure and organization of the human survival motor neurone (SMN) gene. *Genomics* *32*, 479-482.

Burke, R.E., Levine, D.N., Tsairis, P., and Zajac, F.E. (1973). Physiological Types and Histochemical Profiles in Motor Units of Cat Gastrocnemius. *J Physiol-London* 234, 723-&.

Burke, R.E., Levine, D.N., Zajac, F.E., Tsairis, P., and Engel, W.K. (1971). Mammalian Motor Units - Physiological-Histochemical Correlation in 3 Types in Cat Gastrocnemius. *Science* 174, 709-&.

Cairns, S.P., Chin, E.R., and Renaud, J.M. (2007). Stimulation pulse characteristics and electrode configuration determine site of excitation in isolated mammalian skeletal muscle: implications for fatigue. *J Appl Physiol* 103, 359-368.

Campbell, L., Potter, A., Ignatius, J., Dubowitz, V., and Davies, K. (1997). Genomic variation and gene conversion in spinal muscular atrophy: implications for disease process and clinical phenotype. *Am J Hum Genet* 61, 40-50.

Chahin, N., and Sorenson, E.J. (2009). Serum creatine kinase levels in spinobulbar muscular atrophy and amyotrophic lateral sclerosis. *Muscle Nerve* 40, 126-129.

Chami, M., Gozuacik, D., Lagorce, D., Brini, M., Falson, P., Peaucellier, G., Pinton, P., Lecoer, H., Gougeon, M.L., le Maire, M., *et al.* (2001). SERCA1 truncated proteins unable to pump calcium reduce the endoplasmic reticulum calcium concentration and induce apoptosis. *J Cell Biol* 153, 1301-1314.

Chen, G., Carroll, S., Racay, P., Dick, J., Pette, D., Traub, I., Vrbova, G., Egli, P., Celio, M., and Schwaller, B. (2001). Deficiency in parvalbumin increases fatigue resistance in fast-twitch muscle and upregulates mitochondria. *Am J Physiol Cell Physiol* 281, C114-122.

Chevalier-Larsen, E., and Holzbaur, E.L. (2006). Axonal transport and neurodegenerative disease. *Biochim Biophys Acta* 1762, 1094-1108.

Chevalier-Larsen, E.S., O'Brien, C.J., Wang, H., Jenkins, S.C., Holder, L., Lieberman, A.P., and Merry, D.E. (2004). Castration restores function and neurofilament alterations of aged symptomatic males in a transgenic mouse model of spinal and bulbar muscular atrophy. *J Neurosci* 24, 4778-4786.

Chevrel, G., Hohlfeld, R., and Sendtner, M. (2006). The role of neurotrophins in muscle under physiological and pathological conditions. *Muscle Nerve* 33, 462-476.

Chin, E.R. (2004). The role of calcium and calcium/calmodulin-dependent kinases in skeletal muscle plasticity and mitochondrial biogenesis. *Proc Nutr Soc* 63, 279-286.

Chin, E.R., Grange, R.W., Viau, F., Simard, A.R., Humphries, C., Shelton, J., Bassel-Duby, R., Williams, R.S., and Michel, R.N. (2003). Alterations in slow-twitch muscle phenotype in transgenic mice overexpressing the Ca²⁺ buffering protein parvalbumin. *J Physiol* 547, 649-663.

Cifuentes-Diaz, C., Frugier, T., Tiziano, F.D., Lacene, E., Roblot, N., Joshi, V., Moreau, M.H., and Melki, J. (2001). Deletion of murine SMN exon 7 directed to skeletal muscle leads to severe muscular dystrophy. *J Cell Biol* 152, 1107-1114.

Clamann, H.P., and Henneman, E. (1976). Electrical measurement of axon diameter and its use in relating motoneuron size to critical firing level. *J Neurophysiol* 39, 844-851.

Crow, M.T., and Kushmerick, M.J. (1982). Chemical energetics of slow- and fast-twitch muscles of the mouse. *J Gen Physiol* 79, 147-166.

D'Amico, A., Mercuri, E., Tiziano, F.D., and Bertini, E. (2011). Spinal muscular atrophy. *Orphanet J Rare Dis* 6, 71.

Deconinck, N., and Dan, B. (2007). Pathophysiology of duchenne muscular dystrophy: current hypotheses. *Pediatr Neurol* 36, 1-7.

Dekkers, J., Bayley, P., Dick, J.R., Schwaller, B., Berchtold, M.W., and Greensmith, L. (2004). Over-expression of parvalbumin in transgenic mice rescues motoneurons from injury-induced cell death. *Neuroscience* 123, 459-466.

Dentel, J.N., Blanchard, S.G., Ankrapp, D.P., McCabe, L.R., and Wiseman, R.W. (2005). Inhibition of cross-bridge formation has no effect on contraction-associated phosphorylation of p38 MAPK in mouse skeletal muscle. *Am J Physiol Cell Physiol* 288, C824-830.

Di Giorgio, F.P., Carrasco, M.A., Siao, M.C., Maniatis, T., and Eggan, K. (2007). Non-cell autonomous effect of glia on motor neurons in an embryonic stem cell-based ALS model. *Nat Neurosci* 10, 608-614.

Diaz-Amarilla, P., Olivera-Bravo, S., Trias, E., Cragolini, A., Martinez-Palma, L., Cassina, P., Beckman, J., and Barbeito, L. (2011). Phenotypically aberrant astrocytes that promote motoneuron damage in a model of inherited amyotrophic lateral sclerosis. *Proc Natl Acad Sci U S A* 108, 18126-18131.

Dobrowolny, G., Aucello, M., Molinaro, M., and Musaro, A. (2008a). Local expression of mIgf-1 modulates ubiquitin, caspase and CDK5 expression in skeletal muscle of an ALS mouse model. *Neurol Res* 30, 131-136.

Dobrowolny, G., Aucello, M., Rizzuto, E., Beccafico, S., Mammucari, C., Boncompagni, S., Belia, S., Wannenes, F., Nicoletti, C., Del Prete, Z., *et al.* (2008b). Skeletal muscle is a primary target of SOD1G93A-mediated toxicity. *Cell Metab* 8, 425-436.

Dobrowolny, G., Giacinti, C., Pelosi, L., Nicoletti, C., Winn, N., Barberi, L., Molinaro, M., Rosenthal, N., and Musaro, A. (2005). Muscle expression of a local Igf-1 isoform protects motor neurons in an ALS mouse model. *J Cell Biol* 168, 193-199.

Dubowitz, V. (1995). Chaos in the classification of SMA: a possible resolution. *Neuromuscul Disord* 5, 3-5.

Dupuis, L., Gonzalez de Aguilar, J.L., Echaniz-Laguna, A., Eschbach, J., Rene, F., Oudart, H., Halter, B., Huze, C., Schaeffer, L., Bouillaud, F., *et al.* (2009). Muscle mitochondrial uncoupling dismantles neuromuscular junction and triggers distal degeneration of motor neurons. *PLoS One* 4, e5390.

Eagle, M., Baudouin, S.V., Chandler, C., Giddings, D.R., Bullock, R., and Bushby, K. (2002). Survival in Duchenne muscular dystrophy: improvements in life expectancy since 1967 and the impact of home nocturnal ventilation. *Neuromuscul Disord* 12, 926-929.

Ebashi, S., and Endo, M. (1968). Calcium ion and muscle contraction. *Prog Biophys Mol Biol* 18, 123-183.

Ebashi, S., Toyokura, Y., Momoi, H., and Sugita, H. (1959). High Creatine Phosphokinase Activity of Sera of Progressive Muscular Dystrophy. *J Biochem-Tokyo* 46, 103-104.

Eisenberg, E., and Hill, T.L. (1985). Muscle contraction and free energy transduction in biological systems. *Science* 227, 999-1006.

Emery, A.E., and Burt, D. (1980). Intracellular calcium and pathogenesis and antenatal diagnosis of Duchenne muscular dystrophy. *Br Med J* 280, 355-357.

Ervasti, J.M., and Campbell, K.P. (1993). A role for the dystrophin-glycoprotein complex as a transmembrane linker between laminin and actin. *J Cell Biol* 122, 809-823.

Fernando, S.M., Rao, P., Niel, L., Chatterjee, D., Stagljar, M., and Monks, D.A. (2010). Myocyte androgen receptors increase metabolic rate and improve body composition by reducing fat mass. *Endocrinology* 151, 3125-3132.

Fischbeck, K.H. (1997). Kennedy disease. *J Inherit Metab Dis* 20, 152-158.

Fischbeck, K.H., Lieberman, A., Bailey, C.K., Abel, A., and Merry, D.E. (1999). Androgen receptor mutation in Kennedy's disease. *Philos Trans R Soc Lond B Biol Sci* 354, 1075-1078.

Fischbeck, K.H., Souders, D., and La Spada, A. (1991). A candidate gene for X-linked spinal muscular atrophy. *Adv Neurol* 56, 209-213.

Fluck, M., Waxham, M.N., Hamilton, M.T., and Booth, F.W. (2000). Skeletal muscle Ca(2+)-independent kinase activity increases during either hypertrophy or running. *J Appl Physiol* 88, 352-358.

Gentile, M.A., Nantermet, P.V., Vogel, R.L., Phillips, R., Holder, D., Hodor, P., Cheng, C., Dai, H., Freedman, L.P., and Ray, W.J. (2010). Androgen-mediated improvement of body composition and muscle function involves a novel early transcriptional program including IGF1, mechano growth factor, and induction of {beta}-catenin. *J Mol Endocrinol* 44, 55-73.

Gifondorwa, D.J., Robinson, M.B., Hayes, C.D., Taylor, A.R., Pevette, D.M., Oppenheim, R.W., Caress, J., and Milligan, C.E. (2007). Exogenous delivery of heat shock protein 70 increases lifespan in a mouse model of amyotrophic lateral sclerosis. *J Neurosci* 27, 13173-13180.

Gould, T.W., Buss, R.R., Vinsant, S., Pevette, D., Sun, W., Knudson, C.M., Milligan, C.E., and Oppenheim, R.W. (2006). Complete dissociation of motor neuron death from motor dysfunction by Bax deletion in a mouse model of ALS. *J Neurosci* 26, 8774-8786.

Gubbay, S.S., Kahana, E., Zilber, N., Cooper, G., Pintov, S., and Leibowitz, Y. (1985). Amyotrophic lateral sclerosis. A study of its presentation and prognosis. *J Neurol* 232, 295-300.

Gurney, M.E., Pu, H., Chiu, A.Y., Dal Canto, M.C., Polchow, C.Y., Alexander, D.D., Caliendo, J., Hentati, A., Kwon, Y.W., Deng, H.X., *et al.* (1994). Motor neuron degeneration in mice that express a human Cu,Zn superoxide dismutase mutation. *Science* 264, 1772-1775.

Hahnen, E., Schonling, J., Rudnik-Schoneborn, S., Zerres, K., and Wirth, B. (1996). Hybrid survival motor neuron genes in patients with autosomal recessive spinal muscular atrophy: new

insights into molecular mechanisms responsible for the disease. *Am J Hum Genet* 59, 1057-1065.

Harley, H.G., Brook, J.D., Rundle, S.A., Crow, S., Reardon, W., Buckler, A.J., Harper, P.S., Housman, D.E., and Shaw, D.J. (1992). Expansion of an unstable DNA region and phenotypic variation in myotonic dystrophy. *Nature* 355, 545-546.

Harper, P.S., and Dyken, P.R. (1972). Early-onset dystrophia myotonica. Evidence supporting a maternal environmental factor. *Lancet* 2, 53-55.

Harper, P.S. (1989). *Myotonic Dystrophy*. 2nd Ed London: Saunders.

Hartner, K.T., and Pette, D. (1990). Fast and slow isoforms of troponin I and troponin C. Distribution in normal rabbit muscles and effects of chronic stimulation. *Eur J Biochem* 188, 261-267.

Haverkamp, L.J., Appel, V., and Appel, S.H. (1995). Natural history of amyotrophic lateral sclerosis in a database population. Validation of a scoring system and a model for survival prediction. *Brain* 118 (Pt 3), 707-719.

Heatwole, C.R., Miller, J., Martens, B., and Moxley, R.T., 3rd (2006). Laboratory abnormalities in ambulatory patients with myotonic dystrophy type 1. *Arch Neurol* 63, 1149-1153.

Hegedus, J., Putman, C.T., and Gordon, T. (2007). Time course of preferential motor unit loss in the SOD1 G93A mouse model of amyotrophic lateral sclerosis. *Neurobiol Dis* 28, 154-164.

Hegedus, J., Putman, C.T., Tyreman, N., and Gordon, T. (2008). Preferential motor unit loss in the SOD1 G93A transgenic mouse model of amyotrophic lateral sclerosis. *J Physiol* 586, 3337-3351.

Heizmann, C.W., Berchtold, M.W., and Rowlerson, A.M. (1982). Correlation of parvalbumin concentration with relaxation speed in mammalian muscles. *Proc Natl Acad Sci U S A* 79, 7243-7247.

Henneman, E. (1957). Relation between size of neurons and their susceptibility to discharge. *Science* 126, 1345-1347.

Henneman, E., and Olson, C.B. (1965). Relations between Structure and Function in the Design of Skeletal Muscles. *J Neurophysiol* 28, 581-598.

Hennig, R., and Lomo, T. (1985). Firing Patterns of Motor Units in Normal Rats. *Nature* 314, 164-166.

Hoffman, E.P., Brown, R.H., Jr., and Kunkel, L.M. (1987). Dystrophin: the protein product of the Duchenne muscular dystrophy locus. *Cell* 51, 919-928.

Huxley, A.F., and Niedergerke, R. (1954). Structural changes in muscle during contraction; interference microscopy of living muscle fibres. *Nature* 173, 971-973.

Imagawa, T., Takasago, T., and Shigekawa, M. (1989). Cardiac ryanodine receptor is absent in type I slow skeletal muscle fibers: immunochemical and ryanodine binding studies. *J Biochem* 106, 342-348.

Jayaraman, R.C., Latourette, M.T., Siebert, J.E., and Wiseman, R.W. (2006). A rapid algorithm for processing digital physiologic signals: application to skeletal muscle contractions. *Biomed Sign Process Cont* 1, 307-313.

Johansen, J.A., Breedlove, S.M., and Jordan, C.L. (2007). Androgen receptor expression in the levator ani muscle of male mice. *J Neuroendocrinol* 19, 823-826.

Johansen, J.A., Troxell-Smith, S.M., Yu, Z., Mo, K., Monks, D.A., Lieberman, A.P., Breedlove, S.M., and Jordan, C.L. (2011). Prenatal flutamide enhances survival in a myogenic mouse model of spinal bulbar muscular atrophy. *Neurodegener Dis* 8, 25-34.

Johansen, J.A., Yu, Z., Mo, K., Monks, D.A., Lieberman, A.P., Breedlove, S.M., and Jordan, C.L. (2009). Recovery of function in a myogenic mouse model of spinal bulbar muscular atrophy. *Neurobiol Dis* 34, 113-120.

Johnson, R.T., Schneider, A., DonCarlos, L.L., Breedlove, S.M., and Jordan, C.L. (2012). Astrocytes in the rat medial amygdala are responsive to adult androgens. *J Comp Neurol* 520, 2531-2544.

Kaspar, B.K., Llado, J., Sherkat, N., Rothstein, J.D., and Gage, F.H. (2003). Retrograde viral delivery of IGF-1 prolongs survival in a mouse ALS model. *Science* 301, 839-842.

Katsuno, M., Adachi, H., Kume, A., Li, M., Nakagomi, Y., Niwa, H., Sang, C., Kobayashi, Y., Doyu, M., and Sobue, G. (2002). Testosterone reduction prevents phenotypic expression in a transgenic mouse model of spinal and bulbar muscular atrophy. *Neuron* 35, 843-854.

Katsuno, M., Adachi, H., Minamiyama, M., Waza, M., Tokui, K., Banno, H., Suzuki, K., Onoda, Y., Tanaka, F., Doyu, M., *et al.* (2006). Reversible disruption of dynactin 1-mediated retrograde axonal transport in polyglutamine-induced motor neuron degeneration. *J Neurosci* 26, 12106-12117.

Kemp, M.Q., Poort, J.L., Baqri, R.M., Lieberman, A.P., Breedlove, S.M., Miller, K.E., and Jordan, C.L. (2011). Impaired motoneuronal retrograde transport in two models of SBMA implicates two sites of androgen action. *Hum Mol Genet* 20, 4475-4490.

Kennedy, W.R., Alter, M., and Sung, J.H. (1968). Progressive proximal spinal and bulbar muscular atrophy of late onset. A sex-linked recessive trait. *Neurology* 18, 671-680.

Kieran, D., Hafezparast, M., Bohnert, S., Dick, J.R., Martin, J., Schiavo, G., Fisher, E.M., and Greensmith, L. (2005). A mutation in dynein rescues axonal transport defects and extends the life span of ALS mice. *J Cell Biol* 169, 561-567.

Kimura, T., Nakamori, M., Lueck, J.D., Pouliquin, P., Aoike, F., Fujimura, H., Dirksen, R.T., Takahashi, M.P., Dulhunty, A.F., and Sakoda, S. (2005). Altered mRNA splicing of the skeletal muscle ryanodine receptor and sarcoplasmic/endoplasmic reticulum Ca²⁺-ATPase in myotonic dystrophy type 1. *Hum Mol Genet* 14, 2189-2200.

Kinirons, P., and Rouleau, G.A. (2008). Administration of testosterone results in reversible deterioration in Kennedy's disease. *J Neurol Neurosurg Psychiatry* 79, 106-107.

Koenig, M., Monaco, A.P., and Kunkel, L.M. (1988). The complete sequence of dystrophin predicts a rod-shaped cytoskeletal protein. *Cell* 53, 219-228.

Kushmerick, M.J., Moerland, T.S., and Wiseman, R.W. (1992). Mammalian skeletal muscle fibers distinguished by contents of phosphocreatine, ATP, and Pi. *Proc Natl Acad Sci U S A* 89, 7521-7525.

La Spada, A.R., Wilson, E.M., Lubahn, D.B., Harding, A.E., and Fischbeck, K.H. (1991). Androgen receptor gene mutations in X-linked spinal and bulbar muscular atrophy. *Nature* 352, 77-79.

Lapointe, B.M., and Cote, C.H. (1999). Anesthetics can alter subsequent in vitro assessment of contractility in slow and fast skeletal muscles of rat. *Am J Physiol* 277, R917-921.

Lefebvre, S., Burglen, L., Reboullet, S., Clermont, O., Bulet, P., Viollet, L., Benichou, B., Cruaud, C., Millasseau, P., Zeviani, M., *et al.* (1995). Identification and characterization of a spinal muscular atrophy-determining gene. *Cell* 80, 155-165.

Li, W., Brakefield, D., Pan, Y., Hunter, D., Myckatyn, T.M., and Parsadanian, A. (2007). Muscle-derived but not centrally derived transgene GDNF is neuroprotective in G93A-SOD1 mouse model of ALS. *Exp Neurol* 203, 457-471.

Lindenbaum, R.H., Clarke, G., Patel, C., Moncrieff, M., and Hughes, J.T. (1979). Muscular dystrophy in an X; 1 translocation female suggests that Duchenne locus is on X chromosome short arm. *J Med Genet* 16, 389-392.

Lino, M.M., Schneider, C., and Caroni, P. (2002). Accumulation of SOD1 mutants in postnatal motoneurons does not cause motoneuron pathology or motoneuron disease. *J Neurosci* 22, 4825-4832.

Lyon, M.F. (1961). Gene Action in X-Chromosome of Mouse (*Mus Musculus* L). *Nature* 190, 372-&.

Lyon, M.F. (1962). Sex Chromatin and Gene Action in Mammalian X-Chromosome. *American Journal of Human Genetics* 14, 135-&.

MacLean, H.E., Warne, G.L., and Zajac, J.D. (1997). Localization of functional domains in the androgen receptor. *J Steroid Biochem Mol Biol* 62, 233-242.

MacLennan, D.H., Rice, W.J., and Green, N.M. (1997). The mechanism of Ca²⁺ transport by sarco(endo)plasmic reticulum Ca²⁺-ATPases. *J Biol Chem* 272, 28815-28818.

Mankodi, A., Takahashi, M.P., Jiang, H., Beck, C.L., Bowers, W.J., Moxley, R.T., Cannon, S.C., and Thornton, C.A. (2002). Expanded CUG repeats trigger aberrant splicing of ClC-1 chloride channel pre-mRNA and hyperexcitability of skeletal muscle in myotonic dystrophy. *Mol Cell* 10, 35-44.

Mariotti, C., Castellotti, B., Pareyson, D., Testa, D., Eoli, M., Antozzi, C., Silani, V., Marconi, R., Tezzon, F., Siciliano, G., *et al.* (2000). Phenotypic manifestations associated with CAG-

repeat expansion in the androgen receptor gene in male patients and heterozygous females: a clinical and molecular study of 30 families. *Neuromuscul Disord* *10*, 391-397.

Markowitz, J.A., Singh, P., and Darras, B.T. (2012). Spinal muscular atrophy: a clinical and research update. *Pediatr Neurol* *46*, 1-12.

Martin, A.F. (1981). Turnover of cardiac troponin subunits. Kinetic evidence for a precursor pool of troponin-I. *J Biol Chem* *256*, 964-968.

Matsuda, R., Nishikawa, A., and Tanaka, H. (1995). Visualization of dystrophic muscle fibers in mdx mouse by vital staining with Evans blue: evidence of apoptosis in dystrophin-deficient muscle. *J Biochem* *118*, 959-964.

McCord, J.M., Keele, B.B., Jr., and Fridovich, I. (1971). An enzyme-based theory of obligate anaerobiosis: the physiological function of superoxide dismutase. *Proc Natl Acad Sci U S A* *68*, 1024-1027.

McManamny, P., Chy, H.S., Finkelstein, D.I., Craythorn, R.G., Crack, P.J., Kola, I., Cheema, S.S., Horne, M.K., Wreford, N.G., O'Bryan, M.K., *et al.* (2002). A mouse model of spinal and bulbar muscular atrophy. *Hum Mol Genet* *11*, 2103-2111.

McMillan, H.J., Gregas, M., Darras, B.T., and Kang, P.B. (2011). Serum transaminase levels in boys with Duchenne and Becker muscular dystrophy. *Pediatrics* *127*, e132-136.

Mickelson, J.R., and Louis, C.F. (1996). Malignant hyperthermia: excitation-contraction coupling, Ca²⁺ release channel, and cell Ca²⁺ regulation defects. *Physiol Rev* *76*, 537-592.

Miller, T.M., Kim, S.H., Yamanaka, K., Hester, M., Umapathi, P., Arnson, H., Rizo, L., Mendell, J.R., Gage, F.H., Cleveland, D.W., *et al.* (2006). Gene transfer demonstrates that muscle is not a primary target for non-cell-autonomous toxicity in familial amyotrophic lateral sclerosis. *Proc Natl Acad Sci U S A* *103*, 19546-19551.

Mo, K., Razak, Z., Rao, P., Yu, Z., Adachi, H., Katsuno, M., Sobue, G., Lieberman, A.P., Westwood, J.T., and Monks, D.A. (2010). Microarray analysis of gene expression by skeletal muscle of three mouse models of Kennedy disease/spinal bulbar muscular atrophy. *PLoS One* *5*, e12922.

Mohajeri, M.H., Figlewicz, D.A., and Bohn, M.C. (1999). Intramuscular grafts of myoblasts genetically modified to secrete glial cell line-derived neurotrophic factor prevent motoneuron

loss and disease progression in a mouse model of familial amyotrophic lateral sclerosis. *Hum Gene Ther* *10*, 1853-1866.

Monks, D.A., Johansen, J.A., Mo, K., Rao, P., Eagleson, B., Yu, Z., Lieberman, A.P., Breedlove, S.M., and Jordan, C.L. (2007). Overexpression of wild-type androgen receptor in muscle recapitulates polyglutamine disease. *Proc Natl Acad Sci U S A* *104*, 18259-18264.

Monks, D.A., O'Bryant, E.L., and Jordan, C.L. (2004). Androgen receptor immunoreactivity in skeletal muscle: enrichment at the neuromuscular junction. *J Comp Neurol* *473*, 59-72.

Monks, D.A., Rao, P., Mo, K., Johansen, J.A., Lewis, G., and Kemp, M.Q. (2008). Androgen receptor and Kennedy disease/spinal bulbar muscular atrophy. *Horm Behav* *53*, 729-740.

Morton, N.E., and Chung, C.S. (1959). Formal genetics of muscular dystrophy. *Am J Hum Genet* *11*, 360-379.

Murray, L.M., Comley, L.H., Thomson, D., Parkinson, N., Talbot, K., and Gillingwater, T.H. (2008). Selective vulnerability of motor neurons and dissociation of pre- and post-synaptic pathology at the neuromuscular junction in mouse models of spinal muscular atrophy. *Hum Mol Genet* *17*, 949-962.

Musa, M., Fernando, S.M., Chatterjee, D., and Monks, D.A. (2011). Subcellular effects of myocyte-specific androgen receptor overexpression in mice. *J Endocrinol* *210*, 93-104.

Nagai, M., Re, D.B., Nagata, T., Chalazonitis, A., Jessell, T.M., Wichterle, H., and Przedborski, S. (2007). Astrocytes expressing ALS-linked mutated SOD1 release factors selectively toxic to motor neurons. *Nat Neurosci* *10*, 615-622.

Naya, F.J., Mercer, B., Shelton, J., Richardson, J.A., Williams, R.S., and Olson, E.N. (2000). Stimulation of slow skeletal muscle fiber gene expression by calcineurin in vivo. *J Biol Chem* *275*, 4545-4548.

Nedelsky, N.B., Pennuto, M., Smith, R.B., Palazzolo, I., Moore, J., Nie, Z., Neale, G., and Taylor, J.P. (2010). Native functions of the androgen receptor are essential to pathogenesis in a *Drosophila* model of spinobulbar muscular atrophy. *Neuron* *67*, 936-952.

Oki, K., Wiseman, R.W., Breedlove, S.M., and Jordan, C.L. (2013). Androgen receptors in muscle fibers induce rapid loss of force but not mass: Implications for spinal bulbar muscular atrophy. *Muscle Nerve* *47*, 823-834.

Palazzolo, I., Stack, C., Kong, L., Musaro, A., Adachi, H., Katsuno, M., Sobue, G., Taylor, J.P., Sumner, C.J., Fischbeck, K.H., *et al.* (2009). Overexpression of IGF-1 in muscle attenuates disease in a mouse model of spinal and bulbar muscular atrophy. *Neuron* 63, 316-328.

Parsons, B., Szczesna, D., Zhao, J., Van Slooten, G., Kerrick, W.G., Putkey, J.A., and Potter, J.D. (1997). The effect of pH on the Ca²⁺ affinity of the Ca²⁺ regulatory sites of skeletal and cardiac troponin C in skinned muscle fibres. *J Muscle Res Cell Motil* 18, 599-609.

Patel, J.R., McDonald, K.S., Wolff, M.R., and Moss, R.L. (1997). Ca²⁺ binding to troponin C in skinned skeletal muscle fibers assessed with caged Ca²⁺ and a Ca²⁺ fluorophore. Invariance of Ca²⁺ binding as a function of sarcomere length. *J Biol Chem* 272, 6018-6027.

Pearce, J.M., Pennington, R.J., and Walton, J.N. (1964). Serum Enzyme Studies in Muscle Disease. II. Serum Creatine Kinase Activity in Muscular Dystrophy and in Other Myopathic and Neuropathic Disorders. *J Neurol Neurosurg Psychiatry* 27, 96-99.

Pelerson, E., Jeong, G.B., Ross, J.L., Dixit, R., Wallace, K.E., Kalb, R.G., and Holzbaur, E.L. (2009). A switch in retrograde signaling from survival to stress in rapid-onset neurodegeneration. *J Neurosci* 29, 9903-9917.

Pette, D., and Staron, R.S. (2000). Myosin isoforms, muscle fiber types, and transitions. *Microsc Res Tech* 50, 500-509.

Pigino, G., Morfini, G., Atagi, Y., Deshpande, A., Yu, C., Jungbauer, L., LaDu, M., Busciglio, J., and Brady, S. (2009). Disruption of fast axonal transport is a pathogenic mechanism for intraneuronal amyloid beta. *Proc Natl Acad Sci U S A* 106, 5907-5912.

Ranganathan, S., Harmison, G.G., Meyertholen, K., Pennuto, M., Burnett, B.G., and Fischbeck, K.H. (2009). Mitochondrial abnormalities in spinal and bulbar muscular atrophy. *Hum Mol Genet* 18, 27-42.

Rhodes, L.E., Freeman, B.K., Auh, S., Kokkinis, A.D., La Pean, A., Chen, C., Lehky, T.J., Shrader, J.A., Levy, E.W., Harris-Love, M., *et al.* (2009). Clinical features of spinal and bulbar muscular atrophy. *Brain* 132, 3242-3251.

Rinaldi, C., Bott, L.C., Chen, K.L., Harmison, G.G., Katsuno, M., Sobue, G., Pennuto, M., and Fischbeck, K.H. (2012). Insulinlike growth factor (IGF)-1 administration ameliorates disease manifestations in a mouse model of spinal and bulbar muscular atrophy. *Mol Med* 18, 1261-1268.

Ringel, S.P., Murphy, J.R., Alderson, M.K., Bryan, W., England, J.D., Miller, R.G., Petajan, J.H., Smith, S.A., Roelofs, R.I., Ziter, F., *et al.* (1993). The natural history of amyotrophic lateral sclerosis. *Neurology* 43, 1316-1322.

Ripps, M.E., Huntley, G.W., Hof, P.R., Morrison, J.H., and Gordon, J.W. (1995). Transgenic mice expressing an altered murine superoxide dismutase gene provide an animal model of amyotrophic lateral sclerosis. *Proc Natl Acad Sci U S A* 92, 689-693.

Romeo, V. (2012). Myotonic Dystrophy Type 1 or Steinert's disease. *Adv Exp Med Biol* 724, 239-257.

Rosen, D.R., Siddique, T., Patterson, D., Figlewicz, D.A., Sapp, P., Hentati, A., Donaldson, D., Goto, J., O'Regan, J.P., Deng, H.X., *et al.* (1993). Mutations in Cu/Zn superoxide dismutase gene are associated with familial amyotrophic lateral sclerosis. *Nature* 362, 59-62.

Ross, C.A. (2002). Polyglutamine pathogenesis: emergence of unifying mechanisms for Huntington's disease and related disorders. *Neuron* 35, 819-822.

Sandow, A. (1952). Excitation-contraction coupling in muscular response. *Yale J Biol Med* 25, 176-201.

Schmidt, B.J., Greenberg, C.R., Allingham-Hawkins, D.J., and Spriggs, E.L. (2002). Expression of X-linked bulbospinal muscular atrophy (Kennedy disease) in two homozygous women. *Neurology* 59, 770-772.

Schreiber, A., Smith, W.L., Ionasescu, V., Zellweger, H., Franken, E.A., Dunn, V., and Ehrhardt, J. (1987). Magnetic resonance imaging of children with Duchenne muscular dystrophy. *Pediatr Radiol* 17, 495-497.

Schwaller, B., Dick, J., Dhoot, G., Carroll, S., Vrbova, G., Nicotera, P., Pette, D., Wyss, A., Bluethmann, H., Hunziker, W., *et al.* (1999). Prolonged contraction-relaxation cycle of fast-twitch muscles in parvalbumin knockout mice. *Am J Physiol* 276, C395-403.

Sheppard, R.L., Spangenburg, E.E., Chin, E.R., and Roth, S.M. (2011). Androgen receptor polyglutamine repeat length affects receptor activity and C2C12 cell development. *Physiol Genomics* 43, 1135-1143.

Sherrington, C. (1929). Ferrier lecture - Some functional problems attaching to convergence. *P R Soc Lond B-Conta* 105, 332-362.

Sinha-Hikim, I., Taylor, W.E., Gonzalez-Cadavid, N.F., Zheng, W., and Bhasin, S. (2004). Androgen receptor in human skeletal muscle and cultured muscle satellite cells: up-regulation by androgen treatment. *J Clin Endocrinol Metab* 89, 5245-5255.

Sobue, G., Hashizume, Y., Mukai, E., Hirayama, M., Mitsuma, T., and Takahashi, A. (1989). X-linked recessive bulbospinal neuronopathy. A clinicopathological study. *Brain* 112 (Pt 1), 209-232.

Sopher, B.L., Thomas, P.S., Jr., LaFevre-Bernt, M.A., Holm, I.E., Wilke, S.A., Ware, C.B., Jin, L.W., Libby, R.T., Ellerby, L.M., and La Spada, A.R. (2004). Androgen receptor YAC transgenic mice recapitulate SBMA motor neuronopathy and implicate VEGF164 in the motor neuron degeneration. *Neuron* 41, 687-699.

Soraru, G., D'Ascenzo, C., Polo, A., Palmieri, A., Baggio, L., Vergani, L., Gellera, C., Moretto, G., Pegoraro, E., and Angelini, C. (2008). Spinal and bulbar muscular atrophy: skeletal muscle pathology in male patients and heterozygous females. *J Neurol Sci* 264, 100-105.

Sorenson, E.J., and Klein, C.J. (2007). Elevated creatine kinase and transaminases in asymptomatic SBMA. *Amyotroph Lateral Scler* 8, 62-64.

Souccar, C., Lapa, A.J., and do Valle, J.R. (1982). The influence of testosterone on neuromuscular transmission in hormone sensitive mammalian skeletal muscles. *Muscle Nerve* 5, 232-237.

Spencer, M.J., Croall, D.E., and Tidball, J.G. (1995). Calpains are activated in necrotic fibers from mdx dystrophic mice. *J Biol Chem* 270, 10909-10914.

Supinski, G.S., and Callahan, L.A. (2006). Caspase activation contributes to endotoxin-induced diaphragm weakness. *J Appl Physiol* 100, 1770-1777.

Suzuki, K., Katsuno, M., Banno, H., Takeuchi, Y., Atsuta, N., Ito, M., Watanabe, H., Yamashita, F., Hori, N., Nakamura, T., *et al.* (2008). CAG repeat size correlates to electrophysiological motor and sensory phenotypes in SBMA. *Brain* 131, 229-239.

Szent-Gyorgyi, A.G. (2004). The early history of the biochemistry of muscle contraction. *J Gen Physiol* 123, 631-641.

- Takeyama, K., Ito, S., Yamamoto, A., Tanimoto, H., Furutani, T., Kanuka, H., Miura, M., Tabata, T., and Kato, S. (2002). Androgen-dependent neurodegeneration by polyglutamine-expanded human androgen receptor in *Drosophila*. *Neuron* 35, 855-864.
- Talbert, E.E., Smuder, A.J., Min, K., Kwon, O.S., and Powers, S.K. (2013). Calpain and caspase-3 play required roles in immobilization-induced limb muscle atrophy. *J Appl Physiol* 114, 1482-1489.
- Thomas, M., Yu, Z., Dadgar, N., Varambally, S., Yu, J., Chinnaiyan, A.M., and Lieberman, A.P. (2005). The unfolded protein response modulates toxicity of the expanded glutamine androgen receptor. *J Biol Chem* 280, 21264-21271.
- Thomas, P.S., Jr., Fraley, G.S., Damian, V., Woodke, L.B., Zapata, F., Sopher, B.L., Plymate, S.R., and La Spada, A.R. (2006). Loss of endogenous androgen receptor protein accelerates motor neuron degeneration and accentuates androgen insensitivity in a mouse model of X-linked spinal and bulbar muscular atrophy. *Hum Mol Genet* 15, 2225-2238.
- van der Steege, G., Grootsholten, P.M., Cobben, J.M., Zappata, S., Scheffer, H., den Dunnen, J.T., van Ommen, G.J., Brahe, C., and Buys, C.H. (1996). Apparent gene conversions involving the SMN gene in the region of the spinal muscular atrophy locus on chromosome 5. *Am J Hum Genet* 59, 834-838.
- Vassella, F., Richterich, R., and Rossi, E. (1965). The Diagnostic Value of Serum Creatine Kinase in Neuromuscular and Muscular Disease. *Pediatrics* 35, 322-330.
- Vermaelen, M., Sirvent, P., Raynaud, F., Astier, C., Mercier, J., Lacampagne, A., and Cazorla, O. (2007). Differential localization of autolyzed calpains 1 and 2 in slow and fast skeletal muscles in the early phase of atrophy. *Am J Physiol Cell Physiol* 292, C1723-1731.
- Wiseman, R.W., Beck, T.W., and Chase, P.B. (1996). Effect of intracellular pH on force development depends on temperature in intact skeletal muscle from mouse. *Am J Physiol* 271, C878-886.
- Wong, C.I., Zhou, Z.X., Sar, M., and Wilson, E.M. (1993). Steroid requirement for androgen receptor dimerization and DNA binding. Modulation by intramolecular interactions between the NH2-terminal and steroid-binding domains. *J Biol Chem* 268, 19004-19012.
- Wong, M., and Martin, L.J. (2010). Skeletal muscle-restricted expression of human SOD1 causes motor neuron degeneration in transgenic mice. *Hum Mol Genet* 19, 2284-2302.

Wong, P.C., Pardo, C.A., Borchelt, D.R., Lee, M.K., Copeland, N.G., Jenkins, N.A., Sisodia, S.S., Cleveland, D.W., and Price, D.L. (1995). An adverse property of a familial ALS-linked SOD1 mutation causes motor neuron disease characterized by vacuolar degeneration of mitochondria. *Neuron* *14*, 1105-1116.

Wu, H., Kanatous, S.B., Thurmond, F.A., Gallardo, T., Isotani, E., Bassel-Duby, R., and Williams, R.S. (2002). Regulation of mitochondrial biogenesis in skeletal muscle by CaMK. *Science* *296*, 349-352.

Wu, H., Rothermel, B., Kanatous, S., Rosenberg, P., Naya, F.J., Shelton, J.M., Hutcheson, K.A., DiMaio, J.M., Olson, E.N., Bassel-Duby, R., *et al.* (2001). Activation of MEF2 by muscle activity is mediated through a calcineurin-dependent pathway. *EMBO J* *20*, 6414-6423.

Yang, Z., Chang, Y.J., Yu, I.C., Yeh, S., Wu, C.C., Miyamoto, H., Merry, D.E., Sobue, G., Chen, L.M., Chang, S.S., *et al.* (2007). ASC-J9 ameliorates spinal and bulbar muscular atrophy phenotype via degradation of androgen receptor. *Nat Med* *13*, 348-353.

Yu, Z., Dadgar, N., Albertelli, M., Gruis, K., Jordan, C., Robins, D.M., and Lieberman, A.P. (2006). Androgen-dependent pathology demonstrates myopathic contribution to the Kennedy disease phenotype in a mouse knock-in model. *J Clin Invest* *116*, 2663-2672.

Zengel, J.E., Reid, S.A., Sybert, G.W., and Munson, J.B. (1985). Membrane electrical properties and prediction of motor-unit type of medial gastrocnemius motoneurons in the cat. *J Neurophysiol* *53*, 1323-1344.

Zubrzycka-Gaarn, E.E., Bulman, D.E., Karpati, G., Burghes, A.H., Belfall, B., Klamut, H.J., Talbot, J., Hodges, R.S., Ray, P.N., and Worton, R.G. (1988). The Duchenne muscular dystrophy gene product is localized in sarcolemma of human skeletal muscle. *Nature* *333*, 466-469.

Zuloaga, D.G., Morris, J.A., Jordan, C.L., and Breedlove, S.M. (2008). Mice with the testicular feminization mutation demonstrate a role for androgen receptors in the regulation of anxiety-related behaviors and the hypothalamic-pituitary-adrenal axis. *Horm Behav* *54*, 758-766.